The Evolving Search for Positive Electrode Host Materials for the Li-S Battery

by

Connor Hart

A thesis

presented to the University of Waterloo

in fulfillment of the

thesis requirement for the degree of

Master of Science

in

Chemistry-Nanotechnology

Waterloo, Ontario, Canada, 2015

AUTHOR'S DECLARATION

I hereby declare that I am the sole author of this thesis. This is a true copy of the thesis, including any required final revisions, as accepted by my examiners.

I understand that my thesis may be made electronically available to the public.

ABSTRACT

High energy density storage systems are constantly being researched to support the demand for electric vehicles and use for renewable energy systems. One such energy storage system of interest is lithium-sulfur batteries which utilize inexpensive, earth-abundant sulfur as the active material. In order to fully realize the potential of Li-S batteries being commercialized, many problems must still be overcome. Among them are: 1) low conductivity of sulfur species, 2) polysulfide redox shuttle in the electrolyte and self-discharge, 3) volume expansion of active material upon cycling, and 4) lithium metal dendrite formation. The work in this thesis will first focus on a diagnostic method that probes ideal characteristics of sulfur host materials, and then focus on a new material that will address the first three problems.

The exhaustive search for a material that has a high electronic conductivity to facilitate charge transfer, substantial surface area and pore volume to allow high sulfur loading, and well-suited physical/chemical surface properties to inhibit S_n^{2-} diffusion into the electrolyte is still ongoing. It is vital to find a material with these characteristics, so as to bring the Li-S battery one step closer to commercialization. In the first section of this thesis, a versatile, cost-effective electrochemical analysis strategy is described that determines the specific S_n^{2-} adsorptivity of materials. This analytical method for screening sulfur host materials is based on metrics: a quantitative electro-oxidation reaction provides the value for S_n^{2-} adsorptivity – which coupled with surface area – is correlated to the extent of self-discharge at an intermediate state of

discharge during a 5-day cycling protocol. Measurement of nine different materials with varying surface area, and hydrophobicity using the analytical method determined optimum properties for capacity stabilization. In fact, materials (such as MnO_2) that have a high surface area and the ability to chemically interact with intermediate polysulfides realized improved long-term cycling performance and mitigated self-discharge.

In the second part of this thesis, a positive electrode material is proposed as a sulfur host. Surface thiosulfate groups are known to drastically mitigate polysulfide diffusion through the formation of a polythionate complex which acts as an internal mediator catenating long-chain polysulfides. The presence of the polythionate complex through an extrinsic additive was explored for low-cost carbon materials. In this study, carbon materials which contained functional groups able to form the polythionate complex saw up to 60% reduction in the irreversible capacity loss as a result of self-discharge. With 15 wt% additive, polysulfide adsorptivity increased and excellent long-term cycling was realized with a capacity fade of 0.085% per cycle over 200 cycles. By combining a polysulfide adsorber with a carbon matrix, long-term cycling is realized with a sulfur loading of ~1.5 mg/cm^2.

ACKNOWLEDGEMENTS

Completing a Master's Degree thesis does not rely simply on ones gusto and determination to conduct research, process data, and write a 100 page document. In fact, I could not have conducted the research I did without the support of many people.

Firstly, I would like to extend my sincere appreciation to my supervisor Professor Linda F. Nazar for her continued guidance and support throughout the course of this research project. As well, *merci* Dr. Marine Cuisinier for taking me under your 'research' wings and guiding me into the researcher I am today. You both have taught me patience and perseverance in research and for this I will be forever grateful.

Secondly I would like to thank the sulfur group who through continued discussion and friendships has allowed me to progress successfully in my research. Thank you Dr. Xiao Liang, Diane Houtarde, Quan Pang, and Takuto Kwok.

I would also like to extend a huge thanks to my group members of past and present who have always supported me in experiments, and further friendships: Dr. Guerman Popov, Dr. Dipan Kundu, Dr. Victor Duffort, Dr. Momo Safari, Dr. Jaka Sunarso, Dr. Chun Xia, Brian Adams, Parvin Adeli, Kaitlin Town, Robert Black, Russel Fernandes, He Huang, Elahe Pashiri, Yverick Rangom, Abhi Shyamsunder, Xiaoqi Sun, Niranjan Sudhakar, Meng Xu and Kavish Kaup.

Beyond the walls of the Laboratory, I have been involved in my university community. I believe through my involvements I have achieved a well-rounded university experience and it has helped my research gain focus. Thank you to my CHEM120/123 Teaching Assistants Team for your support and guidance in my teaching experience. As well, I would like to thank the

Graduate Student Association and the Graduate Studies Endowment Fund for allowing me to take an active role in contributing to graduate student life at the University of Waterloo.

Finally, I would like to acknowledge the support of my family. Firstly and foremost, I want to say thank you to the love of my life, Amanda Jones, for supporting me through the last two years. Working late into the evening and on weekends is not obviously ideal, but as you supported me and my decisions, I was able to improve as a researcher and a person. Thank you to my parents and siblings for always being a continued support system that I have always wanted and needed.

I will never forget my time here at the University of Waterloo. The last two years has formed me into the researcher and person I am today, and for this I am forever grateful.

Thank you,

Connor Hart

2015

TABLE OF CONTENTS

List of Figures

List of Equations

List of Tables

List of Abbreviations

BET	Brunauer-Emmett-Teller
DME	Dimethoxymethane
DMF	Dimethylformamide
DOL	1,3-dioxolane
EDX	Energy dispersive X-ray spectroscopy
EMD	Electrolytic Manganese Dioxide
F	Faradays Constant
GO	Graphene Oxide
LiTFSI	Bis(trifluoromethanesulfonyl)imide lithium
$LiMO_2$	Lithium metal oxide
Li_2S	Lithium sulfide
NMR	Nuclear Magnetic Resonance Spectroscopy
PVdF	Polyvinylidene fluoride
%RSD	Percent Relative Standard Deivation
SEM	Scanning electron microscopy
S_n^{2-}	Polysulfide (intermediate, soluble in glyme-based electrolytes)
TEGDME	Tetraethylene glycol dimethyl ether
THF	Tetrahydrofuran
TGA	Thermogravimetric analysis
TS	Sodium thiosulfate ($Na_2S_2O_3$)
TTE	tetrafluoroethyl-2,2,3,3-tetrafluoropropyl ether
VC	Vulcan carbon
XPS	X-ray photoelectron spectroscopy
XRD	X-ray diffraction
Δ_D	Self-discharge capacity loss
Δ_C	Irreversible Capacity Loss

Chapter 1
Introduction

1.1 Origin of Rechargeable Lithium Batteries

Around the world, a great transformation is occurring where cities and countries that used to rely on fossil fuels and demand global resources have begun to drive important shifts in urban energy and environmental policy making. Meeting our modern day civilization energy needs typically requires the combustion of fossil fuels to heat homes, power cars, and support industry production. Although society has been built on the consumption of non-renewable energy sources, fossil fuels are problematic as there are political difficulties associated with the production and distribution of this resource. Additionally, the resultant CO_2 emissions are acidifying our oceans and potentially creating global climate change.[1]

Movement away from our current dependence on fossil fuels requires investigation into renewable energy sources such as solar, wind, and hydro. These renewable energy sources, although practical to mitigate air pollution and our impact on global warming, are not reliable as they are dependent on the presence of sun, wind and the flow of water. In order to realize practical application of renewable energy sources to fuel our societal demand, efficient batteries are needed in order to store energy. In practical applications, energy collected from renewable energy sources is stored in efficient batteries for use in electric vehicles, energy grids, and even portable mobile devices. A requirement for society to reduce our dependence on fossil fuels and increase the use of renewable energy sources is that a sustainable, well distributed energy supply for all people is available.[2]

Lead-acid batteries are used in gas-powered vehicles as automotive starters. If society wants to reduce our carbon foot-print, then there needs to be a movement towards electric vehicles. The birth of Li-ion rechargeable batteries has enabled the wireless revolution of cell phones, laptops, and digital cameras, which have transformed global communication. Li-ion batteries have also transformed our transportation industry where they are able to power electric vehicles up to ~300 km. However, Li-ion batteries are expensive and therefore new technologies are needed in order to realize a practical application for electric vehicles.

1.1.1 Basic Concepts of Rechargeable Batteries

Rechargeable batteries, also known as secondary batteries, rely on reversible electrochemical reactions. Secondary batteries are used for automotive starters, portable consumer devices, and grid energy storage applications for load leveling. Typically, a rechargeable battery is made of one or more connected electrochemical cells each providing a current and voltage. All research conducted in this thesis will focus on improving a single electrochemical cell, instead of developing full battery packs.[3]

The typical electrochemical cell design consists of positive (cathode) and negative (anode) electrodes with an electrolyte serving as the ion conductor. The active materials in the anode and the cathode have a difference in chemical potentials, which provides the cell's voltage. Briefly, each electrode must be both electronically and ionically conductive to facilitate charge transfer at the surface and in the bulk. The electrolyte conducts ions between the anode and the cathode, while the electrons traverse an external circuit where they do work.

Electrochemical cells are very complex and require basic understanding of electrochemical terminology which will be used throughout this thesis:[14]

- **Potential:** The potential of an electrode is dependent on its chemical potential (*i.e.* redox potential). A large difference in potential between the cathode and anode (*i.e.* voltage) is desired for a full cell, since the output power is the product of voltage and current. The potential difference has to be within the electrochemical potential window of the electrolyte used, in order to prevent electrolyte decomposition.
- **Current:** Current flows from the positive terminal to the negative terminal but confusingly, electrons flow in the opposite direction. This confusion arises because we tend to assume that electrons are the only current carriers. In fact, positive ions are also current carriers and they flow in the same direction as the current. In a galvanic cell, the positive ions carry the current through the cell and the electrons carry the current in the external circuit.
- **Voltage Profile:** This is a plot of voltage as a function of specific capacity during the galvanostatic cycling of a cell, where a constant discharge/charge current is applied. The profile can explain the redox reactions and at what voltage they occur. A plateau on the plot represents a two-phase transition, whereas a slope corresponds to a single-phase reaction. A minimum voltage difference between the discharge and charge is an indicator of a low degree of polarization (which is desired for efficient batteries).
- **Cycling Rate:** Cycling refers to the repeated discharge and charge of the cell. The current at which a cell is discharged/charged matters when considering the power density. "C/n" rate corresponds to the rate (mA g^{-1}) at which the theoretical specific capacity is achieved in *n* hours upon discharge. For example, C/20 represents the rate to theoretically achieve full capacity in a 20 hour discharge or a 20 hour charge. A larger rate typically achieves more power, but normally leads to greater polarization, lower energy efficiency

and lower specific capacity. A high rate capability is desired as it indicates the ability to maintain capacity, and the degree of polarization upon increased rate.

- **Energy Units:** Specific capacity (mAh g^{-1}) or volumetric capacity (mAh cm^{-3}) is defined by the amount of charge (Q, mAh) stored per mass or volume of electrode for one full discharge/charge. A higher theoretical specific capacity is desired for new electrode systems and battery systems. Energy density is the product of capacity and voltage per mass (Wh kg^{-1}) or volume (Wh L^{-1}).
- **Capacity Retention:** Comparison of the capacity (mAh g^{-1}) achieved in a specific discharge/charge to another discharge/charge a defined number of cycles later. Capacity retention is typically expressed in percent.
- **Cycling Life**: In typical academic research, cycling life is usually studied on a single electrochemical cell and is defined as the capacity retention with prolonged galvanostatic cycling.
- **Coulombic Efficiency:** Typically reported for prolonged cycling, Coulombic efficiency is related to a single cycle via the capacity fade. Coulombic efficiency is calculated from the [Specific $Capacity_{discharge}$/Specific $Capacity_{charge}$]*100%. Coulombic efficiencies close to 100% are ideal for electrochemical systems.

1.1.2 The Origin of Intercalation Electrochemistry

The motivation for using battery technology based on Li metal as an anode relied initially on the fact that lithium is the most electropositive (-3.04 V versus standard hydrogen electrode) and the lightest (specific gravity = 0.53 g cm^{-3}) metal in the periodic table. These properties should theoretically allow for the design and implementation of storage systems with high energy density.

In a lithium ion battery, Li^+ ions shuttle between a layered metal oxide positive electrode host where they are stored upon discharge, and a graphitic negative electrode where they are stored upon charge. Typical cell voltages are in the range of 3.4-3.8V versus Li/Li^+ with theoretical capacities at the positive electrode as high as 280 mAh g^{-1}.[5] Reported in 1980 by Goodenough *et al.*, the layered structure of $LiCoO_2$ functions as an active cathode material for lithium-ion batteries based on intercalation electrochemistry.[6] Intercalation electrochemistry involves reversible (de)insertion of Li+ ions and electrons between the sheets of a layered oxide (positive electrode) or graphitic carbon (negative electrode). Metal oxides ($LiMO_2$) were first commercially viable by SONY Corporation and are now dominating the portable electronic device market. More recently, $LiFePO_4$ with 1D channels of Li^+ ions allow this cathode material to be cycled at a 5C rate for over 30 000 cycles with a capacity of 170 mAh g^{-1}.[7] The $FePO_4$ framework is environmentally friendly, and batteries based on this material are being considered for grid storage application. The challenge for researchers is to develop a battery that will retain high cycle life at an acceptable rate, in a safe and affordable manner, with a much larger energy density. Thus the movement towards electrochemical systems based on integration chemistry.[1]

1.1.3 Movement Towards Integration Electrochemistry

Lithium ion batteries have been prominent over the past two decades, but a further increase in energy density is required. This increase can be achieved through increasing the charge storage capacity of the anode/cathode materials, and/or increasing the overall cell voltage. To overcome the charge-storage issue, materials that undergo integration chemistry while accommodating more ions and electrons are becoming a promising option to replace current Li-ion batteries. Two such examples based on lithium are Li-air (or Li-O_2) and Li-S batteries.

Li-O_2 batteries, which have been more recently explored, employ oxygen as the active agent in the positive electrode. On discharge, Li-metal becomes oxidized releasing Li^+ into the electrolyte, while at the positive electrode, O_2 from the atmosphere enters the porous carbon cathode, dissolves in the electrolyte, and is reduced via $2Li^+ + O_2 + 2e^- \leftrightarrow Li_2O_2$. This system is predicted to have a practical specific energy in the range of 500-900 Wh kg^{-1}, which is sufficient to deliver a driving range of more than 550 km. Before Li-O_2 batteries can be widely employed, there needs to be removal of carbon from the positive electrode, and reduction of metallic lithium in the negative electrode.[8]

1.2 Sulfur as the Active Material

In 1962, elemental sulfur (S_8) was introduced as a positive electrode material by Herbert and Ulam.[9] In a typical Li-S battery, lithium metal is used as the anode (negative electrode), a sulfur composite as the cathode (positive electrode), and are separated by an electrolyte (typically a glyme-based electrolyte with lithium salt dissolved). The Li-S cell undergoes a different discharge/charge mechanism when compared to typical Li-ion batteries. During discharge (**Figure 1.1, left**) of the battery, lithium ions propagate from the lithium metal through the electrolyte and combine with sulfur through a non-topotactic assimilation process. Meanwhile, the electrons leave the anode, travel through an external system to do work, and are then captured by sulfur at the positive electrode. Elemental sulfur in the cathode is reduced upon discharge to form intermediate lithium polysulfides which terminate at the final discharge product of lithium sulfide (Li_2S).[10] Charging (**Figure 1.1, right**) of the cell triggers the reverse reaction where lithium sulfide is oxidized back to sulfur while lithium ions are reduced to lithium metal. This reversible reaction of $S_8 + 16e^- + 16Li^+ \leftrightarrow 8Li_2S$ provides Li-S cells with its large

theoretical energy density of 2,500 Wh kg^{-1} or 2,800 Wh L^{-1} and large theoretical capacity of 1,675 mAh g^{-1}.[10]

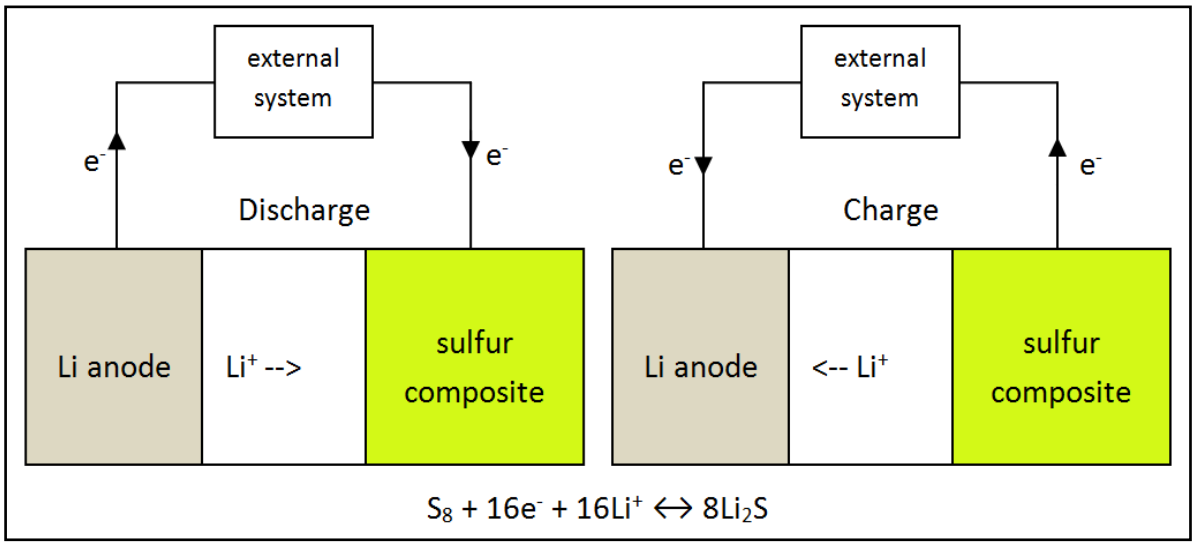

Figure 1.1: Schematic showing the typical discharge (left) and charge (right) mechanism for a Li-S battery.

It is important to note that polysulfides (Li_2S_n, $4 \leq n \leq 8$) are readily soluble in ether-based electrolytes, while Li_2S (and Li_2S_2, if it exists) is not. The seemingly simple chemistry is complicated and yet to be fully understood. Our group has performed *operando* X-ray adsorption near-edge spectroscopy to probe the mechanism behind sulfur discharge in ether-based electrolytes (**Figure 1.2**).[13] It is generally believed that upon discharge, the high-voltage plateau around 2.4 V corresponds to the reaction of S_8 to long-chain polysulfides (Li_2S_n, $4 \leq n \leq 8$) and the low-voltage plateau around 2.1 V represents further reduction into short-chain polysulfides (Li_2S_n, n=1,2) and Li_2S. Upon charge, the long gradual slope corresponds to the oxidation of solid-state Li_2S to long-chain polysulfides and the final short plateau represents further oxidation to S_8. It is worth noting: there is always a certain fraction of unutilized S_8 at all stages, which can be explained by the reaction at the high-voltage plateau: $S^0 + 3/2\ Li^+ + 3/2\ e^- \rightarrow 3/4\ Li_2S + 1/4\ S^0$.[13]

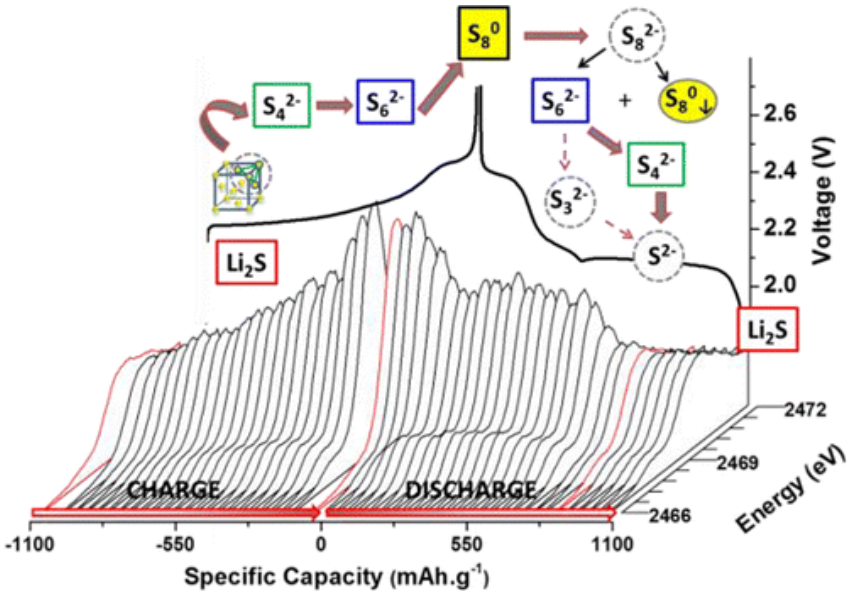

Figure 1.2: Schematic of sulfur discharge mechanism. Figure adopted from reference 13. © American Chemical Society.

1.2.1 Challenges with Li-S batteries

Although Li-S batteries have been studied since the mid-20th century, the problems are formidable, and many efforts have been made to address these struggles. However, many challenges still remain which can be classified into three categories: the physical properties of sulfur species, lack of fidelity of lithium deposition at the anode, and the polysulfide shuttle effect.

1.2.2.1 Physical Properties of Sulfur Species

Sulfur as a cathode material has a large theoretical capacity (1,675 mAh g^{-1}) and an extremely low electric conductivity. In an electrochemical cell, the lithium and sulfur do not come into contact as they are electronically insulated by a separator and electrolyte. Instead, sulfur accepts two electrons from the external circuit which reacts with lithium ions in the cathode where reduction occurs. The physical problems are that sulfur possesses a very low electrical/ionic conductivity, and undergoes a large volume change throughout cycling. At room temperature, sulfur is inherently insulating to both electrons and lithium ions with its electrical

conductivity being $5x10^{-30}$ S cm^{-1}, more than 20 orders of magnitude lower than that of a normal lithium transition metal oxide.[10] As well, sulfur (density = 2.03 g cm^{-3}) expands during reduction to lithium sulfide (density = 1.67 g cm^{-3}) which contracts during oxidation.[10] This 80% volume change can cause deterioration of the positive electrode integrity which is a contributing factor in capacity fading upon cycling.[11]

The volume expansion and conductivity issues have been tackled by many approaches. Carbon has been widely studied as an additive to the positive electrode to increase the conductivity of the composite. Carbon has a high electrical conductivity which can be designed into elegant materials to accommodate for the volume expansion. The ideal configuration for a sulfur-carbon composite is to have a uniform and high sulfur dispersion, complete sulfur enclosure in a confined, but accessible space, and strong sulfur-host affinity.[11]

1.2.2.2 Lithium Dendrite Formation and Physical Problems

Lithium metal is used in the present design of Li-S batteries as the negative electrode material. However, this is not ideal as lithium poses safety concerns that could possibility limit its commercial application. As an example, lithium reacts violently in the presence of water to produce hydrogen gas. If the battery was used in an electric vehicle, and a collision occurred, then immense risk is posed. In addition, dendrites (**Figure 1.3**, growths outward of the planar surface) are formed on the lithium surface when lithium is re-deposited during the charge cycle. These dendrites can penetrate through the separator, and reach the cathode resulting in a short circuit (cell death).[8] When researching Li-S batteries, options to consider for tackling the negative electrode is to protect the lithium anode to prevent dendrite formation, or replace the anode material completely.

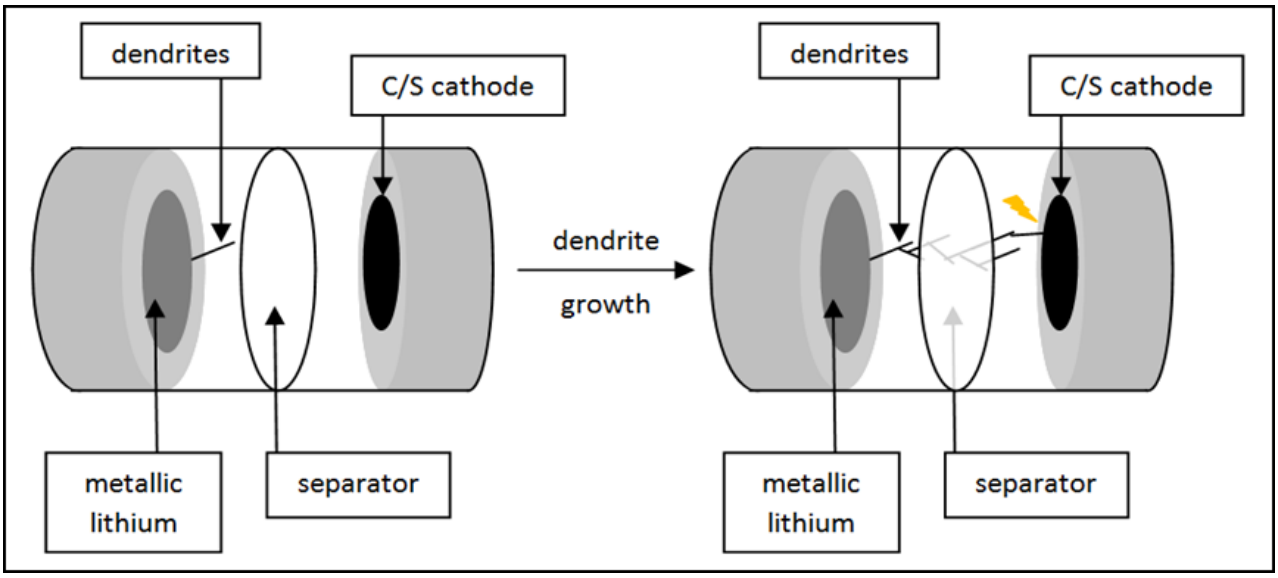

Figure 1.3: Schematic of lithium dendrite formation. Left) functioning cell with minimal lithium dendrite formation through charge cycle. Right) short-circuited cell as a result of electrical connection between anode and cathode.

1.2.2.3 Polysulfide Dissolution and Self-Discharge

The most pressing problem with Li-S batteries is controlling the by-products of the step-wise reduction of sulfur. Typically, Li-S cells are fabricated using glyme-based electrolytes even though intermediate sulfur species are readily soluble.[3,12,13] During discharge, soluble polysulfides that are not fully reduced to solid Li_2S remain in the electrolyte. As shown in **Figure 1.4**, these hydrophilic molecules can diffuse through the separator to the anode side, where they are further reduced by lithium metal to Li_2S which deposits on the lithium metal surface. This newly formed layer results in a solid electrolyte interface which blocks access to the lithium electrode. When the anode is fully coated, more incoming long chain polysulfides will react with this layer to form lower-order (short Li_2S_x, where x = 6 or 4) polysulfides. When there is a high concentration of polysulfides on the anode side, diffusion back to the cathode will occur where they can either be oxidized to sulfur or reduced to Li_2S depending on if in charge or discharge respectively. This polysulfide 'shuttle' is a parasitic process which causes self-

discharge and loss of active materials. As a consequence, capacity fading over cycling is realized.

Self-discharge occurs when batteries are at rest and the active material gradually dissolves and migrates into the electrolyte. Diffusion of polysulfide species during rest can cause active material to precipitate in the positive electrode, be lost in the electrolyte or deposit on the negative electrode.[14]

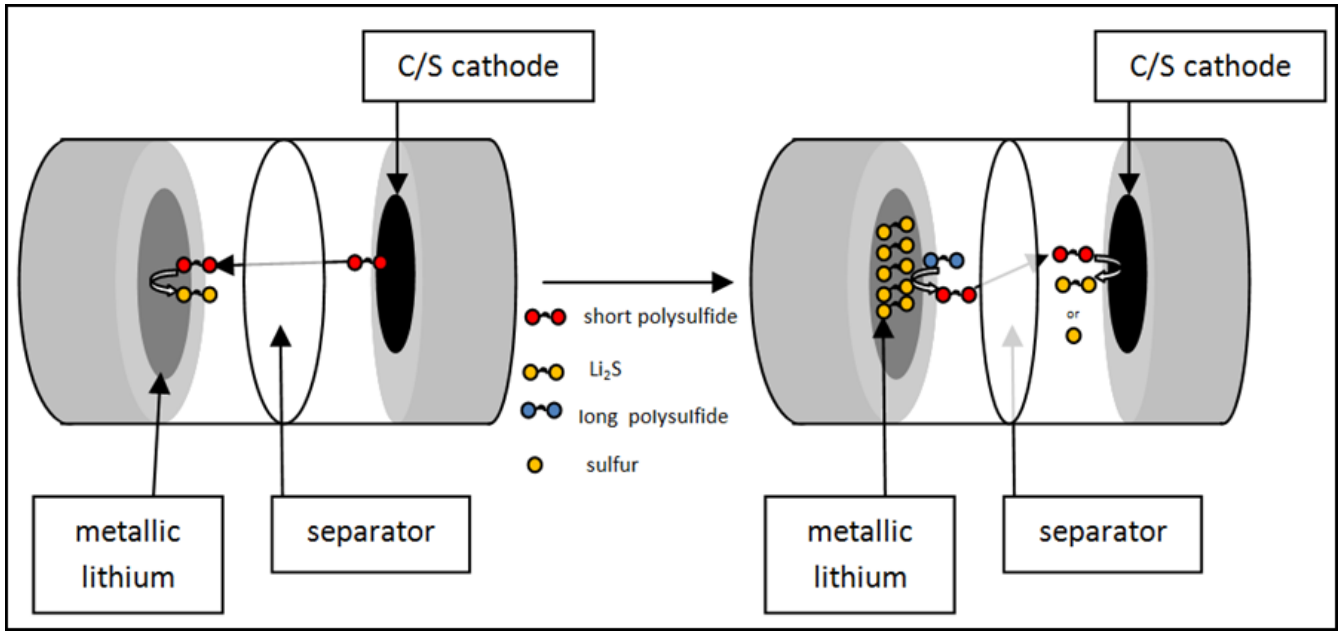

Figure 1.4: Schematic diagram of polysulfide shuttle. Left) soluble polysulfides diffuse through separator to the anode where reduced to Li_2S forming a solid electrolyte interface. Right) polysulfides migrate back through electrolyte to cathode and can either be oxidized or reduced.

There have been studies reported which investigate using different types of electrolytes to mitigate some of the challenges with Li-S batteries. Non-solvents for polysulfides, and high dielectric constant electrolytes both aid in approaching 100% sulfur utilization in the positive electrode upon discharge.[15,16] Although these electrolyte solvents drastically reduce polysulfide diffusion, further issues such as reactivity towards lithium, and increased polarization are realized. This type of research is not in the direct scope of this thesis and will not be discussed

further. This thesis focuses on using glyme-based electrolytes with which polysulfides are readily soluble, and undergo the typical polysulfide shuttle effect.

1.3 A Current Diagnostic Method

The majority of research into Li-S batteries is based on novel materials for the sulfur host. However, research cannot progress in an efficient manner without fundamental understanding of the Li-S electrochemical system. Fundamental research has focused on *operando* measurements to probe for sulfur speciation, and developing analytical methods to probe for certain properties (i.e. polysulfide concentration in the electrolyte during cycling). Many researchers have characterized the Li-S system via X-ray absorption near edge spectroscopy[13,15,16,17], UV-visible spectroscopy[18], and transmission X-ray microscopy[19], which have offered great insight into the intermediate species formed. There are minimal studies on diagnostic methods which can help guide researchers in choosing the right materials/electrolytes for the Li-S system.

One such diagnostic method was proposed by Tarascon *et al.* where they demonstrated the feasibility of using a modified 4-electrode Swagelok (**Figure 1.5a**) cell as an *in situ* analytical tool to determine quantitatively the concentration of dissolved polysulfides formed during discharge of a Li-S battery.[20] Using two different carbon hosts (**Figure 1.5b,c**), a Li-S battery was discharged numerous times and the cyclic voltammetry cathodic peaks were integrated. Integration between 2.25V and 1.5V can be correlated to the concentration of soluble polysulfides in the solution (**Figure 1.5d**). Notably, the sum of all cumulative charges is larger for low surface area carbon/S (XE2/S) composites than for mesoporous carbon/S composites. This analytical method can help determine which materials are more reliable at preventing polysulfides from diffusing into the electrolyte. This 4-electrode cell was claimed as an effective and reliable *in situ* analytical tool which can study the effect of different salts, solvents,

additives, and electrode architectures on the stability of the Li-S battery. No further reports using this 4-electrode cell have been published; however future work should focus on determining how polysulfide concentration changes once the current is turned off, with the addition of temperature and variation of the amount of electrolyte.

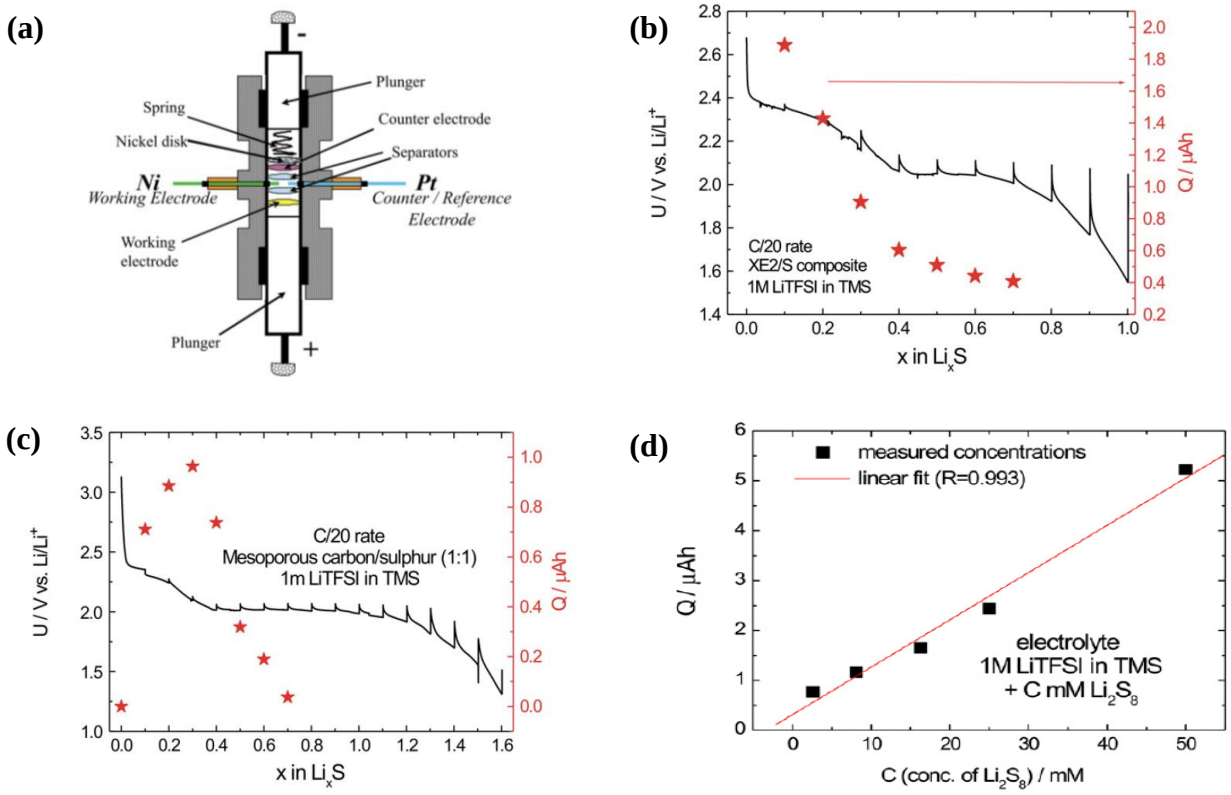

Figure 1.5: (a) Schematic view of the 4-electrode Swagelok cell. Electrochemical behavior during first reduction of (b) XE2/S composite and (c) mesoporous carbon/sulfur composite. Red stars represent partial cumulative charge obtained from integration of cyclic voltammetry peaks. (d) Calibration curve plotting cumulative charge versus known concentration of Li_2S_8 in glyme-based electrolyte. Figure adopted from Reference 20, © 2010 Elsevier B.V.

1.4 Approaches for Positive Electrode Sulfur Host Materials

Research into materials for positive electrode sulfur hosts is driven by a variety of caveats. In general, the cathode consists of sulfur, a conductive additive and polymeric binder. To be a good candidate for the sulfur cathode, the additive has to i) have a good electronic conductivity,

ii) be able to host enough sulfur and iii) reduce the dissolution of intermediate lithium polysulfides into the electrolyte.

1.4.1 Carbonaceous Materials

Seminal work published in 2009 showed that ordered mesoporous carbon materials (CMK-3) with 3-4 nm pores are able to confine sulfur species within the positive electrode and mitigate polysulfide dissolution.[12] With 70 wt% sulfur loaded into CMK-3, the composite material provides an outstanding initial capacity of 1,320 mAh g^{-1}, which is nearly 80% of the theoretical capacity of sulfur with good cycling stability. Since 2009, hundreds of journal articles have been published based on utilizing carbon as the sulfur host. A few highlights include hollow carbon spheres,[21,22] graphene-based composites,[23,24] and carbon nanotube-based[25,26] positive electrodes.

Hollow carbon spheres can be fabricated via a hard template with void space of 200-500 nm and a mesoporous shell of 30-50 nm in thickness (**Figure 1.6**). Jayaprakash *et al.* reported that hollow carbon-sulfur composites achieved high cycling capacity retention of 91% after 100 cycles.[21] The hollow carbon spheres allow for confinement of sulfur species throughout cycling, while the mesoporous shell facilities Li^+ transfer.

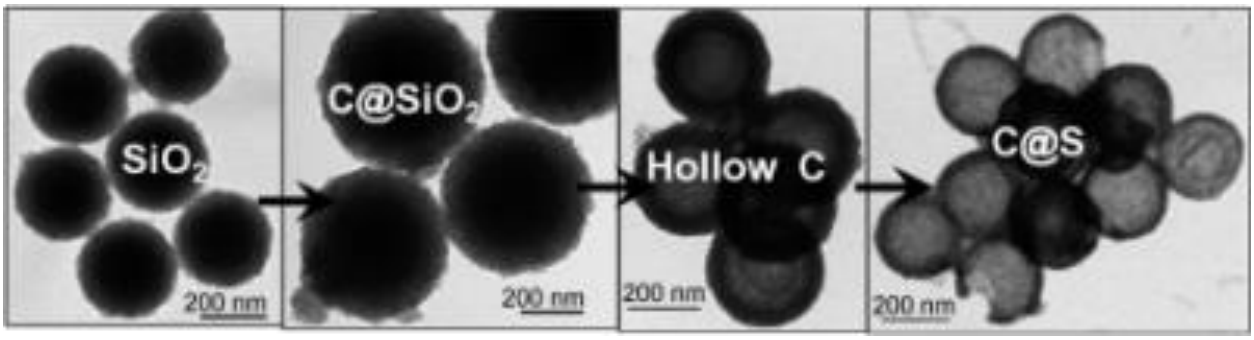

Figure 1.6: Synthesis of hollow carbon spheres impregnated with sulfur. Figure adopted from reference 21, © 2011 Wiley-VCH.

Graphene-wrapped carbon/sulfur particles reported by our lab (including myself) proved very successful at providing long-term cycling (**Figure 1.7**).[23] Sulfur was first melt-infused into Ketjenblack carbon at 155^{o}C at 70 wt%. Using a positively charged polymer, graphene oxide was then wrapped around the carbon/sulfur particles. After partial reduction of the graphene oxide, electrodes exhibited excellent cycling up to 200 cycles where the average stabilized capacity fade rate is only 0.026% per cycle. The large pore volume, small pore diameter, and uniform nanoparticle size of the mesoporous carbon/sulfur composites provides an ideal framework for the electrode architecture, while the graphene wrapping inhibits polysulfide dissolution into the electrolyte.

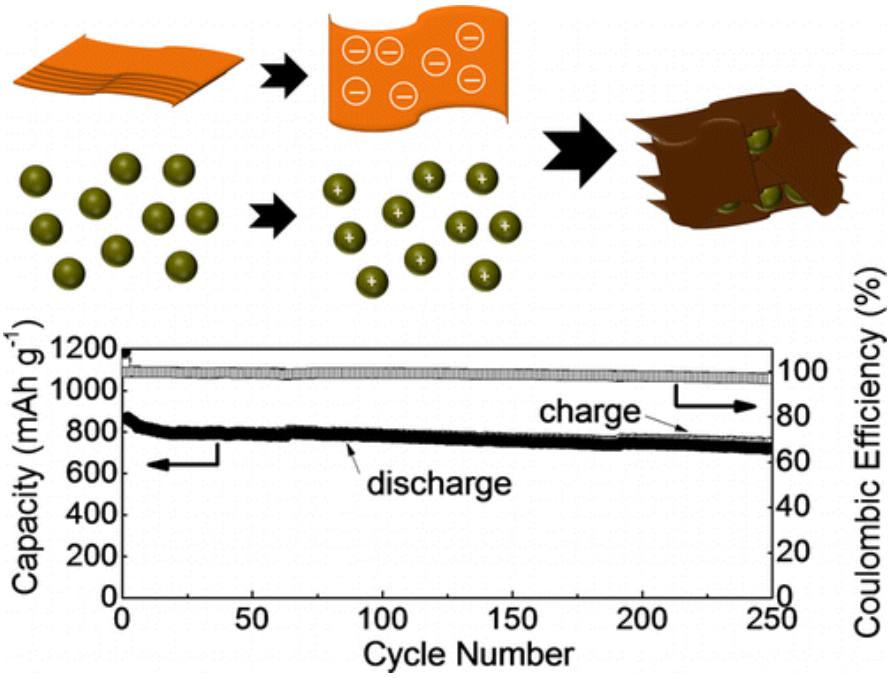

Figure 1.7: Synthesis of the graphene wrapped carbon-sulfur composite, and the respective cycling capability at a C/5 rate. Figure adopted from Reference 23, © 2014 American Chemical Society.

Sulfur can be melt-infused at around 60 wt% in multi-walled carbon nanotubes which manifests a high discharge capacity and long cycle life when compared to electrodes without carbon nanotubes (**Figure 1.8**). In fact, after 100 cycles, there is still 925 mAh g^{-1} discharge

capacity achieved despite the initial charge capacity of ~1,300 mAh g^{-1}. This reasonable cycling can be attributed to the high surface area of multi-walled carbon nanotubes which increase the electron transport capabilities and mitigate the diffusion of polysulfides into the electrolyte.

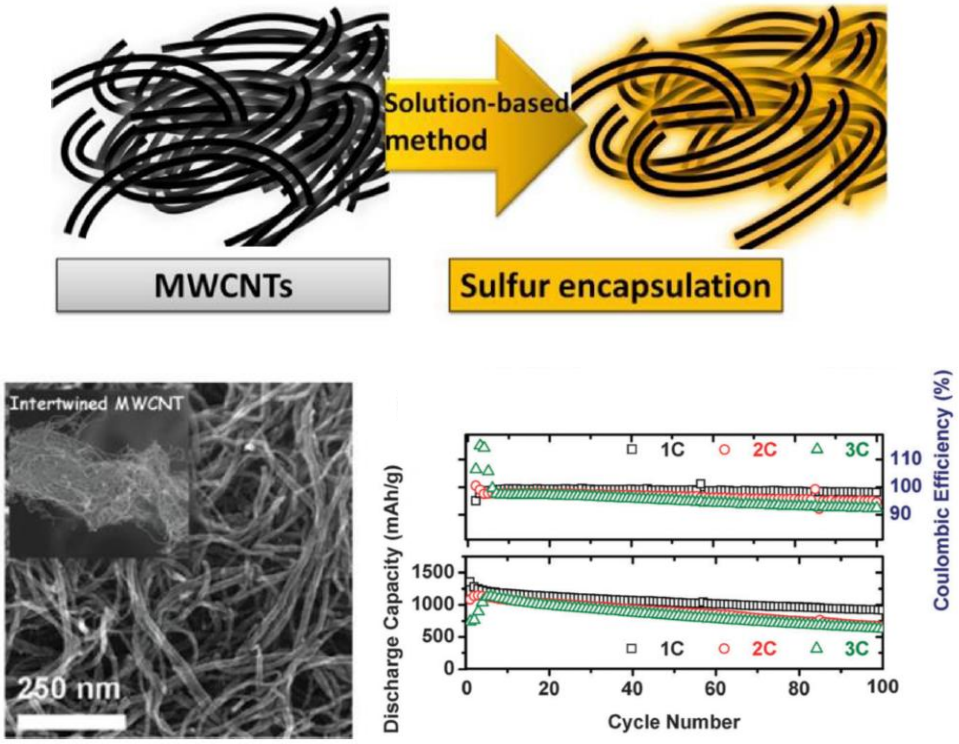

Figure 1.8: Schematic of the synthesis of multi-walled CNT/S composites and their cyclability. Figure adopted from Reference 14, © 2014 American Chemical Society.

The approach adopted for carbon hosts is to confine sulfur and sulfur species within the pores of the carbon matrix. This tactic for Li-S research has afforded reasonable cycling and increased volumetric energy density. Unfortunately, this approach typically only works for short term cycling (~100 cycles) as through ultra-long cycling, the hydrophilic polysulfides diffuse out of the hydrophobic positive electrode and enter the electrolyte which causes capacity decay. A more targeted approach is to exploit chemical interactions or favorable surface interactions

between the host material and polysulfides to realize ultra-long term cycling. This new approach began with research into functionalized carbons and metal oxide host materials.

1.4.2 Metal Oxides as Sulfur Hosts

1.4.2.1 Hydrophilic Physical Interactions

A TiO_2 yolk-shell architecture was developed as a sulfur host which showed stable cycling over 1,000 cycles.[27] Using the yolk-shell structure, an initial capacity of 1,030 mAh g^{-1} at 0.5C (where 1C equals 1,675 mAh g^{-1}) was achieved. The authors attributed the cycling performance to the increased interaction between the hydrophilic metal surface and the intermediate polysulfide species. The electrode integrity is maintained over cycling as the void volume within the yolk-shell allows the active material to expand without compromising the structure (**Figure 1.9a**). Most importantly, **Figure 1.9b** shows that after prolonged cycling over 1,000 cycles, the capacity retention was found to be 67%, which corresponds to a small capacity decay of 0.033% per cycle. The Ti-O and surface hydroxyl groups interact favorably with the dissolved polysulfides inhibiting their diffusion into the electrolyte realizing this exceptional capacity decay per cycle.

Although the TiO_2 yolk-shell concept seems promising, there are some problems. Firstly, the sulfur loading of this material was 0.43 mg/cm^2 which is extremely low as the current trend in Li-S research is a loading of 1.5 mg/cm^2 and only increasing as more research is conducted. As well, most metal oxides are typically non-conductive which can inhibit the rate capability of the electrochemical cell.

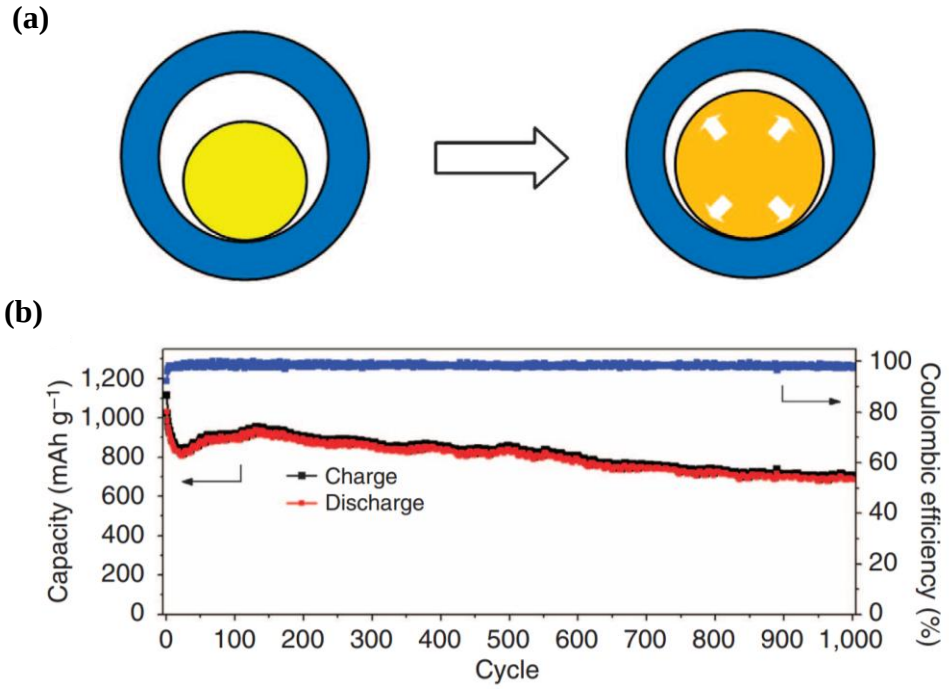

Figure 1.9: (a) Sulfur in the pores of a TiO_2 yolk-shell framework, (b) charge/discharge capacity and Coulombic efficiency over 1,000 cycles at 0.5C. Figure adopted from Reference 27, © Macmillan Publishers Limited.

1.4.2.2 Metallic Bifunctional Sulfur Host

Instead of relying solely on porosity to physically confine polysulfides, a two-in-one approach was taken by Pang et al. where a high surface area metallic Magneli phase Ti_4O_7 was shown to have the ability to chemically bind lithium polysulfides.[28] This metallic oxide triggers surface-mediated reduction of sulfur and oxidation of Li_2S very efficiently. The interaction of both the terminal and bridging sulfur in the polysulfides with the surface of Ti_4O_7 results in the polarization of electrons away from the sulfur atoms to the electropositive titanium (**Figure 1.10a**) causing enhanced interaction and limited polysulfide diffusion. The results of this enhanced interaction are obvious from the electrochemical data (**Figure 1.10b**) where at a 2C rate, an initial capacity of 850 mAh g^{-1} is achieved with a fade rate of only 0.06% over 500 cycles.

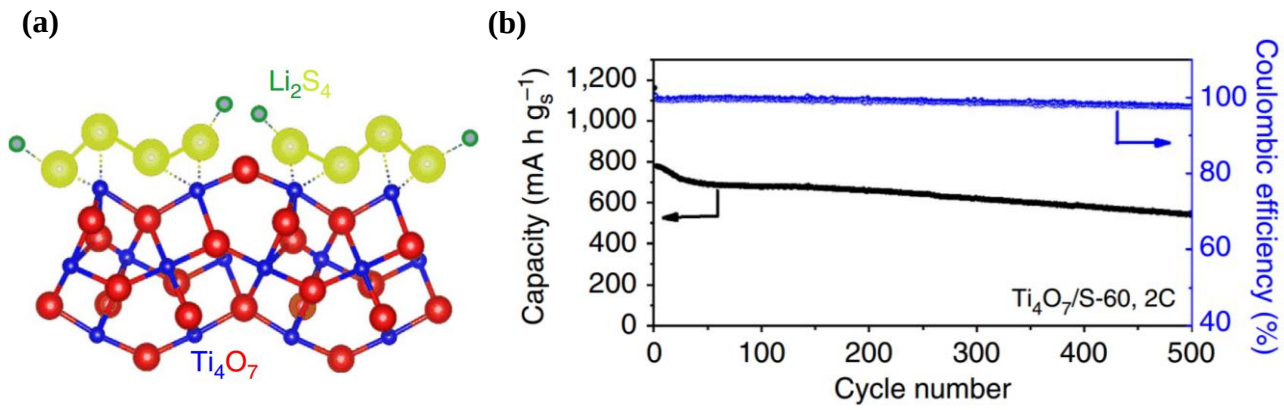

Figure 1.10: (a) Schematic showing the electron density transfer between Li_2S_4 and Ti_4O_7, (b) high rate performance of Ti_4O_7/S at 2C over 500 cycles. Figure adopted from reference 28, © 2014 Macmillan Publishers Limited.

1.4.2.2 Polysulfide Mediator Approach to Solving Polysulfide Dissolution

An approach taken by Liang *et al.* takes a different chemical route to polysulfide retention which relies on mediating polysulfide redox through insoluble thiosulfate species in a two-step process.[29] A pure metal oxide comprised of δ-MnO_2 nanosheets, was synthesized and employed as a sulfur host material. Although it is a poor semiconductor, the interaction with polysulfides is based on a very different principle to that of Ti_4O_7. To illustrate the excellent polysulfide retaining properties, the electrochemical behaviour of MnO_2 and a simple carbon both with 75 wt% sulfur was observed in an optically transparent Li-S cell (**Figure 1.11a**). At the end of discharge, the cell fabricated with MnO_2 had an electrolyte which is colourless suggesting that all polysulfides were retained within the positive electrode. When compared to a simple carbon/sulfur composite, the electrolyte became yellow after discharge suggesting that polysulfides diffused out of the positive electrode (hence, poor retention ability).

The mechanism behind this excellent polysulfide retention is based on the *in situ* generation of thiosulfate surface species which react to form an active complex on the surface of MnO_2 nanosheets. This active complex, called the polythionate complex, serves as an anchor and

transfer mediator to inhibit active mass loss (polysulfide dissolution) into the electrolyte and control the deposition of Li_2S. To evaluate the efficiency of the thiosulfate mediator, long-term cycling was performed at C/5, C/2 and 2C rates (**Figure 1.11b**). The rate was periodically changed to investigate the specific capacity that can be delivered at lower C-rates. After 2,000 cycles at 2C, 245 mA h g^{-1} useable capacity was still available with good Coulombic efficiency (>98.5%) and a very low decay rate of 0.036% per cycle.

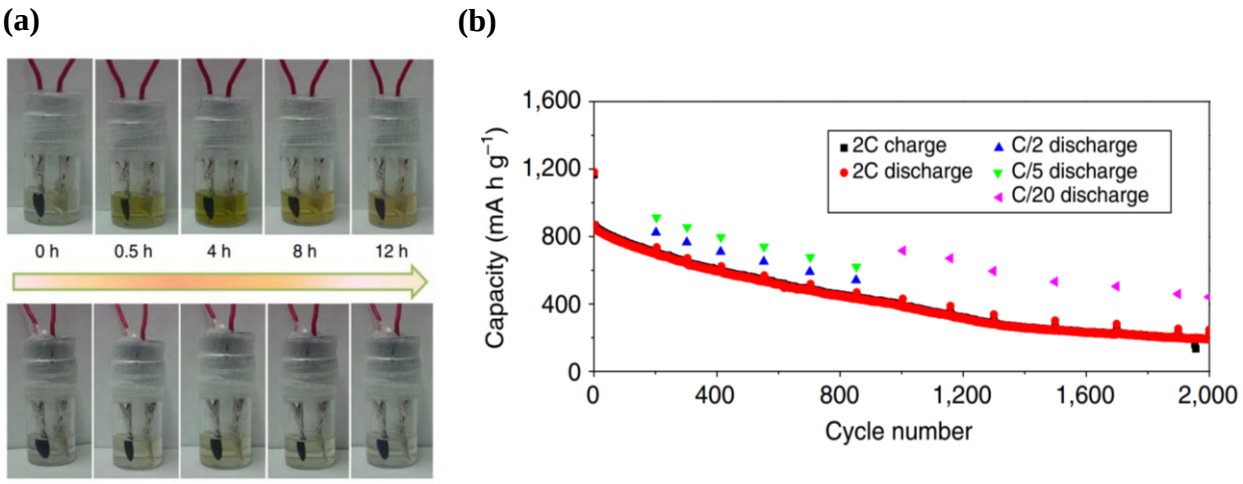

Figure 1.11: (a) Visual confirmation of polysulfide entrapment at specific discharge depths for carbon/sulfur (top) and MnO_2/sulfur (bottom) (b) long-term cycling of 75S/MnO_2 at a 2C rate with periodic slow rate changes over 2,000 cycles. Figure adopted from Reference 29, © 2015 Macmillan Publishers Limited.

The resultant cells deliver high rechargeable capacity at practical current densities and high sulfur loading. It should be further noted that the thiosulfate mediator is not restricted to support on MnO_2 nanosheets, but is broadly applicable to other support materials.[30] Unlike previous strategies to trap polysulfides by physical barriers or simple surface interactions, this chemistry is quite efficient. The discovery and understanding of a transfer mediator, which binds polysulfides and promotes stable redox activity, addresses one of the important challenges that face Li-S chemistry. Along with future anticipated improvements in electrolytes and the lithium negative electrode, this brings the Li–S battery a step closer to practical realization.

1.5 Previous Work to Mitigate Self-Discharge Capacity Loss

As said previously, self-discharge in the Li-S cell is one problem that limits commercial application. Previous work on mitigating the self-discharge capacity loss focused on changing the electrolyte system.[31] In fact, by using tetrafluoroethyl-2,2,3,3-tetrafluoropropyl ether (TTE) instead of dimethyl ether (DME) in the electrolyte, the extent of self-discharge reduced as shown in **Figure 1.12**. These results are achieved because of: 1) lower solubility of intermediate polysulfides in the fluorinated electrolyte and 2) formation of a solid electrolyte layer on the surface of the positive electrode. Although this electrolyte helps to mitigate self-discharge, it is not ideal for use in Li-S batteries as it can only be charged up to 2.6V before decomposing. Therefore, the full sulfur theoretical capacity may not be realized due to the limited potential window.

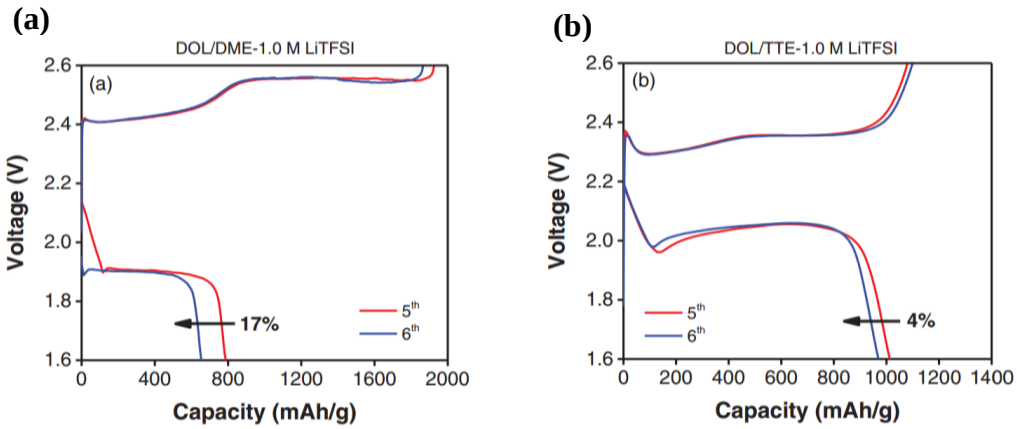

Figure 1.12: 5th and 6th cycle voltage profile for Li-S cells with high-loading sulfur cathodes rested at room temperature for 24 hours between the 5th and 6th discharge: (a) DOL:DME and (b) DOL:TTE electrolyte.

1.6 Summary

Li-S batteries have been studied as a positive electrode host since 1962 when first proposed by Ulam *et al.*[9] Sulfur as the active material affords a high specific capacity of 1,675 mAh g^{-1} and is plentiful in our earth's crust. However, there are many scientific issues with this

system that inhibit its commercial applicability. One main issue is that intermediate polysulfides are soluble in glyme-based electrolytes. When polysulfide solubility is coupled with the lack of affinity between the sulfur host and polysulfides, diffusion into the electrolyte, self-discharge and the parasitic 'shuttle' mechanism is realized. One such property that is required in order for this system to become commercially viable is the mitigation of the extent of self-discharge during rest.

Taking a survey of Li-S based papers published; the majority of research has been conducted on new materials for the positive electrode host. Initial research focused on carbon materials and their analogs to physically entrap sulfur species throughout cycling. However, over long-term cycling (>100 cycles) the physical entrapment fails so the hydrophilic polysulfides escape into the electrolyte due to the poor interaction. Recently, our lab has investigated metal oxides as sulfur host materials which can either provide a hydrophilic surface enhancing the interaction with polysulfides, or form a transfer mediator mitigating polysulfide dissolution. The redox mediator approach proved very beneficial showing cycling up to 2,000 cycles with an excellent decay rate of 0.036% per cycle; there was only one other paper published at that time which displayed this length of ultra-long cycling.[29,32]

Beyond the positive electrode, fundamental research of the Li-S systems needs to be conducted. Research into electrolytes and protection of the lithium anode is underway, but are out of the scope of this thesis. Ultimately a holistic approach needs to be taken to develop a high energy density ultra-long cycling lithium-sulfur cell. This is where the positive electrode contains sulfur species in electrical contact, the electrolyte prevents dissolution of polysulfides while being stable towards lithium and having high conductivity, and the lithium anode is protected to prevent safety issues and dendrite formation.

As one can observe, there is much more research needed to be done for Li-S batteries, and it is with hope that the research in this thesis brings this battery system one-step closer to commercialization.

1.7 Scope of this thesis

The work in this thesis focuses on developing a new diagnostic method which correlates properties of potential cathode materials, and then utilizing this method to search for a new sulfur host material. **Chapter 1** provided a background of the energy demand and the need for high energy density rechargeable batteries. This section explored multiple recent publications on current Li-S advances, two of which were published from our group where I was second author contributing highly to experimental, discussion and manuscript writing.[23,29] **Chapter 2** describes the characterization methods and techniques used in this thesis. **Chapter 3** proposes a new method for probing the polysulfide adsorptivity of materials and correlating this property to cyclability and extent of self-discharge (Connor Hart and Marine Cuisinier *et al. Chem. Commum.,* **2015**, 51, 2308, © 2015 The Royal Society of Chemistry).[33] **Chapter 4** focuses on utilizing the developed method to search for a sulfur host material by utilizing thiosulfate as an additive to inexpensive carbon hosts (Connor Hart and Xiao Liang *et al.,* **2015**, to be submitted pending BASF approval).

Chapter 2:
Characterization Methods and Techniques

2.1 X-ray Diffraction

The X-ray diffraction (XRD) technique relies on X-ray radiation striking a powder sample at a certain incident angle and crystals will diffract these X-rays for collection by the detector. The sample platform is rotated with respect to the incident X-ray radiation and a pattern containing the characteristic diffractions of the sample are obtained. The X-ray diffraction pattern is unique to each crystal structure and can be used for identification.

Bragg's Law (**Equation 2.1**) provides the angles for coherent and incoherent scattering from a crystal lattice.[34] It can explain the appearance of a diffraction pattern through interference of X-ray reflections from crystal planes in a sample.

$$n\lambda = 2d\ \sin\theta \qquad (\mathbf{2.1})$$

This law is schematically shown in **Figure 2.1** where θ represents the incident angle of the incoming X-ray radiation with respect to the crystallographic planes. Parallel X-ray beams can be diffracted by neighboring parallel atomic planes which maintain a distance of d with each other. Bragg's law is satisfied when $2d \cdot sin\theta$ is a multiple (n) of the wavelength (λ), and as a consequence, the two parallel beams will be in phase after being diffracted causing an observable diffraction peak.

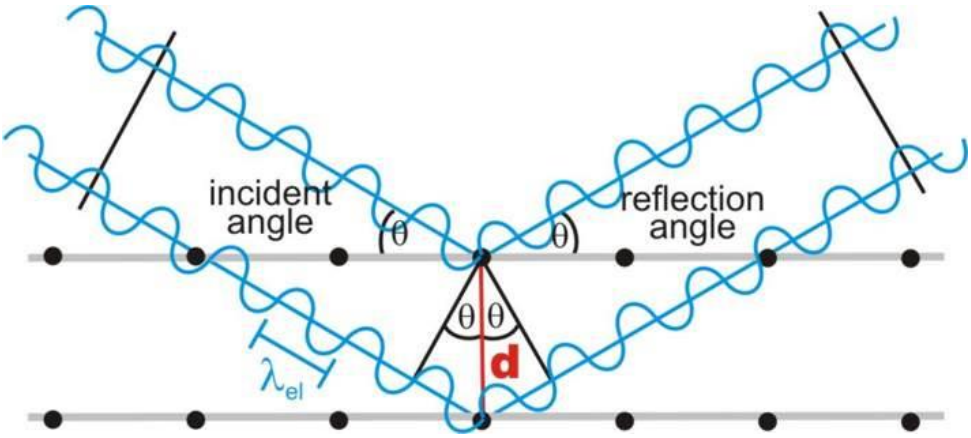

Figure 2.1: Schematic illustration of Bragg's Law

The X-ray diffractometer scans the sample over a range of θ (or 2 θ) and measures the intensity of diffracted X-rays as a function of the angle. Any plane that possibly diffracts X-rays will be detected. The overall area under all peaks belonging to one phase on the XRD pattern is proportional to the weight fraction of this phase in the sample powder. The pattern achieved is affected by a variety of properties; the more crystalline the sample, the more intense the peaks. As well, at the nanoscale, peaks in the diffraction pattern will begin to widen as the crystalline size diminishes. XRD patterns in this thesis were collected on a Bruker D8-Advance powder X-ray diffractometer operating at 40 kV and 30 mA and using Cu-Kα radiation (λ=0.15405 nm).

2.2 Scanning Electron Microscopy and Energy Dispersive X-ray Spectroscopy

Being able to see on the nanometer scale has been a great achievement in science and engineering. Scanning electron microscopy (SEM) is an important tool which allows researchers to probe the morphology of solid samples. SEM fundamentally operates when electrons of high energy hit the surface of the solid which generates a variety of byproducts: secondary electrons, back-scattered electrons, transmitted elections, and X-rays characteristic to the specific elements in the sample. The collection of electrons can be transformed into a high-resolution image and

this image is dependent on the types of electrons collected. Secondary electrons provides more information on the surface topography, while back-scattered electrons are more informative on the molecular mass.

Elemental distribution occurs via Energy Dispersive X-ray Spectroscopy (EDX) and operates via formation of an X-ray from the lowering in energy of an electron filling a hole from a previously ejected electron. As X-rays are characteristic of the host element, a database informs the researcher of the elements in the bulk when using EDX technique.

SEM imaging and EDX measurements in this thesis were carried out on a LEO 1530 field emission SEM equipped with an EDX attachment (Zeiss). Secondary electron mode was used when taking images.

2.3 Surface area/pore size characterization

Surface area and pore size characterizations rely on measuring N_2 adsorption/desorption which is collected at 77K in a liquid nitrogen bath. A N_2 adsorption isotherm is a plot of volume of nitrogen adsorbed on the surface of a sample as a function of the relative pressure in the sample chamber. Previous to the measurement, the sample is outgassed at a defined temperature to ensure the surface is free of gas molecules. During the measurement, nitrogen gas is periodically introduced into the sample tube and measurement of the amount of gas that physisorbs onto the material is collected. In this thesis, surface area and pore volume are respectively determined from Brunauer-Emmett-Teller (BET) theory and from the amount of N_2 adsorbed at a relative pressure P/P_0 of 0.99.

2.4 Thermogravimetric Analysis

Thermogravimetric analysis (TGA) is a thermal analysis which can measure chemical and physical properties while under a constant heating ramp rate. Thermal decomposition

temperatures and phase transformation can be obtained from TGA measurements. For the research presented in this thesis, TGA was performed under air or N_2 with a standard temperature program of 10 ^{o}C/min. The weight percent of sulfur and sodium thiosulfate is of interest and is determined by the weight loss between 200-400 ^{o}C, and by the mass remaining after carbon oxidizes at 600-700 ^{o}C respectively.

2.5 X-ray Photoelectron Spectroscopy

X-ray photoelectron spectroscopy (XPS) is a surface sensitive technique that is able to determine elemental composition and oxidation state. This technique is very powerful as it can be used to elucidate many surface reactions. XPS relies on the detection of emitted electrons from the ground state upon photoradiation from X-rays. When an atom receives energy from X-ray radiation, it gets excited from the ground state, during which core electrons are emitted into vacuum. The energy transfer during this process can be described in **Equation 2.2**.

$$E_{binding} = \mathrm{hv} - E_{kinetic} - \phi \qquad (\mathbf{2.2})$$

The spectrometer probes the kinetic energy and the intensity of the photoelectrons ejected by X-ray radiation. By knowing the work function(ϕ) of the instrument (irrelative of the sample), and the kinetic energy of the ejected electrons, the binding energy of the electrons ejected from the surface can be calculated. XPS was performed on a Thermo ESCALAB 250 instrument configured with a non-monochromatic Al Kα (from twin anode) for non-conductive materials (Li_2S_4, $Na_2S_2O_3$) and a monochromatic Al Kα (1486.6 eV) for conductive composite materials. All spectra were fit with Gaussian-Lorentzian functions and a Shirley-type background using CasaXPS software. The binding energy values were all calibrated using the C 1s peak at 285.0 eV. For S 2p spectra, three constraints were used on the fitting: position difference of 1.2 eV

between S $2p_{1/2}$ and $2p_{3/2}$, peak area ratio of 2:1 for $2p_{3/2}$:$2p_{1/2}$ and equal full width half maximum.

2.6 Electrochemical Measurements

In this thesis, a variety of electrochemical measurements were made. The experimental protocol listed below is of general use, and if deviations from these descriptions are made, it will be noted.

2.6.1 Fabrication of Coin Cells

In this thesis, 2325 type coin cells were used to investigate the electrochemical performance of electrode materials. A coin cell configuration is shown in **Figure 2.2**. The positive electrode was fabricated by mixing the active material composite, conductive carbon additive and polymeric binder in a solvent to form a slurry and then drop-casting onto a carbon paper current collector (P50, AvCarb). The electrode was then dried at 60 ^{o}C overnight to vaporize the solvent. The cell was assembled inside an Ar-filled glovebox. The electrolyte consists of a lithium salt dissolved in a mixture of ether-based solvents, with the presence of lithium nitrate for protection of the lithium metal anode. The use of separators is to electronically isolate the positive electrode from the negative electrode.

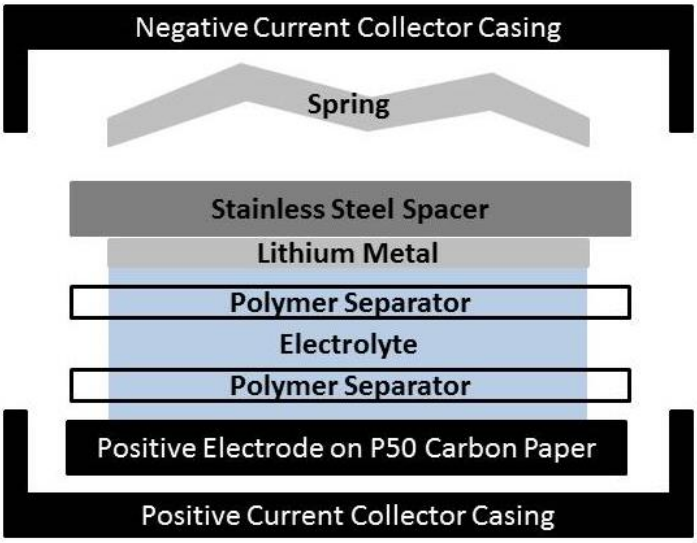

Figure 2.2: Schematic diagram of a 2325 type coin cell.

2.6.2 Galvanostatic Cycling

Generally, electrochemical measurements in this thesis occur by using a galvanostatic technique where a constant current is applied to the cell until predetermined cut-off voltages are reached. Long-term cycling is probed by plotting the specific capacity (y-axis) versus the cycle number (x-axis). The analytical method developed in Chapter 3 utilizes a potentiostatic technique where a potential is applied, and the current is measured. Galvanostatic cycling was carried out using a BT2000 battery cycler (Arbin Instruments).

2.6.3 Self-Discharge

Self-discharge is the intrinsic ability for the active material in a battery to dissolve into the electrolyte and diffuse out of the positive electrode causing active mass loss and poor cyclability. Self-discharge experiments were conducted using 2325 type coin cells which were fabricated as mentioned above. Galvanostatic cycling at a C/2 rate for 9 cycles allowed for stabilization and on the 10^{th} discharge cycle, cells were stopped at 2.1V (before supersaturation) to rest for three days. After resting, cells were resumed to discharge to 1.8V, where normal

galvanostatic cycling continued. As elemental sulfur does not dissolve in electrolyte, the most effective way to measure self-discharge in a Li-S battery is by discharging to form soluble polysulfides and measure the amount of polysulfides that diffuse out of the positive electrode into the electrolyte. In a typical Li-S cell, the onset of the second discharge plateau typically begins at 2.0V. Stopping the cell at 2.1V allowed for maximal polysulfide concentration to exist in the cell and thus measurement of self-discharge capabilities occurred under harsh conditions.

2.7 ^{1}H Nuclear Magnetic Resonance Experiments

Nuclear Magnetic Resonance (NMR) is a powerful scientific research tool which has been used since the second half of the previous century. NMR is a non-invasive, non-destructive atom/isotope selective method which provides information on a microscopic scale. Proton NMR (^{1}H NMR) is an application of NMR which focuses on the hydrogen-1 nuclei within molecules. Typically, NMR spectra are recorded using deuterated (^{2}H) solvents so as to not have signal from the solvents and allow the molecular structure of the material of interest to be elucidated.

A solution of the sample in a uniform 5 mm glass tube is oriented between the poles of a powerful magnet, and is spun to average any magnetic field variations. Radio frequency radiation of appropriate energy is broadcast into the sample from an antenna coil. A receiver coil surrounds the sample tube, and emission of absorbed rf energy is monitored by dedicated electronic devices and a computer.

^{1}H NMR provides spectra that are unique for all molecules as the peak position indicates a lot of information about the local environment of the hydrogen atoms. This thesis will not delve into all the theory of proton NMR, but this instrument will be utilized to monitor electrolyte decomposition.

2.8 Statistical Analysis

In Chapter 3, an analytical method for determining the polysulfide adsorptivity of a material will be proposed. As this is a novel method, a variety of statistical and analytical analysis occurred in order to validate the method. In order to facilitate better understanding, definitions are explained below:[35]

- **Calibration Curve:** A calibration curve is a general method for determining the concentration of a substance in an unknown sample by comparing the unknown to a set of standard solutions of known concentrations. Generally a graph is plotted where the y-axis is the response (i.e. peak area, capacity) and the x-axis is concentration. By creating a graph of standard solutions, a linear fit linear regression can be drawn and any unknown concentration can be determined through interpolation of the Line of Best Fit. Generally a calibration curve is deemed valid if the correlation coefficient (R^2) of the calibration line generated is greater than 0.99. The correlation coefficient is a measure of how well the data fits into a statistical model. In the case for the calibration curves shown in this thesis, the statistical model used is a linear fit.
- **Standard Deviation:** Measures the amount of variation or dispersion in a set of values. A standard deviation close to 0 indicates the data points are close to the mean (or expected value). The standard deviation (s) can be calculated by **Equation 2.3**:

For a set of "n" data points having values "x_i"

$$s = \sqrt{\frac{\sum_{i=1}^{n}(x_i - \bar{x})^2}{n-1}} \qquad \textbf{(2.3)}$$

where $\sum$ = "the sum of"

and $\bar{x} = \frac{\sum_{i=1}^{n} x_i}{n}$, the mean of the sample set

- **Percent Relative Standard Deviation (%RSD):** The %RSD is widely used in analytical chemistry to express the precision and accuracy of a specific assay. The %RSD can be calculated via **Equation 2.4**:

$$\% \, RSD = \frac{s}{\bar{x}} \times 100 \qquad (\mathbf{2.4})$$

- **Precision:** Precision (repeatability) is generally calculated by repeated measurements of a standard solution to determine how well the same value can be achieved. From the results of this analysis, the %RSD is calculated. To determine whether the results are acceptable, the %RSD is compared to the modified Horwitz equation (**Equation 2.5**):

$$\% \, RSD < 2^{(1-0.5 \log C)} \times 0.67 \qquad (\mathbf{2.5})$$

$$C = \frac{Average Concentration \, of \, the \, analyte}{D}$$

Where, for example: $D = 10^6$ if concentration is in mg/L

- **Accuracy**: Accuracy is the nearness of a measured value to the real value. In this thesis, the real value is based off a theoretical calculation of achieved capacity. Accuracy is generally determined by calculating the percent recovery (actual/theoretical*100). Based off the low concentration levels analyzed for the standard solutions, the percent recovery must be from 80-120% to be deemed valid.

Chapter 3
Rational Design of Sulfur Host Materials for Li-S Batteries: Correlating Lithium Polysulfide Adsorptivity and Self-Discharge Capacity Loss

3.1 Introduction

There are several challenges with sulfur electrochemistry that hinder the commercialization of this energy storage system. Unquestionably, a main problem is the soluble nature of the S_n^{2-} intermediates, allowing their diffusion through the electrolyte. Such undesired mass transport of electroactive species is at the origin of three major performance barriers. At open-circuit, the spontaneous reduction of S_n^{2-} on the surface of the negative electrode (known as self-discharge) can eventually result in Li_2S poisoning of the lithium electrode.[36] During charge, the oxidation of S_n^{2-} at the positive electrode is accompanied by their diffusion and reduction at the negative electrode in a similar fashion. This redox shuttle can proceed endlessly and therefore causes poor coulombic efficiency and capacity decay due to the loss of active material in the electrolyte or on the negative electrode.[36]

Previous work on mitigating the detrimental effects of S_n^{2-} solubility focused on two different aspects of the cell. Regarding the electrolyte, additives such as $LiNO_3$ that passivate the negative electrode prove effective to alleviate self-discharge over short rest times and improve coulombic efficiency, while S_n^{2-} dissolution can be decreased by using low polarity fluorinated ethers as co-solvents.[37,38,39] On the other hand, considerably more effort has been placed on the material used as the sulfur host, i.e. the positive electrode matrix. Materials such as mesoporous carbons[12] and semiconducting or metallic oxides[28,29] to name a few, with varying surface area

and polarity, have all been designed in an attempt to limit S_n^{2-} diffusion out of the positive electrode.

The exhaustive search for a material that has a high electronic conductivity to facilitate charge transfer, substantial surface area and pore volume to allow high sulfur loading, and well-suited physical/chemical surface properties to inhibit S_n^{2-} diffusion into the electrolyte is still ongoing. It is vital to find a material with these characteristics so as to bring the Li-S battery one step closer to commercialization. Before spending valuable resources (money and time) on fabricating electrochemical cells to assess the long-term cyclability of a sulfur-based electrode composite, it is critical to ensure that the material envisaged as sulfur host meets all the criteria listed above. Herein, we report a facile yet rational method for screening sulfur host candidates, based on metrics: A quantitative electro-oxidation reaction provides the value for S_n^{2-} adsorptivity - which coupled with the surface area - is correlated to the extent of self-discharge at an intermediate state of discharge during a 5-day cycling protocol. The results prove more pertinent than 100 galvanostatic cycles to predict long-term cyclability.

3.2 Novel Developed Method

3.2.1 Synthesis of Polysulfide Standard (Li_2S_4)

In an argon filled glove box, sulfur (99.5%, Sigma-Aldrich) was dissolved in Super-Hydride® solution (1.0 M lithium triethylborohydride in tetrahydrofuran, Sigma-Aldrich) in a mole ratio of 2.75:1 respectively. The resulting solution was dried under vacuum, followed by a final wash with toluene and centrifugation to isolate the yellow precipitate, Li_2S_4.

3.2.2 Experimental Protocol

In an argon filled glovebox, standard solutions are prepared by accurately weighing a known mass of Li_2S_4 into 16 mL of 1.0M lithium perchlorate ($LiClO_4$, battery grade, Sigma-

Aldrich) in tetraethylene glycol dimethyl ether (TEGDME) solvent. Typically, in an argon filled glovebox, the sample is prepared by dispersing a specific host material accurately weighed into a stock solution of Li_2S_4 in tetraethylene glycol dimethyl ether (TEGDME) (**Figure 3.1(i)**). The suspension is allowed to stir and saturation of the material surface with S_n^{2-} is ensured by adding more of the Li_2S_4 stock solution until coloration persists after 18 hours. The suspension is then centrifuged and the supernatant collected for titration of the excess S_n^{2-} (**Figure 3.1(ii)**). As displayed in **Figure 3.1(iii)**, titration consists of the electrochemical oxidation of a 16 mL solution of S_n^{2-} in 1.0 M $LiClO_4$ in TEGDME, placed in the left hand compartment of an H-cell, with a nickel foam current collector. The right hand compartment is filled with an electrolyte solution of 1.0 M $LiClO_4$ in TEGDME with 2 wt% $LiNO_3$, wetting a Li foil counter electrode. A constant voltage of 3.0 V under potentiostatic technique is applied until the measured current reaches 0 mA (**Figure 3.1(iv)**). At this point, the total capacity resulting from oxidation of the excess Li_2S_4 to elemental sulfur is integrated over time. A straightforward subtraction of the amount of S_n^{2-} titrated from the total amount initially added, allows one to determine the amount of S_n^{2-} removed from solution via adsorption onto the matrix of interest.

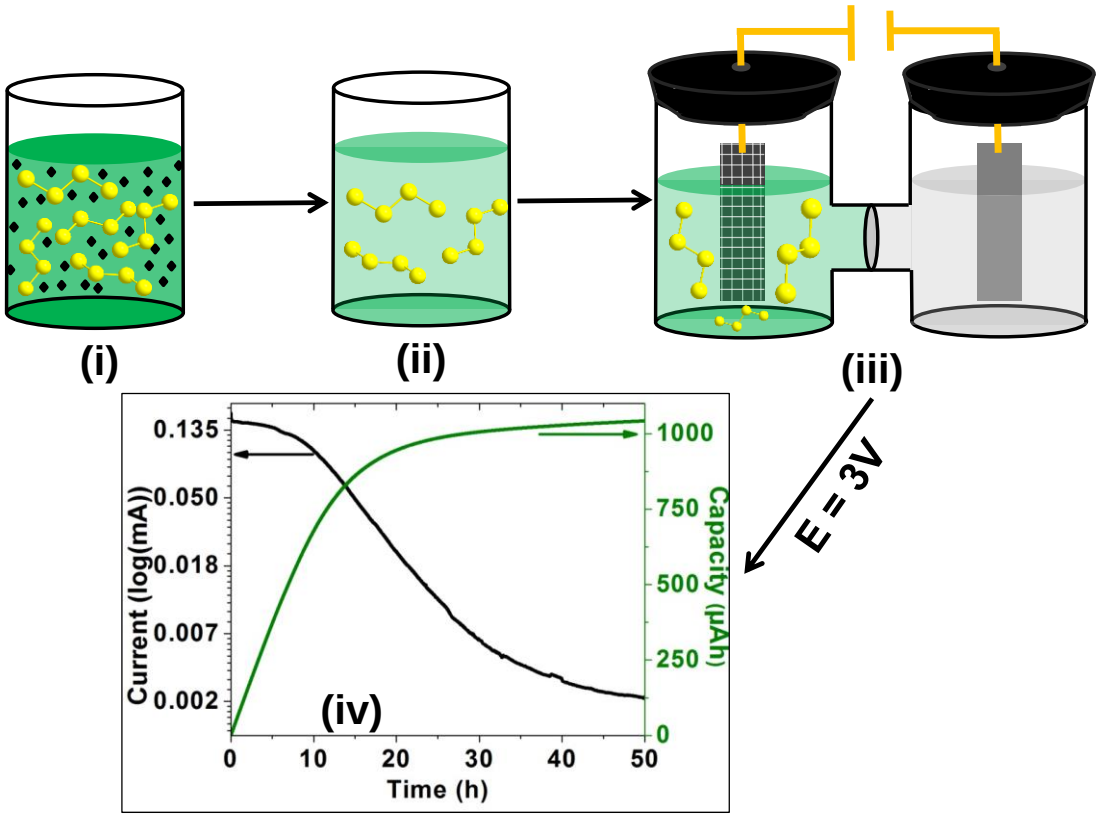

Figure 3.1: Method developed to determine the polysulfide adsorptivity via electrochemical oxidation.

3.2.3 Linearity Validation

A total of 4 standard solutions were prepared and analyzed according to the developed method to generate a calibration curve. The 4 calibration standards which span a wide concentration range (0.15 mM to 2.96 mM) remain linear. In fact, an excellent R^2 value of 0.9986 was achieved thus proving this method to be valid in terms of first order linearity of the standard solutions.

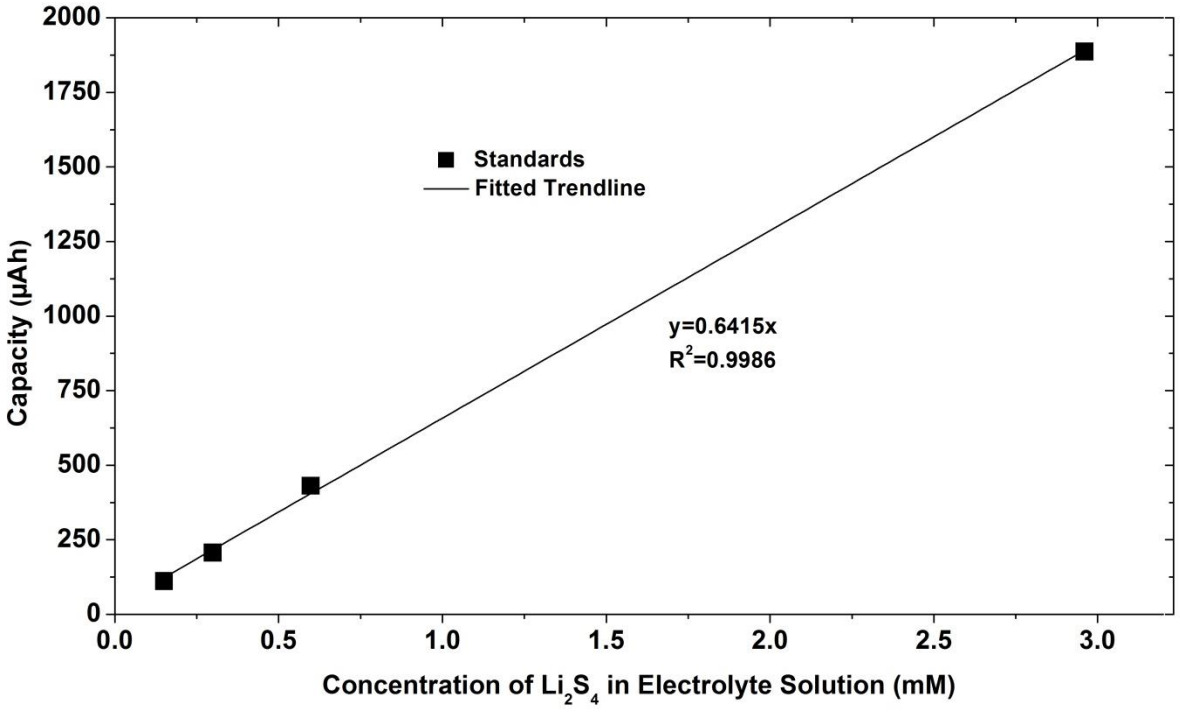

Figure 3.2: Calibration plot for achieved capacity of known concentration of Li_2S_4 in 1M $LiClO_4$ in TEGDME.

3.2.4 Precision and Accuracy Validation of the Developed Method

Accuracy is the closeness of the experimental results to the theoretical results. In the developed method, capacity was used as the dependent variable of the defined concentration of the Li_2S_4 solution. The theoretical capacity of Li_2S_4 in the electrolyte can be calculated using Faraday's Law of Electrolysis via **Equation 3.1** which states that the mass of a substance altered at an electrode during electrolysis is directly proportional to the quantity of electrical charge.[40]

$$\boldsymbol{Q = \frac{m_{Li_2S_4} * F * n_e^-}{MM_{Li_2S_4} * t_h}} \qquad \textbf{(3.1)}$$

Where: m_{Li2S4} = mass of Li_2S_4 in grams from each 16 mL standard solution

F = Faradays constant (965,000 A s mol^{-1})

MM_{Li2S4} = molar mass of Li_2S_4 (142.15 g mol^{-1})

t_h = time in hours (3600s/h)

Plotting the experimental and theoretical capacities with respect to the concentrations of the standard solutions resulted in **Figure 3.3a**. According to the values present in **Table 3.1** and shown in **Figure 3.3a**, this developed method achieved 81% recovery of the theoretical capacity. Based on the validation limits, this percent recovery falls within the range of 80-120% and thus this method is deemed accurate within the calibration range of 0.15 mM to 2.96 mM.

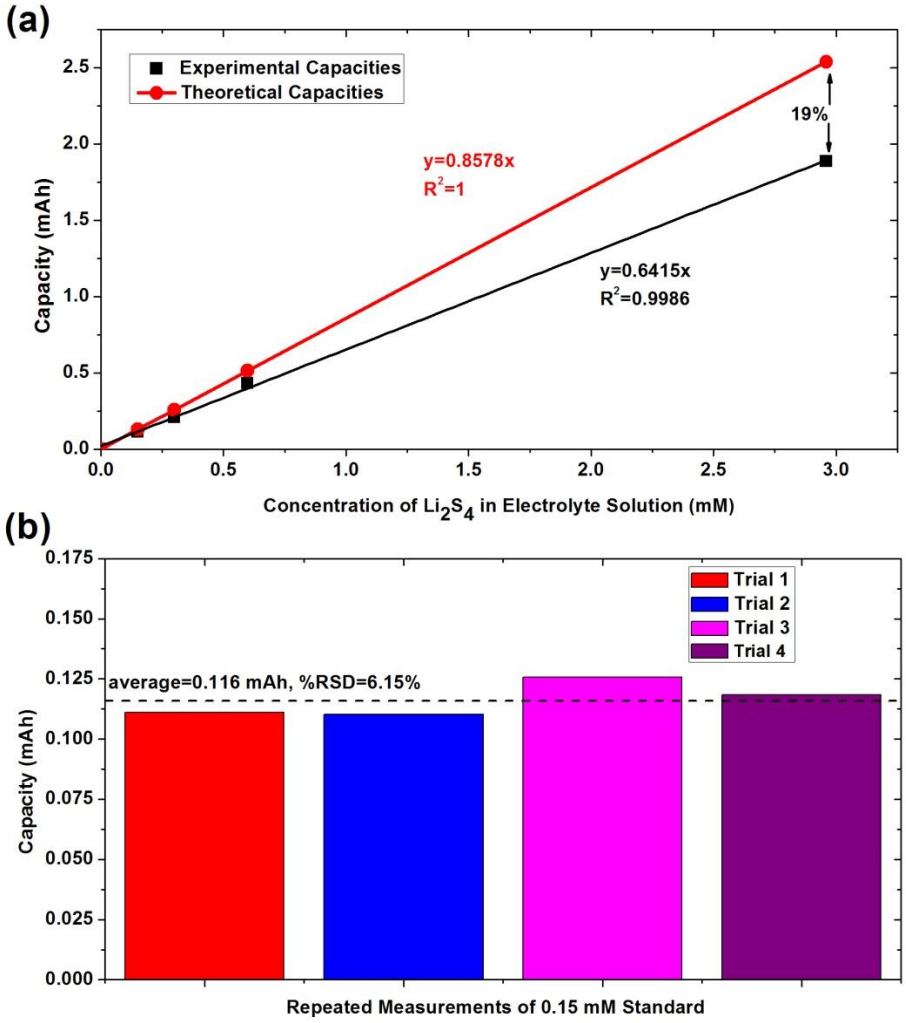

Figure 3.3: (a) Experimental and theoretical capacities versus concentration of standard solutions for accuracy determination. (b) Repeated measurements of the 0.15 mM standard solution probing precision abilities of the developed method.

Table 3.1: Comparison of experimental and theoretical capacity values and average percent recovery calculation.

Standard Conc. (mM)	Q (mAh) Experimental	Q (mAh) Theoretical	Percent Recovery (%)	Average Percent Recovery (%)
0.150	0.11	0.13	86.4	81.3
0.299	0.21	0.26	80.5	
0.598	0.43	0.51	84.0	
2.96	1.89	2.54	74.3	

Parameters that could affect the percent recovery are experimental errors (such as the H-cell set up is not optimal) and the Li_2S_4 is not 100% pure. In fact, the synthesis route for Li_2S_4 creates amorphous Li_2S_4 that is surrounded by THF molecules. It is believed that there are several THF molecules per Li_2S_4 and therefore when weighing the Li_2S_4 to make standard solutions, the mass also includes that of THF (believed to be less than %5 by mass). It is difficult to know the exact purity as it requires heating up to 250^{o}C for several hours to remove all the THF molecules, but at this temperature the Li_2S_4 will melt.

Precision calculations were conducted in accordance to **Section 2.8** where repeated measurements of the 0.15 mM standard solution were conducted and the capacity was calculated for each trial. Data for the repeated measurements are displayed in **Figure 3.3b** which shows that after conducting statistical treatment, the %RSD is 6.15%. As the experimental %RSD is less than the calculated %RSD based off the modified Horwitz equation (**Equation 2.5,** 19.5%), this method is deemed precise.

3.3 Additional Experimental

3.3.1 Preparation of sulfur composites

Sulfur was infiltrated into all studied materials with the exception of graphene oxide using a melt infusion method at 155°C. Infiltration of sulfur into graphene oxide required an aqueous solution of 255 mg $Na_2S_2O_3$ and 278 µL concentrated HCl to be added to an aqueous dispersion of graphene oxide followed by filtration and drying at 60°C. **Figure 3.4** shows the thermogravimetric analysis of all sulfur composites under a nitrogen atmosphere. All composites had similar sulfur loadings with a final content of 70 wt% which was determined by the weight loss at ~300^{o}C when sulfur evaporates.

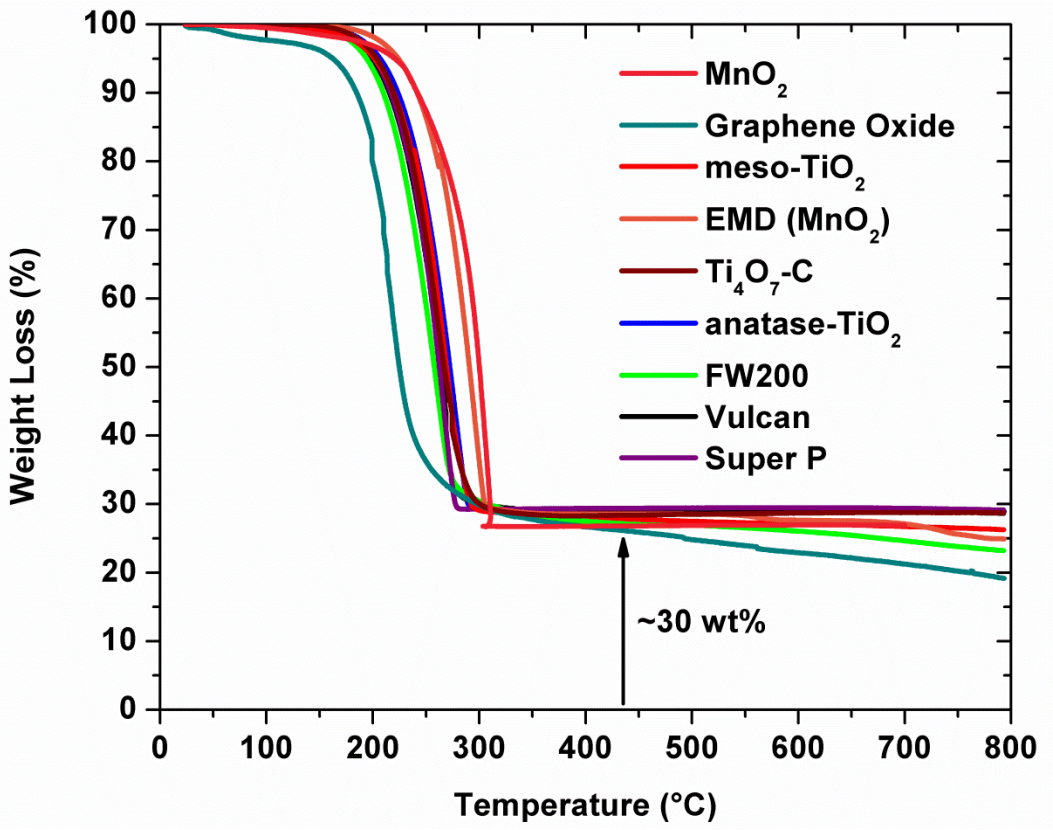

Figure 3.4: Thermogravimetric analysis of all sulfur composites under nitrogen atmosphere.

3.3.2 Electrochemical Analysis

Positive electrodes were prepared from a uniform distribution of material/sulfur, Super P carbon, and poly(vinylidene fluoride-co-hexafluoropropylene) (PVdF) in a 80:10:10 mass ratio in dimethylformamide (DMF) solvent followed by sonication and drop-casting onto P50 carbon paper (AvCarb, Fuel Cell Earth) current collector before being dried at 60ºC overnight. The only exception was when preparing the slurry for the graphene oxide/sulfur material, ball milling of the components occurred to ensure no agglomeration of graphene oxide. This ball milled material was stirred (not sonicated) in DMF prior to being drop-cast onto P50 carbon paper.

To alleviate any electrochemical differences from cathode composition, sulfur loading for all electrodes of all materials was kept constant at 0.9 mg±1%/cm^2. Each positive electrode was tested in a 2325 type coin cells using 50 µL of 1M lithium bis(trifluoromethanesulfonyl)imide in a 1:1 v/v ratio of 1,3-dioxolane (DOL) and 1,2-dimethoxyethane (DME) with 2 wt% $LiNO_3$ electrolyte. Lithium metal foil was used as the negative electrode, and physically isolated using 2 sheets of Celgard 3501 separators. For long-term cycling, cells were cycled between 1.8 and 3.0V using a BT2000 Arbin battery cycler at room temperature at a discharge/charge rate of C/2 (1C = 1,675 mA/g) which corresponds to a current density of 0.625 mA/cm^2.

Self-discharge experiments were conducted for each material and 2325 type coing cells were fabricated as mention above. Galvanostatic cycling at a C/2 rate for 9 cycles allowed for stabilization and on the 10^{th} discharge cycle, cells were stopped at 2.1V (before supersaturation) to rest for three days. After resting, cells were resumed to discharge to 1.8V, where normal galvanostatic cycling continued.

3.3.3 ^{1}H NMR Study

Proton-NMR experiments were conducted in DMSO-d_6 solution (Sigma Aldrich, dried on 4 Å molecular sieves) on a Bruker Advance 300 MHz instrument at room temperature. ^{1}H spectra were referenced to the residual DMSO peak at 2.49 ppm (TMS at 0 ppm).

3.4 Results and Discussions

3.4.1 Polysulfide Adsorptivity of Materials

A total of 9 different materials with varying surface areas and hydrophobicity's were analyzed to specifically probe the role of these properties. Materials included carbon based materials such as Super P, Vulcan and FW200. Oxide materials include, anatase-TiO_2 (anatase, Alfa Aesar, 99%), mesoporous-TiO_2 (meso-TiO_2, mesotech), Ti_4O_7-C[28] (contains ~15 wt% carbon), Electrolytic Manganese Dioxide (EMD, Kerr-McGee Chemical Corporation), MnO_2 nanosheets[29] and graphene oxide (GO, ACS Materials). All samples analyzed had a concentration of supernatant falling within the calibration curve (**Figure 3.5**), thus these measurements were considered valid. Utilizing the achieved capacity and the calibration curve, the concentration of polysulfides in the H-cell can be determined. From this, a mass of polysulfides that were adsorbed can be calculated and compared to other materials.

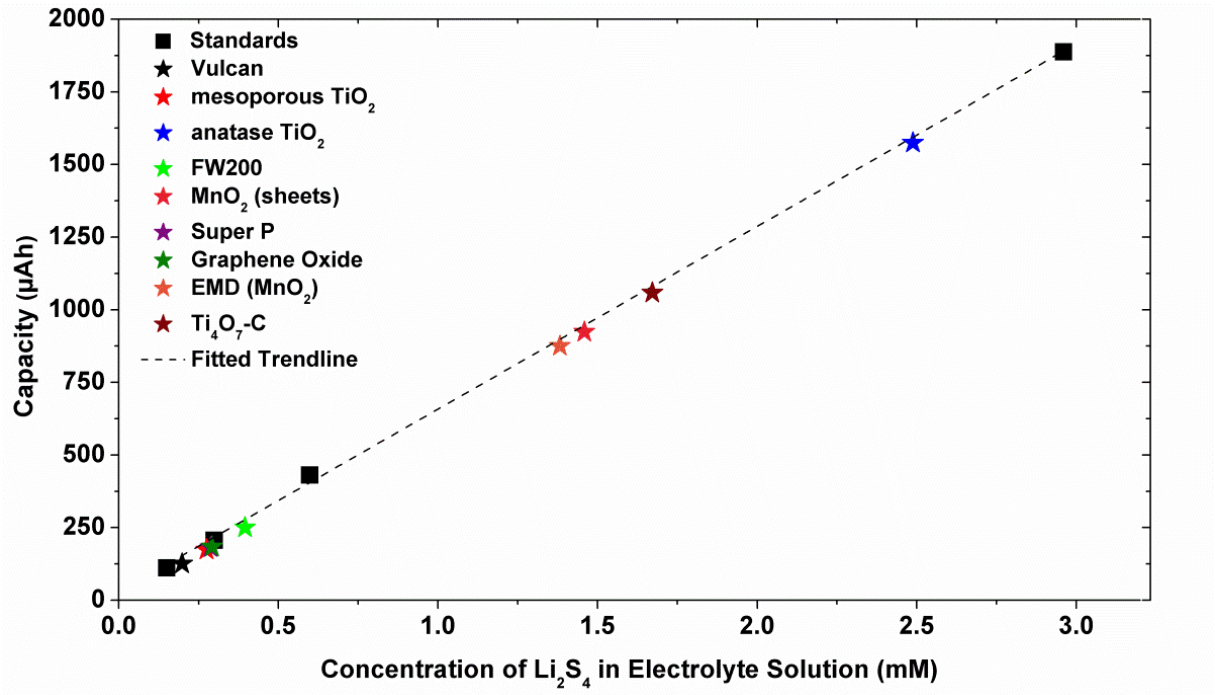

Figure 3.5: Calibration plot (squares) for achieved capacity of known concentration of Li_2S_4 in TEGDME. Experimental points (stars) for polysulfide adsorptivity onto a variety of different samples.

A summary of the experimentally determined S_n^{2-} adsorptivity of materials are displayed in **Figure 3.6** where the effects of the physical and chemical properties can be assessed. As a general trend, non-polar materials (i.e. carbons such as Super P and Vulcan) adsorbed much less S_n^{2-} compared to polar materials (i.e. metallic oxides such as TiO_2 and MnO_2). These results are in agreement with recent publications, in which polar materials demonstrated the ability to readily bind polysulfides, especially in comparison with still prevailing non-polar carbons.[27,28,29]

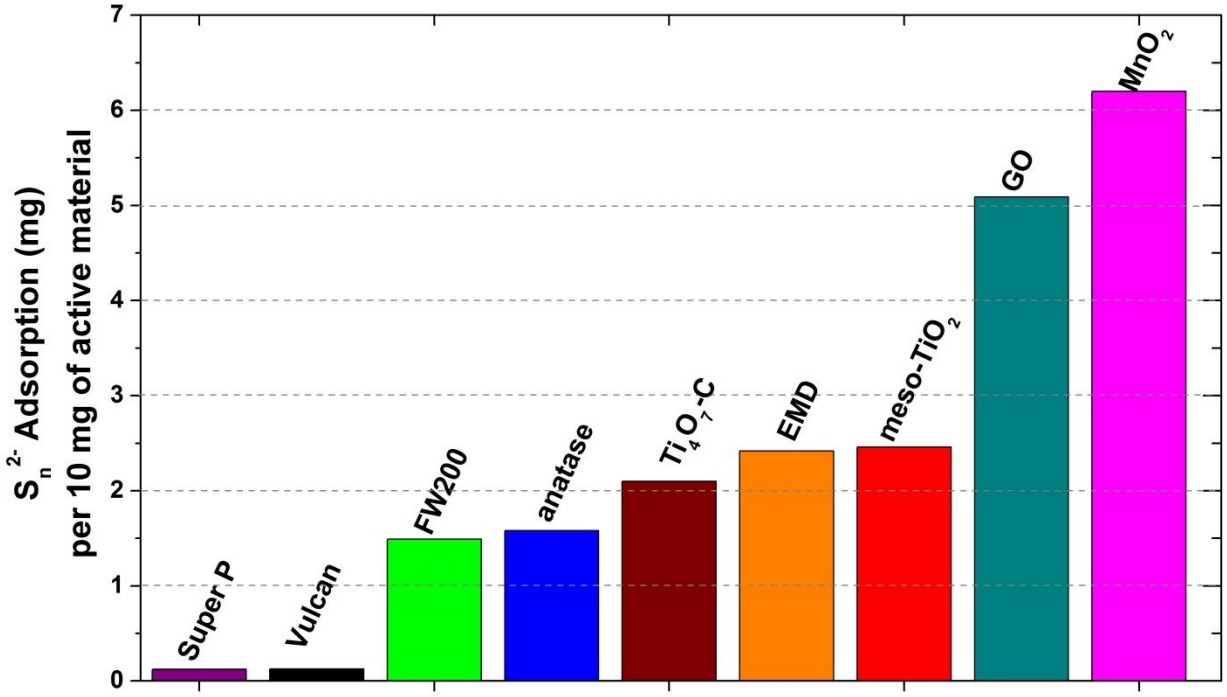

Figure 3.6: Summary of calculated polysulfide adsorptivity per 10 mg of active material from experimental data.

Further correlations can be drawn between the S_n^{2-} adsorptivity of various samples and their respective surface area determined by the Brunauer-Emmett-Teller (BET) method (**Table 3.2**). Polarity is an intrinsic characteristic of a specific material, so that mesoporous and non-porous anatase-TiO_2 have the same affinity for S_n^{2-}. In practice, mesoporous TiO_2 adsorbs 1.8 times more S_n^{2-} than the non-porous sample due to its higher surface area (indeed, more surface is available for adsorption), however the specific adsorptivity (i.e. per mass unit) does not scale linearly with the surface area. A similar comparison was drawn between EMD and MnO_2 nanosheets, indicating the surface accessed by S_n^{2-} in electrolyte solutions is not as high as gaseous N_2 adsorptivity which determines the BET surface area. For screening sulfur host candidates, polysulfide specific adsorptivity is a more relevant parameter: not only are electrode composites typically formulated by weight, but the experimental conditions for its determination closely mimic those of actual Li-S cells.

Table 3.2: Nitrogen sorption surface area measurements of all materials degassed at 100°C.

Sample	Surface Area (m^2/g)
Super P	67.70
Vulcan	212.1
FW200	357.7
Graphene Oxide	26.40
Non-porous anatase	54.04
Mesoporous Anatase	271.5
Ti_4O_7-C	291.2
MnO_2 sheet	103.9
EMD MnO_2	24.53

3.4.2 Long-Term Cyclability

In an attempt to correlate the S_n^{2-} adsorptivity of materials to the long-term cycling ability of composite electrodes in Li-S cells, galvanostatic cycling was performed at a current density of C/2 (836 mA/g; corresponding to discharge or charge in two hours). The results are displayed in **Figure 3.7a** and **b**. As a general trend, samples with the highest S_n^{2-} adsorptivity achieved the highest capacity retention over 100 cycles. This was expected, as materials with a stronger affinity for S_n^{2-} can retard diffusion into the electrolyte, thus minimizing capacity fading. High surface area MnO_2 (nanosheets) and TiO_2 (mesoporous) exhibit slightly higher capacity retention than their lower surface area counterparts, but the difference is not as drastic as the S_n^{2-} adsorptivity would suggest. Again, the surface available for adsorption in the composite electrode is reduced compared with the previous experiment, owing to binder coverage for example. This suggests that developing better cathode architecture to take advantage of the higher surface area is critical. Nonetheless, the trends drawn from **Figure 3.6** are respected and the adsorptivity scale can be used to benchmark any new possible sulfur host material. Comparing the 100^{th} cycle capacity to the 20^{th} cycle rather than the 1^{st} cycle (**Figure 3.7b** and **Table 3.3**) is reasonable as time was allowed for full wetting of the positive electrode by the electrolyte. This enables better assessment of the long-term behaviour of cells; for example,

graphene oxide (GO) which exhibits rapid fading followed by a steady capacity and FW200, an oxygen-rich carbon that shows slow but continuous decay. From the 20^{th} to the 100^{th} cycle, all cells based on polar sulfur hosts - transition metal oxides or oxidized carbons - have a capacity retention > 90%. This confirms that the S_n^{2-} adsorptivity indeed benefits prolonged cyclability. In contrast, sulfur electrodes using carbonaceous materials all exhibit poorer capacity retention (< 90%). Moreover, while graphene oxide[27] and MnO_2 nanosheets[29] both recently demonstrated cyclability up to 2000 cycles with record minimal fading rate of < 0.04% per cycle, the performance of Li-S cells incorporating non-polar carbon hosts keep steadily degrading even after 100 cycles (**Figure 3.7**).

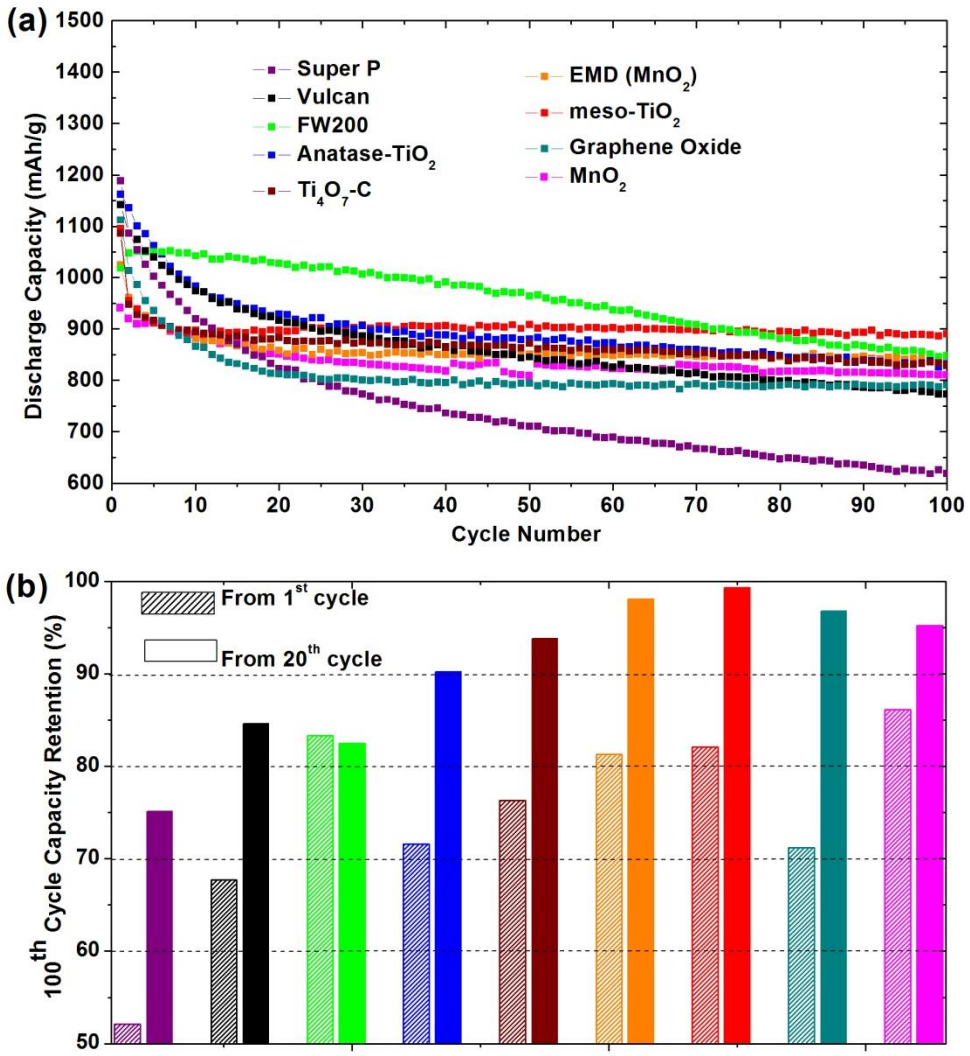

Figure 3.7: (a) Galvanostatic cycling of all Li-S cells at a C/2 rate. (b) plotted summary of capacity retention from the 1st cycle and then from the 20th cycle.

Table 3.3: Capacity retention of galvanostatically cycled cells at C/2 rate

Material	Initial Discharge Capacity (mAh/g)	Capacity Retention from 1st Cycle (%)	Capacity Retention from 20th Cycle (%)
MnO_2 (sheets)	941.1	86.1	95.2
Graphene Oxide	1012.4	71.2	96.8
Mesoporous TiO_2	1095.6	82.1	99.3
EMD	1025.3	81.3	98.1
Ti_4O_7-C	1081.4	76.3	93.8
anatase	1161.9	71.6	90.2
FW200	1018.1	83.3	82.5
Vulcan	1141.9	67.7	84.6
Super P	1188.1	52.1	75.1

3.4.3 Self-Discharge Experiments

As reported by Urbonaite *et al.*,[41] capacity retention after 100 cycles may be misleading, since physical confinement will eventually be breached. After 500 cycles, typical meso-structured carbons (i.e. FW200) behaved as poor sulfur hosts, equivalent to carbon blacks, and a novel cell testing protocol was necessary. Self-discharge experiments were therefore conducted at an intermediate state of discharge on Li-S cells incorporating each of our nine materials.[42] **Figure 3.8a** displays the typical voltage profile exhibited by all materials. After 9 formation cycles, the 10^{th} discharge was interrupted at 2.1 V, where the fraction of sulfur under the form of soluble S_n^{2-} is maximal.[20] After resting for 3 days, discharge was resumed and resulted in a lower capacity compared to the 9^{th} discharge (Δ_D), while the subsequent 10^{th} charge suffered even a further capacity drop when compared to the 9^{th} charge (Δ_C). As displayed in the inset of **Figure 3.8a**, the specific capacity remained stable during the subsequent cycles (11 – 20), and therefore Δ_C was irreversibly lost for any of the materials. This is explained more fully below.

Figure 3.8b compiles Δ_D and Δ_C for all the different materials studied. To assess internal chemical reactions at open-circuit, self-discharge in batteries is typically measured as Δ_D, and in the case of Li-S batteries, one would attribute it to polysulfide diffusion. Although there is no direct correlation between Δ_D and specific S_n^{2-} adsorptivity of each host material, Δ_C clearly scales inversely with the amount of S_n^{2-} retained in the positive electrode by adsorption onto the host matrix. Simply, materials with a large S_n^{2-} adsorptivity (as seen in **Figure 3.6**) have the lowest irreversible capacity loss (Δ_C) compared to those materials with a lower S_n^{2-} adsorptivity. Although such a trend was anticipated, the quantification makes it quite clear: Super P based sulfur electrodes lose more than 40% of their capacity after only 3 days shelving at intermediate

state of discharge. In contrast, hosts such as graphene oxide or MnO_2 nanosheets retain 91% and 94% of their active sulfur content, respectively.

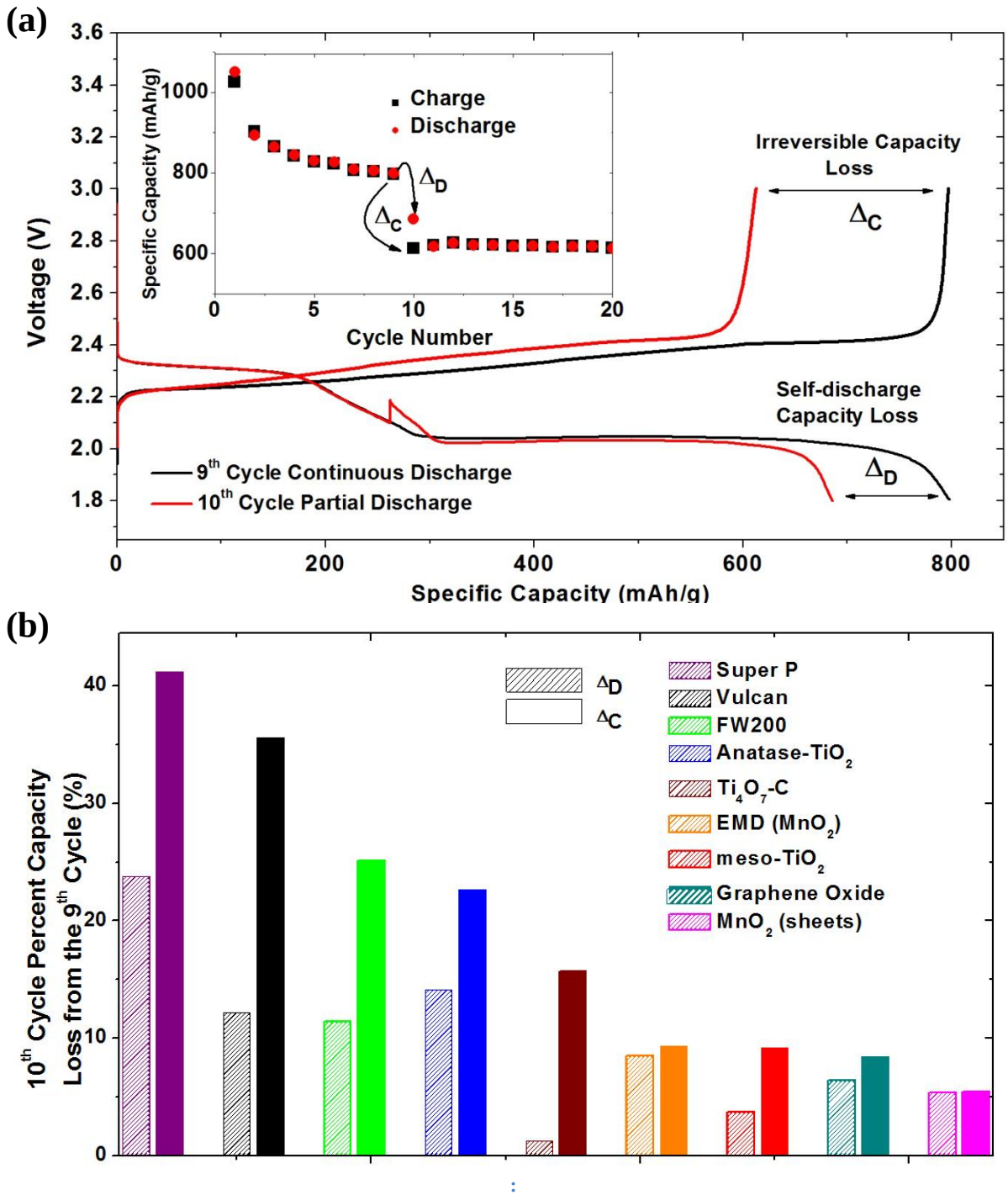

Figure 3.8: (a) Voltage/capacity profile of 9th cycle (continuous discharge) and 10th cycle (3-day rest period during discharge). Inset: typical capacity/cycle index plot, illustrating Δ_D and Δ_C upon self-discharge; (b) summary of Δ_D and Δ_C for different materials.

3.4.4 Origin of Irreversible Capacity

The origin of the irreversible capacity loss that varies between different materials is explained using a simple mechanism in **Figure 3.9**. In the first scenario, a non-polar host (black circles) is coated with sulfur (yellow, A) which upon discharge to 2.1 V is reduced to soluble S_n^{2-} (green, B). Since non-polar surfaces interact poorly with ions, S_n^{2-} readily diffuses into the electrolyte during the 3 day rest (C). In open-circuit mode, polysulfides can form Li_2S via dismutation, which could precipitate anywhere: the positive electrode, the separator or the negative electrode. Upon subsequent charge (D) the active material lost from the positive electrode - either in the form of S_n^{2-} in the separator or electrochemically inaccessible Li_2S - is not reoxidized to sulfur and as such, the reversible storage capacity of the Li-S cell is irreparably diminished. Polar host materials inherently mitigate irreversible capacity loss by binding S_n^{2-}. In this second scenario, the S_n^{2-} remains in close interaction with the host material upon discharge to 2.1 V (B) and over the 3 day rest minimal S_n^{2-} diffuse into the electrolyte (C). Upon full charge, electrochemically accessible Li_2S or S_n^{2-} oxidize to sulfur, leaving a marginal concentration of S_n^{2-} in the electrolyte which results in the small irreversible capacity loss observed with these polar host materials (**Figure 3.8b**). As mentioned earlier, while the exact chemistry of host-S_n^{2-} binding varies with the nature of the host[28,29], increasing the specific surface area available for adsorption (**Table 3.2**) maximizes S_n^{2-} adsorptivity (**Figure 3.6**). Hence the retention of polysulfides in the positive electrode composite is enabled under closed and open-circuit conditions.

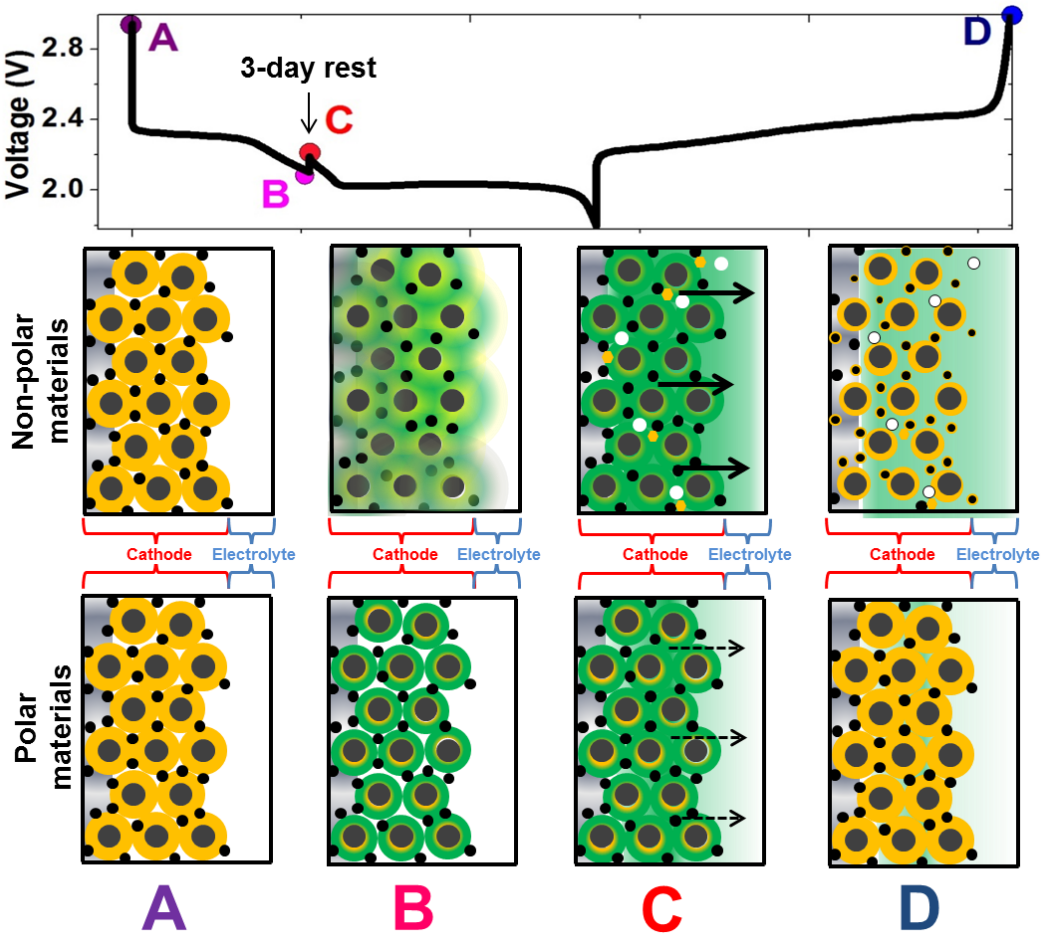

Figure 3.9: Schematic displaying a typical electrochemical half-cell undergoing self-discharge using either non-polar or polar sulfur host materials.

3.4.5 Attempts to Recover/Mitigate Capacity Loss During Self-Discharge

Experiments were conducted using varying cut-off voltages, or cycling rates to try and recover any capacity that was lost as a consequence of self-discharge. Lost capacity could be in the form of electrochemically inaccessible Li_2S, or polysulfides being left in solution due to cycling at a rate that is too fast. For all experiments, Super P / sulfur positive electrodes were fabricated and galvanostatically cycled as mentioned in **Section 3.3.2**, with any exceptions mentioned in the subsequent subsections.

3.4.5.1 Activation of Self-Discharged Li-S Cell

Experiments were conducted to charge the self-discharged cell to 4.0V (only on the 10^{th} cycle) in an attempt to re-activate the Li_2S to mitigate the irreversible capacity loss. **Figure 3.10a** displays the cycling behaviour for the self-discharged cells. On the 10^{th} cycle, there is a 21% discharge capacity loss after the self-discharge (Δ_D), and an equal charge capacity loss on the subsequent charge to 4.0 V (Δ_C-act). As detailed previously, when recharging to 3V, a further capacity drop is typically observed upon charge (i.e $\Delta_C >> \Delta_D$, see the blue square in **Figure 3.10a**) after which both charge and discharge capacities stabilize. In the present case, a further capacity drop is observed on the 11^{th} charge at 3 V (30% from the 9^{th} cycle).

The mitigated capacity loss on the 10^{th} charge most probably arises from the oxidation of $LiNO_3$ around 3.5 V, as observed in **Figure 3.10b** (red curve). Hence, a Li-S cell damaged by self-discharge cannot be electrochemically reactivated. The conclusion is that, if polysulfides reduce to Li_2S by dismutation during a rest or storage period an intermediate state of discharge, this Li_2S is not in contact with the positive electrode (therefore either in the separator or on the negative electrode) and is essentially electrochemically 'dead'.

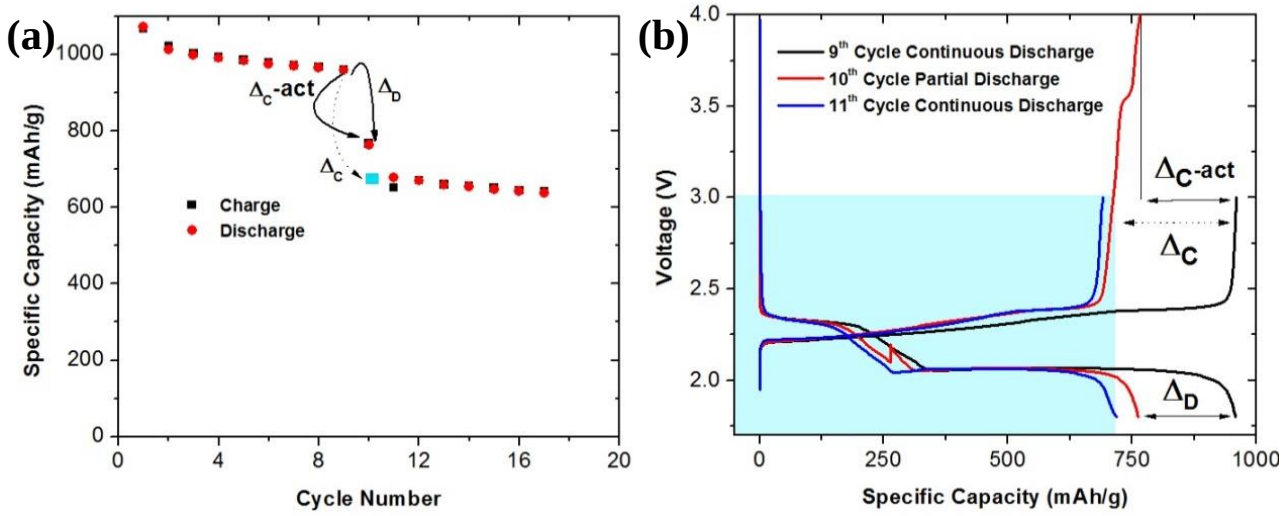

Figure 3.10: Super P/ sulfur electrodes: (a) self-discharge capacity drop as exemplified through galvanostatic cycling at C/2 rate and a activation 10th charge cycle. (b) Voltage profile of 9th (black) continuous discharge cycle, 10th (red) partial discharge, and 11th (blue) continuous discharge cycles. The blue box shows the capacity achieved on the 10th charge if only charged to 3.0V.

3.4.5.2 Slow Rate Self-Discharge / Charge

One possible reason for the extent of the irreversible capacity is the cycling rate is too fast. A fast rate does not providing enough time for polysulfides to be fully reduced to electrochemically active Li_2S, or to be re-oxidized to sulfur upon charge. Galvanostatic cycling was conducted at C/2, with the exception that cycle 9 and 10 were conducted at a C/10 rate.

From **Figure 3.11**, the first 8 cycles show a typical behaviour at C/2 rate. Upon reducing the rate to C/10 on the 9th cycle, the specific capacity increased slightly suggesting a higher utilization rate of sulfur in the positive electrode. The subsequent 10th partial discharge and 10th charge resulted in a Δ_D and Δ_C of 8% and 4% respectively. This is drastically lower than previously reported (25% and 42% respectively), suggesting that slow rates can help mitigate self-discharge.

More importantly, when increasing the current rate back to C/2 on the 11th cycle (**Figure 3.11a** and **b**), the overall capacity loss for $\Delta_{D(8\text{-}11)}$ and $\Delta_{C(8\text{-}11)}$ are 17% and 18% respectively. This

capacity loss is lower than previously reported for only C/2 cycling which suggests a slower self-discharge and re-charge rate may be able to mitigate the irreversible capacity loss. Further experiments will need to be conducted in order to fully understand the physical meaning, and the practical implications for Li-S batteries.

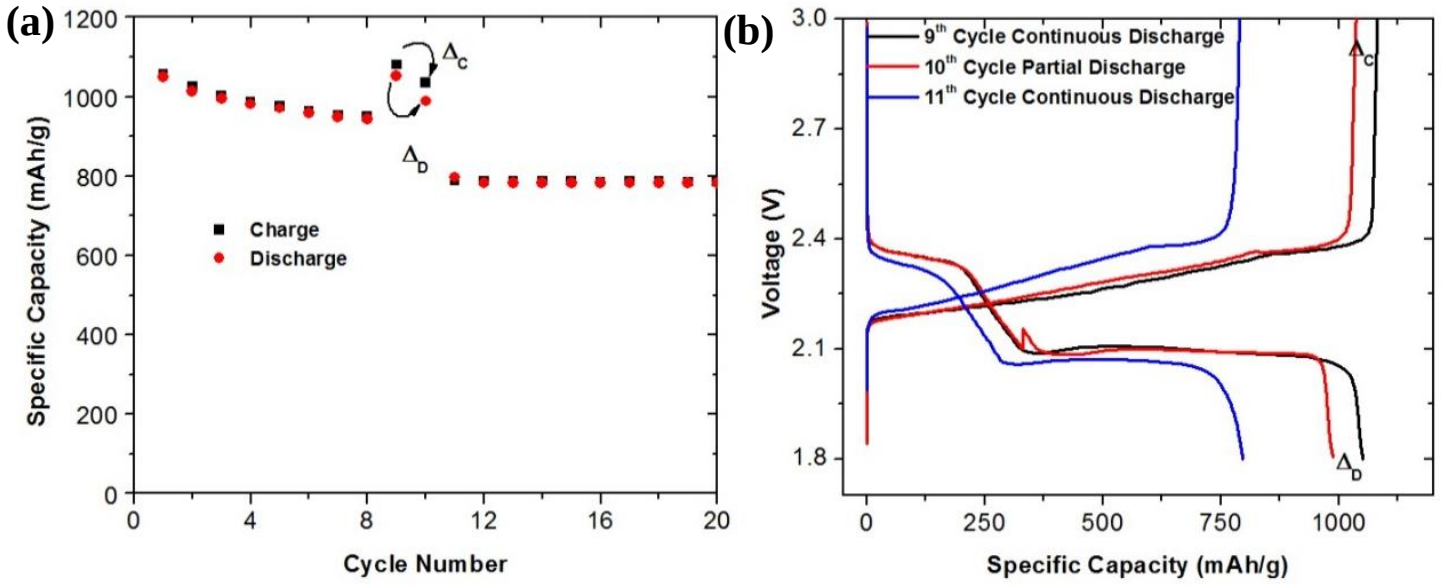

Figure 3.11: (a) Slow rate self-discharge cycling profile. 9th and 10th cycle are conducted at C/10 rate. (b) Voltage profile of 9th (black) continuous discharge cycle, 10th (red) partial discharge, and 11th (blue) continuous discharge cycles.

3.4.6 Investigation of Electrolyte Decomposition by ^{1}H NMR

Electrolyte decomposition is often reported among aging or failure modes of lithium batteries. For instance, carbonate solvent undergo nucleophilic attack by contact with charged transition metal oxide surfaces. Similarly, polysulfide dianions or radicals in high concentration (rest at 2.1 V) may attack 1,3 dioxolane (DOL) from the typical glyme-based electrolyte to form electrochemically inactive sulfur compounds. Decomposition will have long term detrimental effects on the cell performance, thus exacerbating the irreversible capacity from self-discharge.

In order to exacerbate any possible reactivity from the S_3^- radical (formed in high dielectric solvents), a bulk experiment was carried out in DMSO by subjecting DOL to

extremely high concentrations of dianions and radicals. In an argon-filled glovebox, 1 mmol Li_2S_6 was synthesized in 4 mL deuterated DMSO by reacting appropriate amounts of Li_2S and elemental sulfur. After 12 hours, an equimolar amount of DOL was added and left to react for 24 hours at room temperature. The ^1H NMR spectra of Li_2S_6 in DMSO, DOL in DMSO and Li_2S_6+DOL in DMSO are shown in **Figure 3.12**. All the NMR peaks observed can be attributed to either DOL or to DMSO, and no impurity or decomposition products can be detected, even at the scale of the satellite peaks (^{13}C-^1H coupling, so that their intensity is ~1% of the central peaks). Qualitatively, the coloration of the polysulfide solution does not fade upon mixing with DOL, suggesting that colored species (S_6^{2-}, $S_3^{\cdot-}$) are not consumed in any chemical reaction.

Therefore, the results showed that there were no electrolyte decomposition products from DOL detectable using ^1H NMR at room temperature. Therefore, electrolyte decomposition is probably not a source of the irreversible capacity observed after self-discharge. DME solvent was not tested for electrolyte decomposition as it is much more stable towards nucleophilic attack.[16]

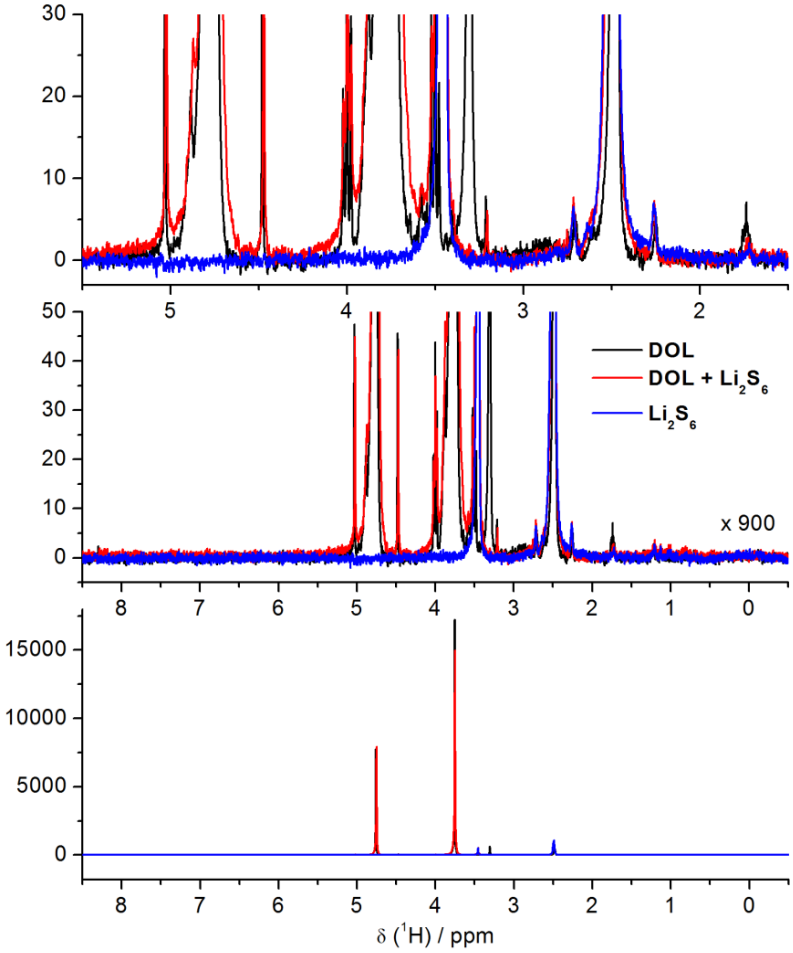

Figure 3.12: ^{1}H NMR of Li_2S_6 in DMSO (blue), DOL in DMSO (black) and Li_2S_6+DOL in DMSO (red). Peaks at 3.8 ppm and 4.8 ppm are assigned to DOL, peaks at 2.5 ppm and 3.5 ppm to DMSO and water contaminant in DMSO, respectively. Expanded views do not reveal any additional peak after mixing polysulfides and DOL for 24 hours.

3.5 Conclusions and Final Thoughts

Comparison with a previously reported, 4-electrode Swagelok™ cell designed to estimate S_n^{2-} concentration in the electrolyte shows the versatility of our approach.[20] The Swagelok™ cell, although able to detect S_n^{2-} concentration *in situ*, required a complex assembly procedure and four electrodes, whereas the strategy developed herein is a versatile, cost-effective method that determines the specific S_n^{2-} adsorptivity of materials prior to cell development. This method can be extended to any new candidate for use as a sulfur host in a Li-S cell prior to fabricating

expensive electrochemical full cells. Second, a vital 5-day cycling protocol allows prediction of the long-term performance of sulfur composite electrodes by measuring the ability of the host to retain the active sulfur mass under real operating conditions. In **Figure 3.13**, the parameters relevant for a sulfur host material (surface area and S_n^{2-} adsorptivity), are put in perspective together with the capacity retention following a self-discharge experiment. From this forward-looking plot, one easily visualizes how critical S_n^{2-} adsorptivity and surface area is in the capacity retention after self-discharge.

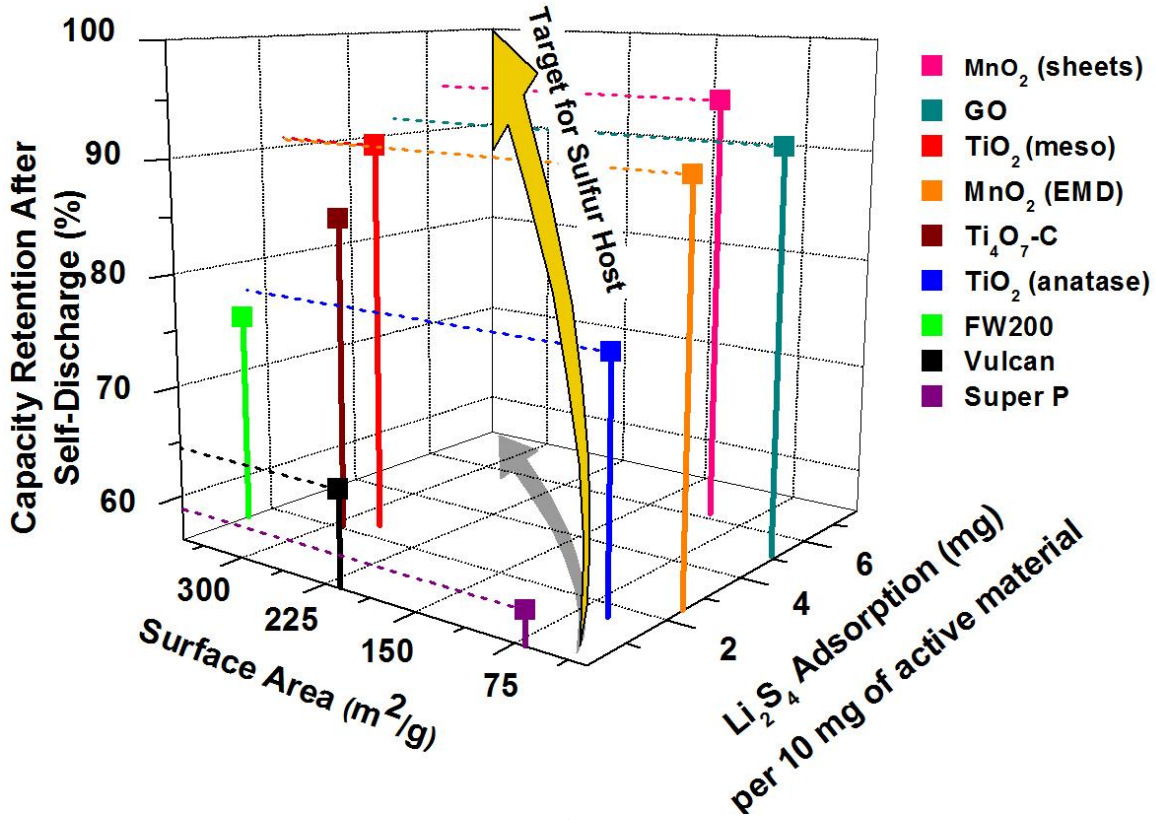

Figure 3.13: Target for sulfur host based on S_n^{2-} adsorption, surface area and capacity retention following a self-discharge experiment.

The fact that the Li-S cell operates at about 2.2 V particularly allows it to benefit from optimization of both factors, which would not be the case for a conventional Li-ion (or Li-O_2) cell because of the aggravated reactivity of electrolytes (or intermediate species) at higher

potentials. However, clever and efficient electrode architecture is equally important in order to take advantage of these properties. Although this is also key for conventional Li-ion cells, for the chemical transformation chemistry underlying the Li-S cell, it is paramount. The search for novel sulfur hosts should therefore first focus on tailoring their surface for maximum interaction before engineering such materials with expanded surface area, in order to achieve even higher capacity retention upon cycling.

Chapter 4
Thiosulfate as an Additive for the Sulfur-Based Electrode

4.1 Introduction

The race to commercialization of Li-S batteries rapidly began in the early 2000's, but has been hindered by the numerous technical issues within this system. The solubility of intermediate sulfur species (polysulfides, S_n^{2-}) throughout discharge and charge causes a redox shuttle between electrodes which affects capacity fading and lowers Coulombic efficiency over cycling.[43] Furthermore, the insulating nature of sulfur requires a conductive additive in the positive electrode resulting in a lower sulfur fraction, and a compromised energy density.[5,8,14,43] The most popular route to solving these problems and enhancing sulfur utilization was by trapping S_n^{2-} within the pores of carbon.[12,22,23,25,44,45] As is now understood, a practical Li-S cell is not realized only through physical confinement of sulfur within pores because degradation overtime can occur as a result of the 80% volume change throughout cycling. Polymeric coatings are promising as electrode materials because structural integrity remains throughout cycling.[46,47,48]

Recently, our group showed that MnO_2 nanosheets, as the sulfur host, suppresses active mass loss during cycling resulting in an ultra-low capacity decay rate of 0.036% per cycle over 2,000 cycles at a rate of 2C.[29] The stable electrochemical performance is due to the formation of thiosulfate on the surface of MnO_2 as outlined in **Chapter 1**. Upon discharge, the surface thiosulfate groups anchor soluble 'higher' order polysulfides through catenation and further mediate S_n^{2-} redox forming 'lower' order insoluble polysulfides. The *polythionate* complex that mediates this redox process curtails active mass loss which results in the improved electrochemical performance.

Carbon materials, although practical due to their high energy density, may not completely inhibit polysulfide diffusion into the electrolyte as physical confinement fails over ultra-long term cycling. Metal oxides offer minimal polysulfide diffusion, but are typically semiconductors at room temperature with decreased energy density compared to carbons. To exploit the capabilities of electrode hosts of both categories, thiosulfate was used as an additive to low-cost carbon hosts. The additive, through the formation of the *polythionate* complex, inhibits polysulfide diffusion into the electrolyte; meanwhile, the carbon host maintains electronic conductivity. Through this combination, FW200-thiosulfate sulfur hosts have 89% capacity retention after 100 cycles at C/2, and a 0.085% capacity decay rate per cycle over 200 cycles. This performance is 33% better than similar electrodes cycled without the additive. Although not yet superior (in terms of cycling) than some previous studies, it is important to note that the thiosulfate mechanism improved cycling of low-cost simple carbons.

4.2 Experimental

4.2.1 Preparation of Carbon-Sulfur Composites

Four different Vulcan (VC) carbon / sulfur composites were prepared with 63, 66, 70, and 74 wt% sulfur and one FW200 carbon / sulfur composite with 74 wt% sulfur via a melt infusion method at 155^{o}C. Notation for materials is as follows: VC/S – XX% or FW200/S – XX%, where XX is the weight percent of sulfur in the carbon composite.

4.2.2 Preparation of Carbon-sodium thiosulfate composites

Sodium thiosulfate ($Na_2S_2O_3$, Sigma-Aldrich) was dissolved in deionized water and the mixture was stirred and sonicated with carbon for two hours before being dried at 55^{o}C for a period of three days to ensure all the water was removed. Notation for materials is as follows:

VC – XX% TS or FW200 – XX% TS where XX is the weight percent of $Na_2S_2O_3$ in the carbon composite.

4.2.3 Preparation of carbon-sulfur-sodium thiosulfate composites

$Na_2S_2O_3$ was dissolved in deionized water in a pre-determined amount and added to samples VC/S – XX% and FW200/S – XX% to ensure a final sulfur loading of 63% in all composites. This realized a $Na_2S_2O_3$ weight percent in three carbon/sulfur composites of 5, 10, or 15%. Notation for materials are as follows: VC/S – XX% or FW200/S – XX% where XX is weight percent of $Na_2S_2O_3$.

4.2.4 Preparation of Li_2S_4 Reference Powder

Li_2S_4 was synthesized by mixing 1.0M lithium triethylborohydride in tetrahydrofuran (Super-Hydride Solution, Aldrich) and sulfur (Sigma-Aldrich) in a 2.75:1 molar ratio. After dissolution, the solution was vacuum dried until a yellow powder formed, followed by a final wash with toluene and isolation of the yellow Li_2S_4 powder.

4.2.5 Polysulfide Adsorption Analysis

Standard solutions used to generate the calibration plot were prepared by mixing desired amounts of Li_2S_4 with 16 mL of 1M $LiClO_4$ (battery grade, Sigma Aldrich) in tetraethylene glycol dimethyl ether (TEGDME). Sample solutions were prepared by adding a known mass of material into a solution of Li_2S_4 in TEGDME and allowing the mixture to stir for 18 hours. The coloured supernatant was isolated via centrifugation and diluted to 16 mL with 1M $LiClO_4$ in TEGDME. Oxidations of the standard and sample solutions were conducted using an electrochemical H-cell design. The left hand compartment contained the sample/standard solutions with an immersed nickel mesh electrode. The right-hand compartment contained a lithium foil electrode wetted by 1M $LiClO_4$ in TEGDME with 2 wt% $LiNO_3$. Electrochemical

oxidation occurred at a potential of 3.0V and the capacity was determined based on the integrated current until it reached 0 mA.

4.2.6 Electrochemical Measurements

Positive electrodes of all materials were fabricated by mixing a 8:1:1 mass ratio of the sulfur composite, Super P carbon, and poly(vinylidene fluoride-co-hexafluoropropylene) in dimethylformamide (DMF) and dropcasting the slurry onto P50 carbon paper (AvCarb, Fuel Cell Earth) current collectors. Electrodes were dried at 60^{o}C before being assembled in 2325 type coin cells using Li foil as the negative electrode, two 3501 Celgard separator sheets and 50 µL of 1M lithium bis(trifluoromethanesulfonyl)imide with 2wt% $LiNO_3$ in DOL:DME (1:1 v/v ratio) electrolyte. Long-term cycling experiments were conducted on a BT2000 Arbin battery cycler at room temperature between 1.8 and 3.0V using a charge/discharge rate of C/2 (1C=1,675 mA g^{-1}), following the first conditioning cycle at C/20. Self-discharge experiments required galvanostatic cycling at C/2 rate for 9 cycles before they were stopped on the 10th discharge at 2.1V (directly before supersaturation – the point of maximal polysulfide formed) to rest for three days. After resting, cells were resumed to discharge to 1.8V where normal cycling continued.

4.3 Results and Discussions

4.3.1 Synthesis and Characterization of Materials

A variety of materials were prepared from Vulcan carbon (VC) and FW200 carbon to study the effect of sodium thiosulfate ($Na_2S_2O_3$, TS) addition to the sulfur host of two different surface area carbons. Materials used for S_n^{2-} adsorption analysis were prepared by dissolving a certain amount of $Na_2S_2O_3$ in deionized water and mixing it with a known amount of carbon to fabricate carbon composites with different amounts of thiosulfate. TGA of these carbon/thiosulfate materials are shown in **Figure 4.1 a** and **b** which shows that 5, 10, and 15%

wt% TS composites were prepared**.** Materials used for electrochemical measurements were prepared by first melt infusing sulfur at 155^{o}C into carbon materials (VC/S – XX%, **Figure 4.1c**) and subsequently adding a aqueous solution of $Na_2S_2O_3$ to create carbon/sulfur composites with 63 wt% sulfur loading and a defined thiosulfate content (VC/S-XX% TS or FW200/S-15% TS, **Figure 4.1b** and **d**).

Thermogravimetric analysis (TGA) was used to quantify the amount of $Na_2S_2O_3$ present in each material. Upon heat treatment in air, thiosulfate is experimentally determined to oxidize to form sulfate with SO_2 as a by-product following **Equation 4.1**.

$$Na_2S_2O_{3(s)} + 3/2O_{2\,(g)} \rightarrow Na_2SO_{4(s)} + SO_{2(g)} \qquad \textbf{(4.1)}$$

This reaction was confirmed by X-ray diffraction (XRD, **Figure 4.2b)**, where Na_2SO_4 was clearly obtained after heat treatment of a VC-TS composite. The XRD of $Na_2S_2O_3$ is shown in **Figure 4.2a** as a reference to the starting material. Therefore, weight conversion from Na_2SO_4 to $Na_2S_2O_3$ was accounted for to quantify the amount of thiosulfate present in the original composites.

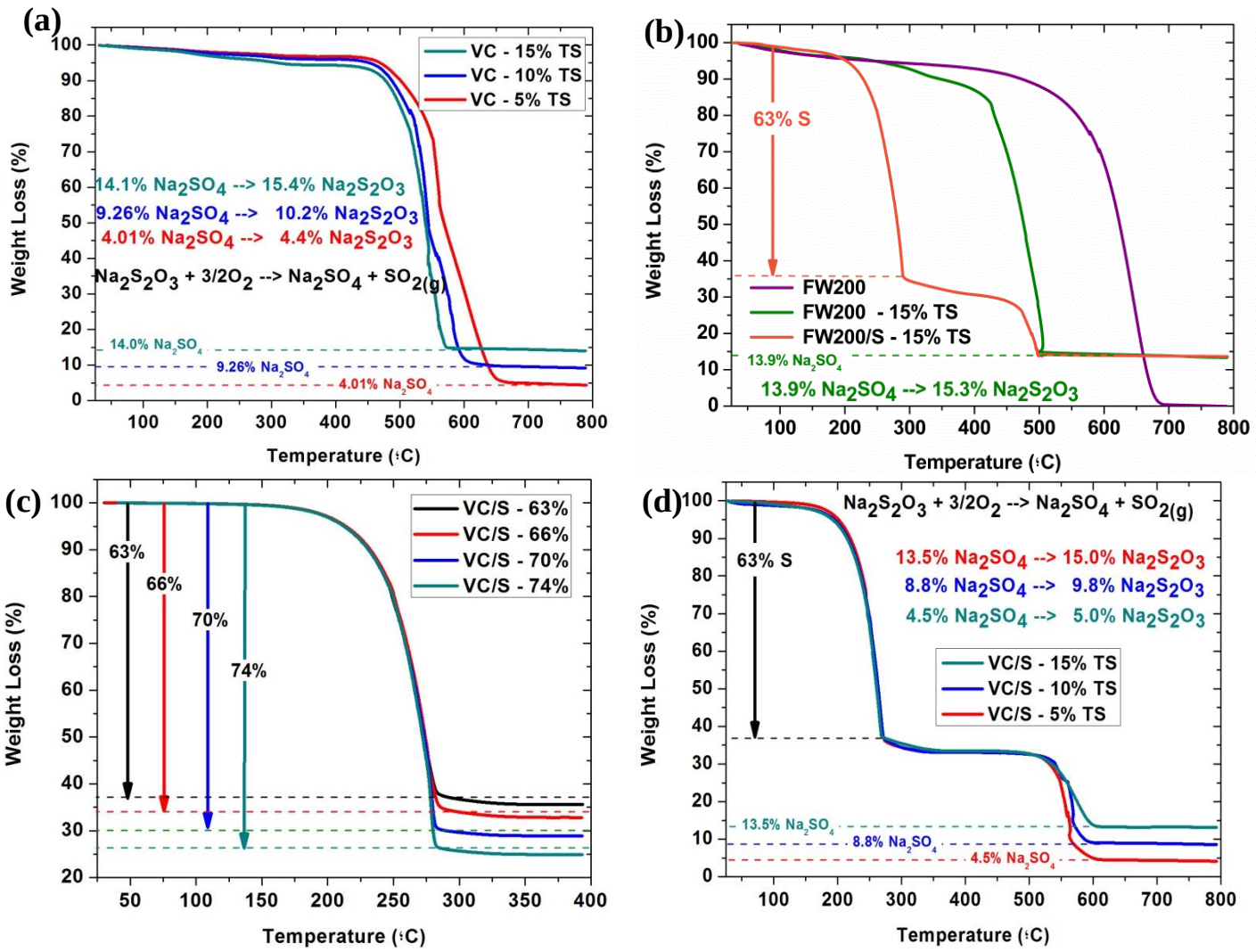

Figure 4.1: Thermogravimetric analyses conducted in air for (a) Vulcan carbon mixed with $Na_2S_2O_3$ as an additive (VC – XX% TS), and (b) FW200 carbon mixed with $Na_2S_2O_3$ as an additive (FW200 – 15% TS) and a FW200/S composite mixed with the thiosulfate additive (FW200/S – 15% TS), (c) Vulcan carbon – sulfur composites (VC/S), (d) Vulcan carbon – sulfur composites mixed with $Na_2S_2O_3$ as an additive (VC/S – XX% TS).

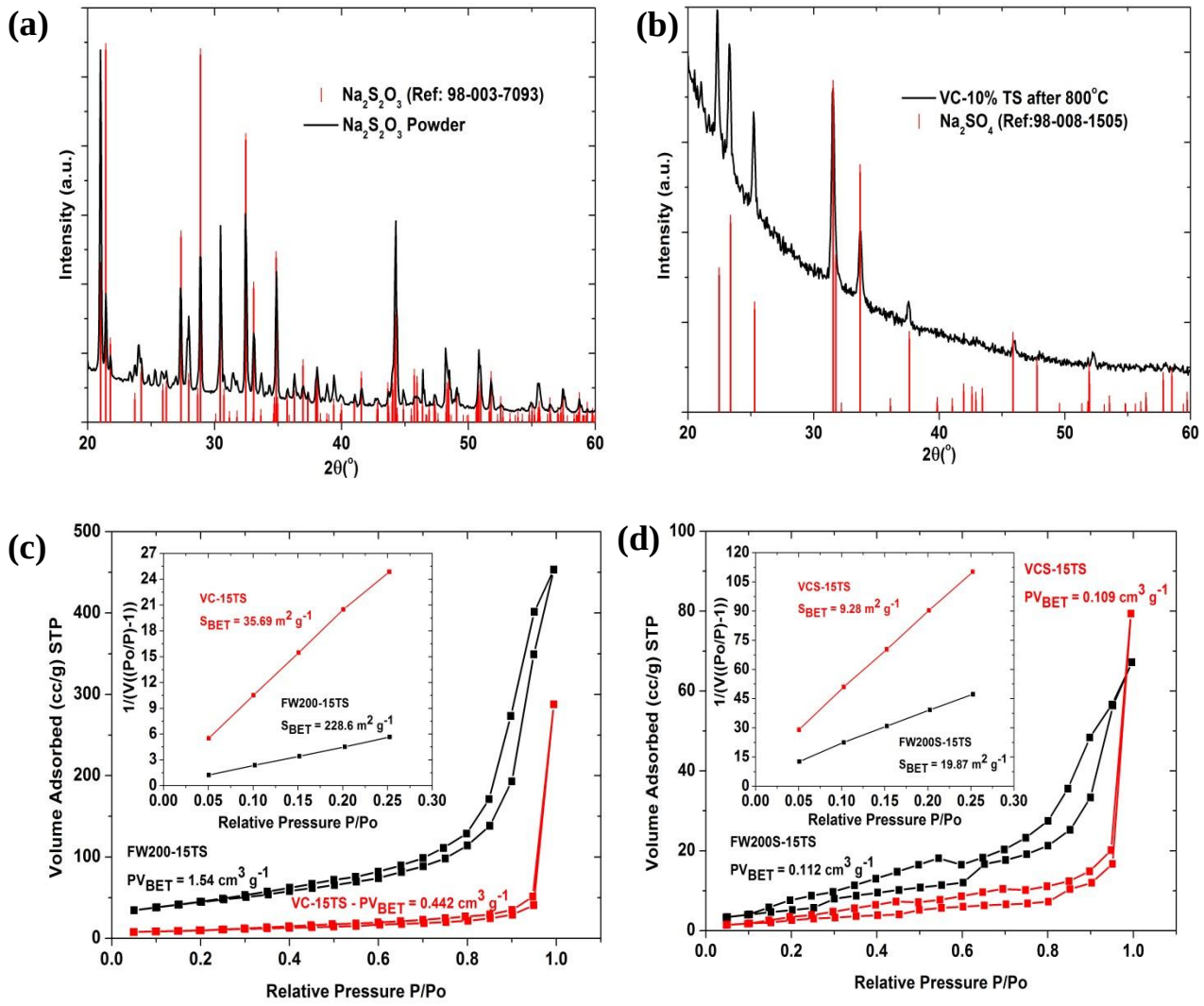

Figure 4.2: X-ray diffraction pattern of (a) commercial $Na_2S_2O_3$ and (b) VC-10% TS after heat treatment in air at 800°C; adsorption/desorption isotherms, inset: BET data used to determine surface area for (c) carbon/thiosulfate composites and (d) carbon/sulfur-thiosulfate composites.

Table 4.1: Summary of BET surface area and pore volume measurements of a variety of carbon composites.

Sample	Surface Area (m^2/g)	Pore Volume (cm^3/g)
FW200	341.1	2.44
FW200/S-74%	75.42	0.445
FW200-15TS	228.6	1.54
FW200S-15TS	19.87	0.112
VC	202.2	0.784
VC/S-74%	11.09	0.126
VC-15TS	35.69	0.442
VCS-15TS	9.28	0.109

Scanning electron microscopy images of VC/S – 63% and FW200/S – 63% (**Figure 4.3a** and **b**) reveal a very uniform sulfur coating with no large sulfur agglomerations. The low surface area and pore volume of 11.09 $m^2 g^{-1}$ and 0.126 $cm^3 g^{-1}$ (**Table 4.1**) respectively rationalizes that VC/S-74% does not allow for a uniform coating of 15wt% $Na_2S_2O_3$ as evident by the large thiosulfate particles found in the SEM image (**Figure 4.3 c).** However, FW200/S-15%TS displays a very uniform morphology of sulfur and thiosulfate as evident from **Figure 4.3 d,e,f** where no large agglomerations are visible and the elemental mapping of sulfur and sodium are very uniform. The uniform morphology after addition of $Na_2S_2O_3$ is likely a result of the initially high surface area and pore volume of 75.42 $m^2 g^{-1}$ and 0.445 $cm^3 g^{-1}$ for FW200/S-74%. Sulfur infiltration and subsequent $Na_2S_2O_3$ addition fully fills all the pores and limits the surface area in the materials used for electrochemical measurements (mainly in VC/S-15%TS). However, due to the large pore size and surface area of FW200, the morphology of this composite is more uniform and thus ideal for electrochemical measurements.

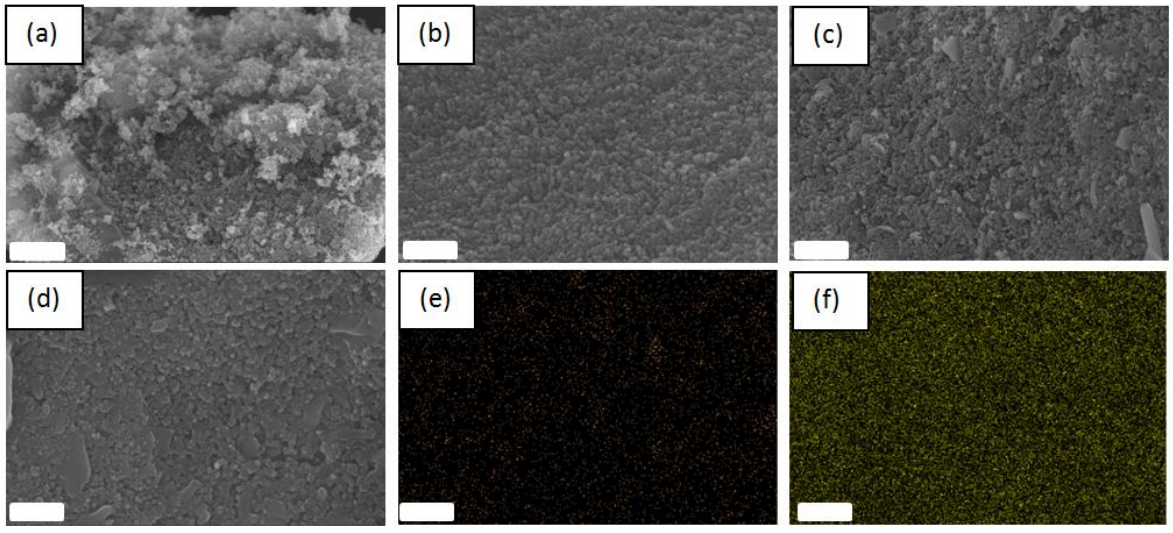

Figure 4.3: Scanning electron microscopy images of (a) VC/S-63%, (b) FW200/S-63%, (c) VC/S-15%TS, (d) FW200/S-15%TS and elemental mapping of FW200/S-15%TS for elements (e) sodium and (f) sulfur. Scale bars are (a) 1 µm, (b) 200 nm, (c) 1µm, (d) 200 nm, (e) 2 µm, (f) 2 µm.

4.3.2 Polysulfide Adsorption

As reported in Chapter 3, a facile and rational method for screening sulfur host candidates was developed by determining the specific polysulfide (S_n^{2-}) adsorptivity of materials.[33] The ability of a material to adsorb strongly S_n^{2-} species can be correlated to enhanced long-term performance of sulfur-based electrodes in a Li-S cell. Carbonaceous materials with the $Na_2S_2O_3$ additive were analyzed according to the outlined method in order to determine how the S_n^{2-} adsorptivity changes. Briefly, to determine the adsorptivity of these carbonaceous materials, a known concentration of Li_2S_4 was dissolved in TEGDME and stirred overnight with a known mass of material. After allowing substantial time for adsorption to occur, centrifugation of the solution resulted in a coloured supernatant which was oxidized at 3.0V to sulfur in the liquid H-cell set-up. The polysulfide adsorptivity was calculated based on the measured current using the valid calibration curve based standard solutions (**Figure 4.4**).

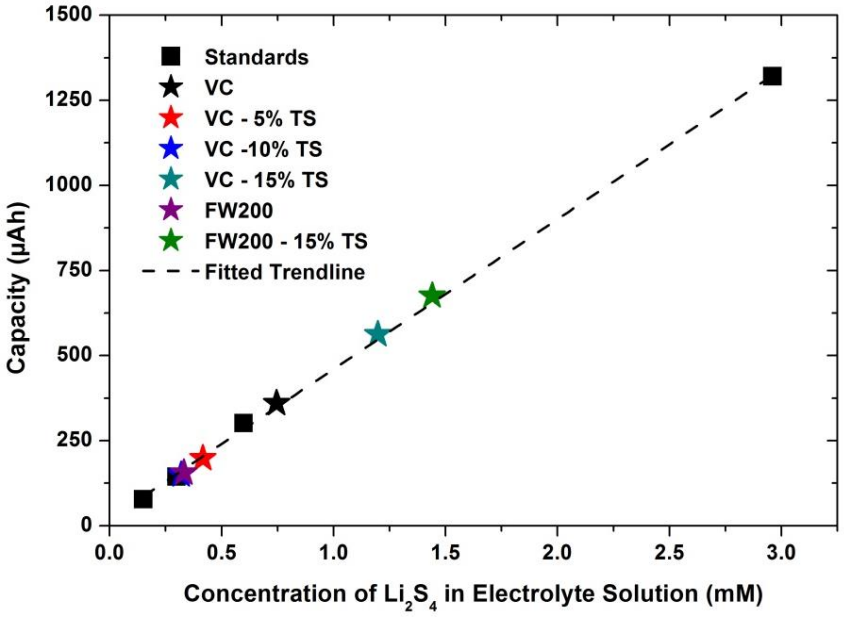

Figure 4.4: Calibration plot (squares) derived from oxidative capacity generated by a solution of Li_2S_4 in TEGDME to sulfur. Experimental points (stars) were mapped on the curve for a variety of different materials. Equation of fitted trendline: y=573.15x, R^2 = 0.9967.

Figure 4.5a displays the summary of the S_n^{2-} adsorptivity of all 6 materials studied. The polysulfide adsorptivity of carbon materials increased with increasing thiosulfate additive concentration. There is a 2.68 times greater adsorptivity for Vulcan carbon with 15 wt% additive compared to the pristine Vulcan carbon. The S_n^{2-} adsorptivity for VC is not linear with increasing thiosulfate weight percent. As the weight percent increases, the difference in polysulfide adsorptivity becomes less significant. This suggests a maximum effect of the thiosulfate is reached when the surface area becomes too saturated for further beneficial effects for S_n^{2-} adsorption. As shown in **Figure 4.2c** and summarized in **Table 4.1**, the addition of 15 wt% thiosulfate caused the surface area to decrease by 82% to 35.69 m^2 g^{-1} causing saturation of the carbon surface by the additive.

In light of the surface area limitation, FW200 with a higher surface area of 341.1 m^2 g^{-1} was functionalized with 15wt% $Na_2S_2O_3$ additive and the results of the S_n^{2-} adsorptivity analysis shown in **Figure 4.5a.** There was a 1.67 fold increase in S_n^{2-} adsorptivity for FW200-15%TS bringing the adsorptivity on par with the previously reported (**Figure 3.6**) mesoporous-TiO_2 (**Figure 4.5b)**. One can see from **Figure 4.5b** that FW200 has an adsorptivity of 1.5 mg/10mg material, and is increased up to ~2.5 mg/10mg material with 15 wt% additive. The elemental mapping and the absence of very large (>1 μm) $Na_2S_2O_3$ particles confirms uniformity of $Na_2S_2O_3$ in the material, thus, maybe one reason for an enhanced S_n^{2-} adsorptivity. The S_n^{2-} adsorptivity for the FW200-15%TS did not double as it did with VC suggesting that the higher surface area of FW200 is not exploited efficiently. As shown in **Figure 4.2c**, the surface area and pore volume after FW200-thiosulfate infusion remained at 228.6 m^2 g^{-1} and 1.54 cm^3 g^{-1} respectively, indicating that carbon surfaces were incompletely coated with thiosulfate. This allows for weak physisorption interaction between the carbon and polysulfides.

In terms of S_n^{2-} adsorptivity, the results demonstrated that a carbonaceous host with thiosulfate additive performs similarly to that of a metal oxide (**Figure 4.5b**). Metal oxides offer a polar host for increased polysulfide interaction instead of relying on physical entrapment as observed in elegant (mesoporous) carbons. This new approach utilizes a polysulfide adsorber with an inexpensive carbon which now adsorbs polysulfides in solution more readily.

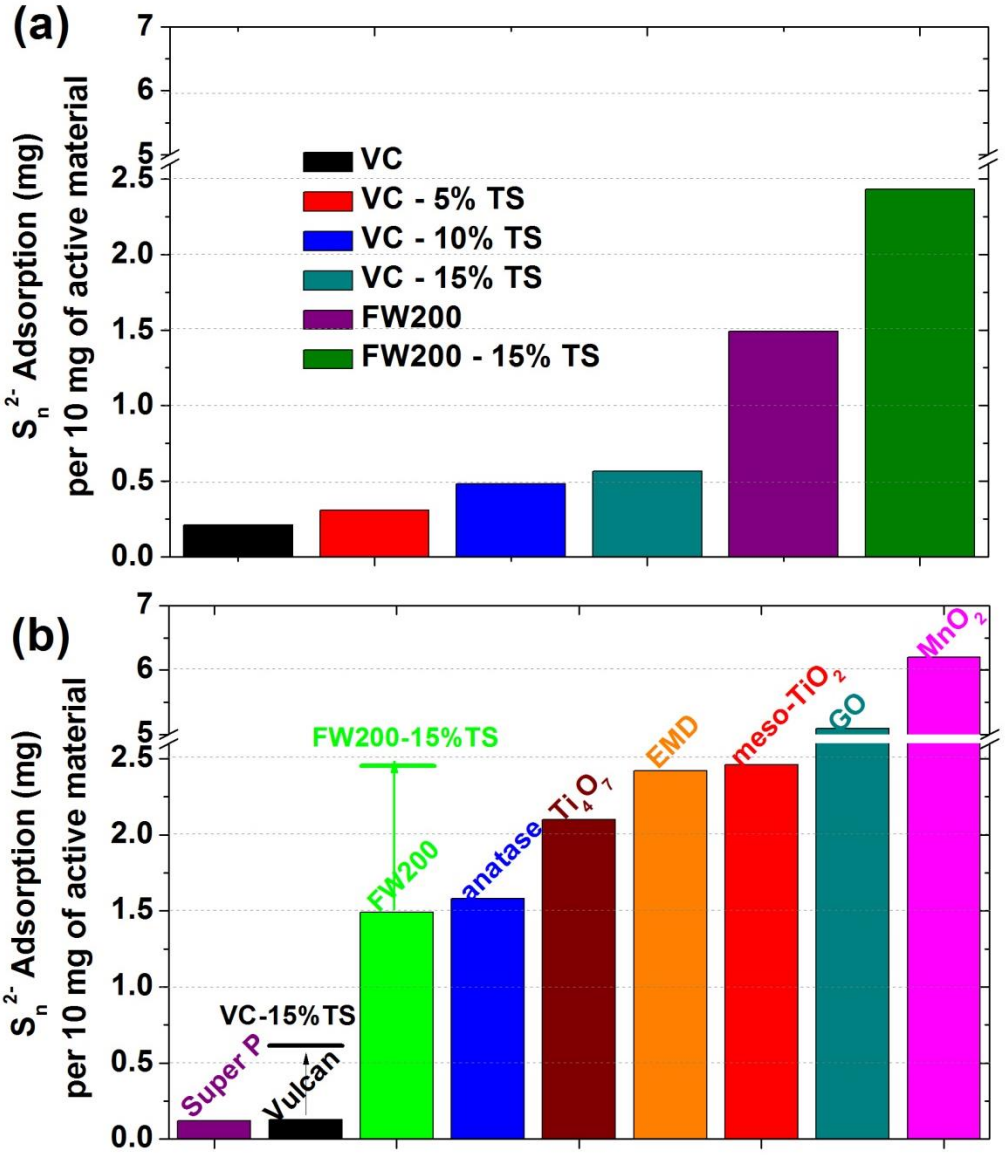

Figure 4.5: (a) Summary of the calculated polysulfide adsorptivity per 10 mg active material from experimental data and (b) Figure 3.6 from Chapter 3 which has been modified to add the increase (see vertical arrows) in S_n^{2-} adsorptivity from the addition of the thiosulfate additive.

4.3.3 Self-Discharge Experiments for Carbon-Additive Composites

Experiments were conducted on each carbon material functionalized with the $Na_2S_2O_3$ additive to probe the extent of irreversible capacity loss as a result of a 3 day rest at an intermediate state of discharge. The irreversible capacity loss is directly influenced by the amount of S_n^{2-} the host material is able to retain; where a higher S_n^{2-} adsorptivity, results in less capacity loss.[33] **Figure 4.6 a** and **b** display the cycling profile of the electrochemical cells under a self-discharge protocol resulting in a decreased discharge/charge capacity after the 3 day rest. A summary of self-discharge results are displayed in **Figure 4.6c** showing no direct correlation in the self-discharge capacity loss (subsequent discharge capacities, Δ_D). However, the irreversible capacity loss (subsequent charges, Δ_C) decreases as the S_n^{2-}adsorptivity increases. Although still not satisfactory, Vulcan carbon typically loses 40% of its capacity during a three-day rest, whereas with 15 wt% thiosulfate additive, the degree of irreversible capacity decreases to 33%. By adding 15 wt% $Na_2S_2O_3$ to FW200, there is a 60% reduction in the irreversible capacity after a 3 day rest making the self-discharge characteristics now comparable to mesoporous-TiO_2. Mechanistically, polar materials like metal oxides have an intrinsic ability to retain S_n^{2-} in the positive electrode to prevent irreversible capacity. However, non-polar materials such as carbons do not intrinsically retain polysulfides on its surface due to the incompatibility between S_n^{2-} and carbon. By adding $Na_2S_2O_3$ to a non-polar material, the extent of self-discharge decreases as a result of increased S_n^{2-} adsorptivity; compelling evidence that this additive is advantageous in a Li-S positive electrode matrix.

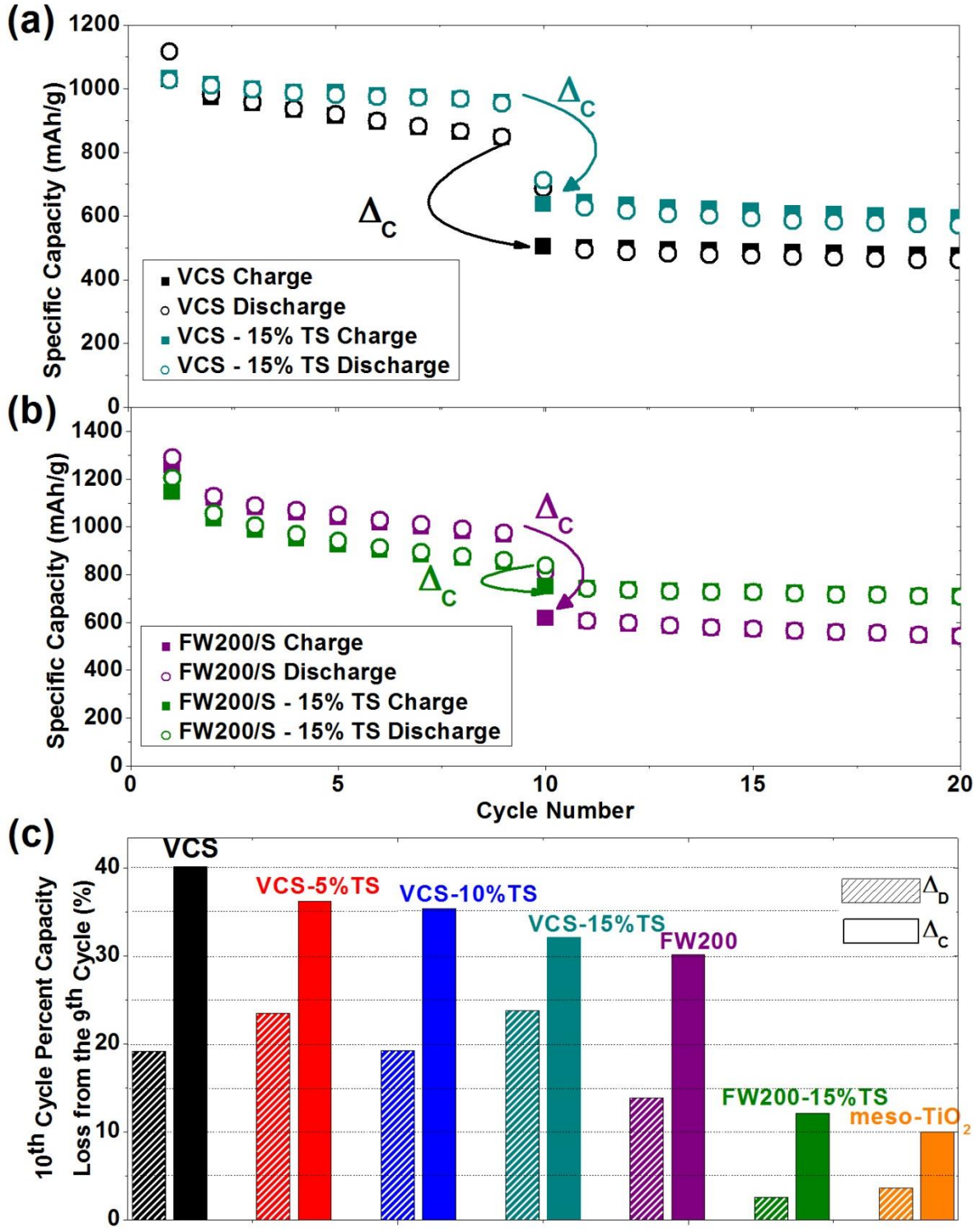

Figure 4.6: (a) and (b) capacity/cycle index plot, illustrating Δ_C upon self-discharge, (c) summary of Δ_D and Δ_C for Vulcan carbon and FW200 with and without the $Na_2S_2O_3$ additive.

4.3.4 Probing the Interaction Between Thiosulfate and Li_2S_4 by XPS Analysis

The nature of the interaction of MnO_2 nanosheets with S_n^{2-} has been reported by our group; the insoluble $S_2O_3^{2-}$ on the surface of MnO_2 anchors the long chain polysulfides and converts them to lower order polysulfides via an internal disproportionation reaction.[29] The interaction between carbon-thiosulfate-S_n^{2-} was determined using S 2p, C 1s and O1s X-ray photoelectron spectroscopy (XPS) analysis. Following convention, only the lower binding energy component (S $2p_{3/2}$) of the S2p spin orbit doublet is quoted.

As reference standards to probe for spectral energy features, synthesized Li_2S_4 and commercial $Na_2S_2O_3$ were analyzed by XPS (**Figure 4.7**). The XPS spectrum of Li_2S_4 shows two sulfur environments in a 1:1 area ratio at 161.7 eV and 163.1 eV corresponding to the terminal (S_T^{-1}) and bridging (S_B^{0}) sulfur atoms. There is a 1:1 area ratio between the two sulfur environments in $Na_2S_2O_3$ at 162.1 eV and 168.1 eV corresponding to the peripheral sulfur and the central sulfur respectively (inset, **Figure 4.7b**).

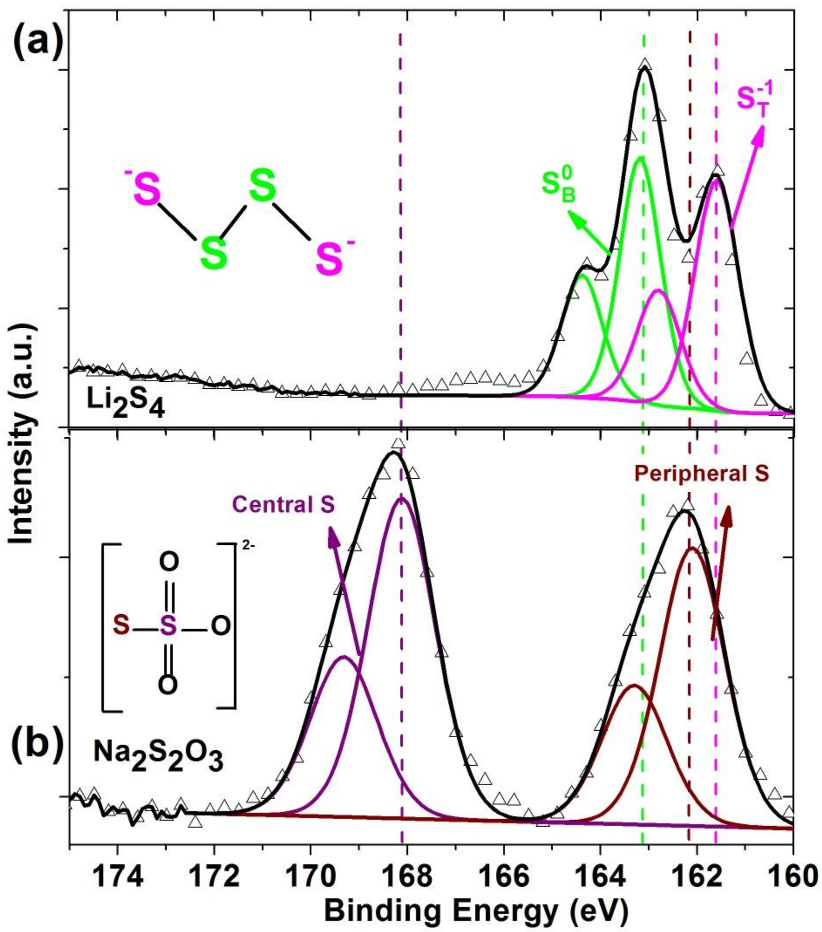

Figure 4.7: XPS S 2p core spectra for reference materials (a) Li_2S_4 powder and (b) $Na_2S_2O_3$.

Figure 4.8a displays the data collected on the recovered powder (VC + Li_2S_4) from mixing a solution of Li_2S_4 in glyme-based solvent with a known amount of Vulcan carbon. There is a minor contribution at 166 to 170 eV characteristic of sulfite arising from trace concentration of water in the solvent. The peak at 163.8 eV is assigned to elemental sulfur (S^0) which readily deposits on the non-polar surface of Vulcan carbon through disproportionation of Li_2S_4 in solution. Simultaneously, the disproportionation reaction of varying chain length S_n^{2-} species forms Li_2S_4 upon drying which can be seen from the peaks at 161.7 and 163.1 eV. The C1s and O1s core spectra (**Figure 4.9 a** and **d**) reveal only organic interactions (C-H and C-O bonds) and thus no interaction with sulfur is detected. The interactions between polysulfide and Vulcan

carbon can be summarized in **Figure 4.10a**, where there is Li_2S_4 and elemental sulfur on the surface of the carbon host.

Figure 4.8b displays three characteristic sulfur environments obtained on incorporation of $Na_2S_2O_3$ into Vulcan carbon as an additive. The first two sulfur environments are in a 6:1 area ratio corresponding to the central and peripheral sulfur from $Na_2S_2O_3$ at 168.1 eV and 162.1 eV respectively. The third environment is measured at 163.8 eV which corresponds to the formation of a S^0-C bond from the peripheral sulfur of thiosulfate binding with carbon. The peripheral sulfur species of $Na_2S_2O_3$ that did not remain in an oxidation state of (-1) formed a S^0-C bond as rationalized through the shift in peak area. There is now a 6:5 (central thiosulfate sulfur : S^0-C bond) peak area ratio confirming that 84% of the peripheral sulfur of thiosulfate made a bond with carbon. The C 1s spectrum in **Figure 4.9b** indicates the formation of a C-S^0 bond, while the O 1s (**Figure 4.9e)** spectrum confirms the presence of thiosulfate on the surface. Summarized in **Figure 4.10b**, partial deposition of thiosulfate occurs onto the surface of the carbon host, while, the remaining thiosulfate binds to carbon through the peripheral sulfur.

The interaction of polysulfides in the presence of VC-15%TS was studied by XPS with results displayed in **Figure 4.8c**. The peaks at 168.1 eV and 162.1 eV correspond to the central and peripheral sulfur of the free thiosulfate respectively. The peak area at 163.8 eV corresponds to S^0 which originates from the thiosulfate-carbon bond and from the disproportionation reaction of Li_2S_4 in solution forming elemental sulfur. The higher energy spectral feature at 168.8 eV corresponds to the formation of the polythionate complex as previously reported.[29] At lower binding energy, there are spectral features corresponding to the terminal and bridging sulfur of Li_2S_4 at 161.7 and 163.1 eV respectively. C 1s spectra (**Figure 4.9c)** offers further confirmation of the presence of a S^0-C bond which remained after mixing with Li_2S_4. Summarized in **Figure**

4.10c, there are free sulfur, thiosulfate and Li_2S_4 species on the surface of carbon, along with catentated sulfur species forming the polythionate complex.

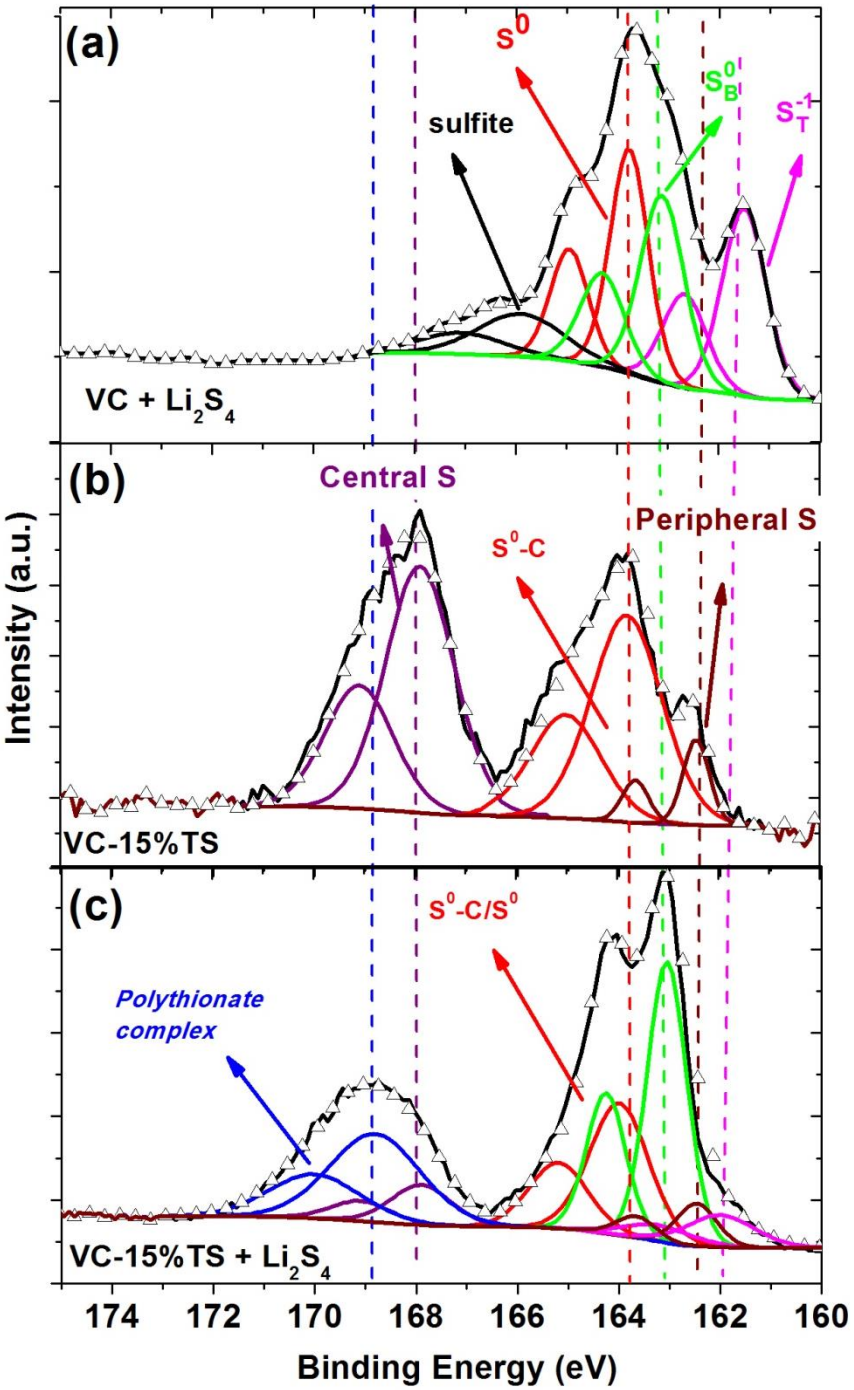

Figure 4.8: (a) Vulcan carbon mixed with Li_2S_4 exhibiting the formation of elemental sulfur and remaining Li_2S_4, (b) Vulcan carbon mixed with 15 wt% $Na_2S_2O_3$ showing the typical reference peaks from thiosulfate and the formation of a S^0-C bond, and (c) Vulcan carbon with 15 wt% $Na_2S_2O_3$ mixed with Li_2S_4 showing the formation of the polythionate complex.

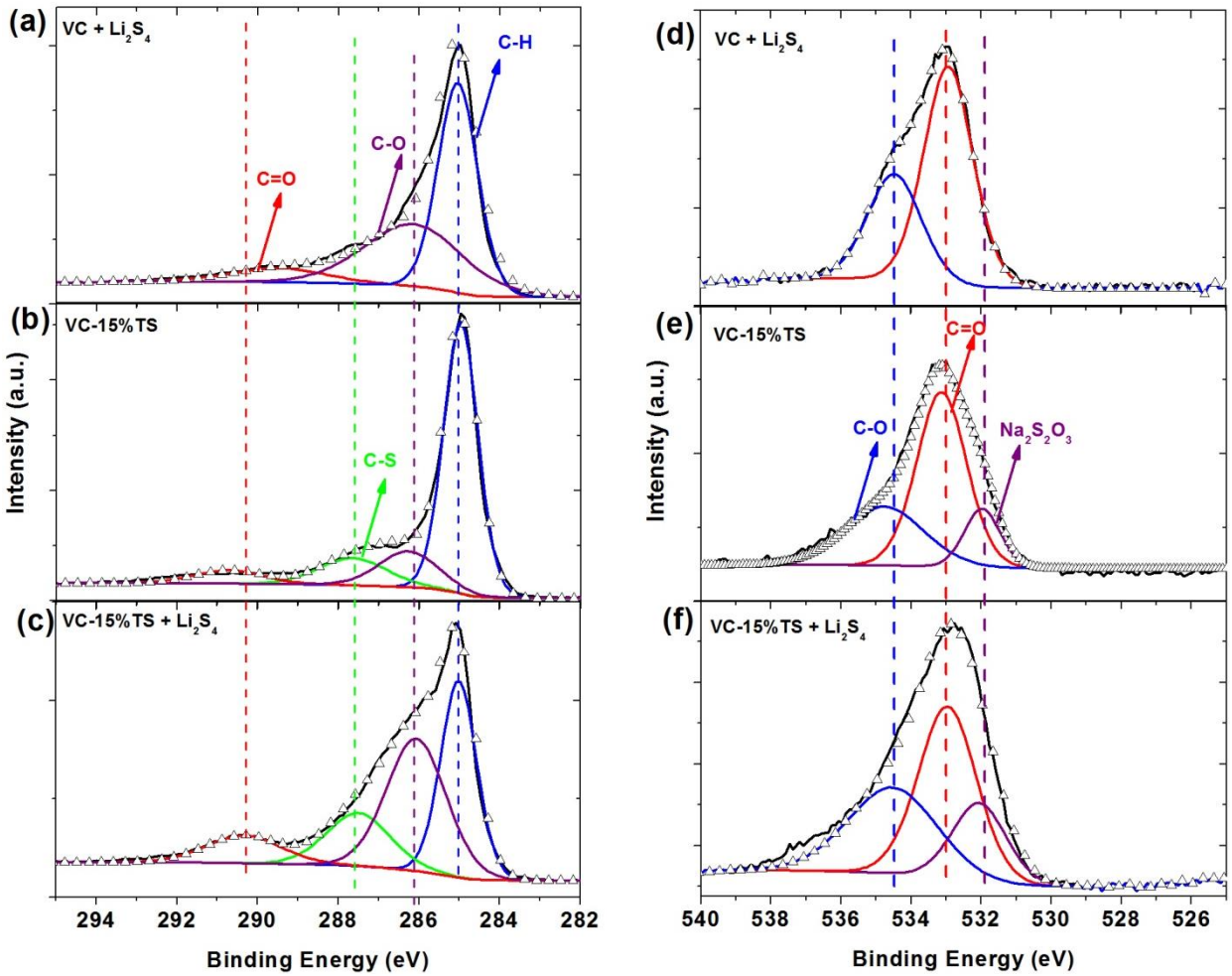

Figure 4.9: C 1s spectra of (a) Vulcan carbon mixed with Li_2S_4, (b) Vulcan carbon mixed with 15 wt% $Na_2S_2O_3$ and (c) Vulcan carbon with 15 wt% $Na_2S_2O_3$ mixed with Li_2S_4 and O1s spectra of (d) Vulcan carbon mixed with Li_2S_4, (e) Vulcan carbon mixed with 15 wt% $Na_2S_2O_3$ and (f) Vulcan carbon with 15 wt% $Na_2S_2O_3$ mixed with Li_2S_4.

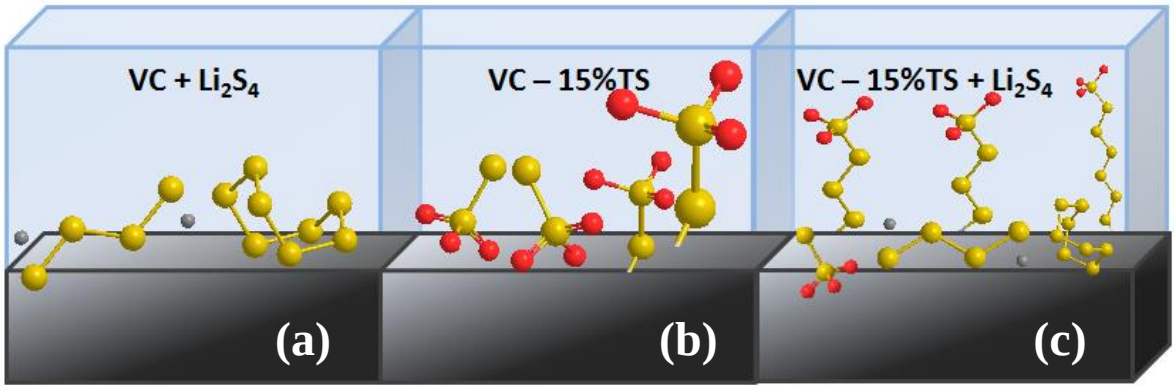

Figure 4.10: Pictorial representation of thiosulfate mechanism based on XPS data (a) VC + Li_2S_4, (b) VC-15%TS, (c) VC15%TS + Li_2S_4. Atoms: sulfur (yellow), grey (lithium), and red (oxygen).

Carbon materials that are not structured to physically entrap polysulfides suffer detrimental capacity loss due to the diffusion of S_n^{2-} into the electrolyte. However, this problem can be alleviated through the addition of $Na_2S_2O_3$ to a carbon host which actively binds the polysulfides through a catenation process.

4.3.5 Electrochemical Measurements

Long-term cycling capability of these materials was assessed through galvanostatic cycling at a C/2 current density (836 mA g^{-1}, corresponding to discharge or charge of the theoretical capacity in two hours) with the first conditioning cycle at C/20 to fully wet the electrode with the electrolyte. **Figure 4.11** shows the cycling profile and behavior of coin cells using Vulcan carbon composites as the sulfur host. There was only a 7% enhancement in the capacity retention for the VC/S-15%TS over the pristine carbon (**Figure 4.11b).** This low capacity retention enhancement is not surprising as the polysulfide adsorptivity of these materials did not increase drastically with the additive present in the composite. Therefore, for low surface area carbon materials (i.e. VC), the addition of thiosulfate does not prove advantageous for cycling and therefore should not be used in practical Li-S batteries.

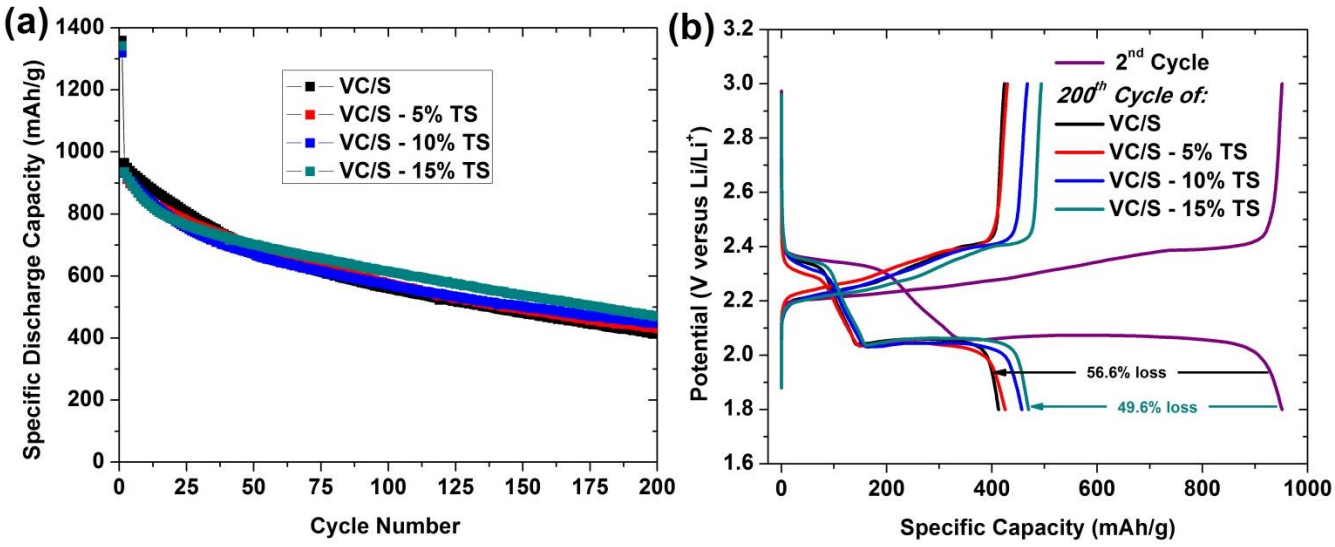

Figure 4.11: (a) Galvanostatic cycling of Vulcan carbon composite materials at C/2 rate after an activation cycle at C/20, (b) cycling profile of Vulcan carbon composite materials.

In contrast, the modified FW200 possesses excellent cycling compared to the bare FW200 as exemplified in **Figure 4.12 a** and **b** where a drastic difference in the cycling behavior of these materials is obtained. Over 200 cycles, FW200 drastically fades, whereas the additive composite is able to retain 33% more capacity after 200 cycles. Overall, the addition of 15 wt% $Na_2S_2O_3$ to high surface area FW200 resulted in 89% capacity retention from the 100th cycle, and 83% capacity retention from the 200th cycle. This excellent cycling for a carbon sulfur host correlates to a capacity fade rate of 0.085% per cycle.

The enhanced cycling of the FW200/S-15%TS composite is realized as the polysulfide adsorptivity increased drastically. It is expected that the uniform coating of sulfur and thiosulfate played a role in providing an ideal electrode architecture for stable cycling as well. This uniformity exacerbated the effect of the polythionate complex as it would be present all over the surfaces of the FW200 composite further enhancing the quantity of interactions. Whereas pristine FW200 relies only on hydrophobic interaction with the polysulfides, which is very weak and causes a high degree of polysulfide dissolution, when compared to FW200/S-15%TS.

From elemental mapping shown in **Figure 4.3,** the amount of sodium present in the composite is low (~5 wt%). It is expected that the sodium is not participating in any electrochemistry as it originates from the sodium thiosulfate that is sitting freely on the surface of the carbon host and is insoluble in the ether-based electrolyte.

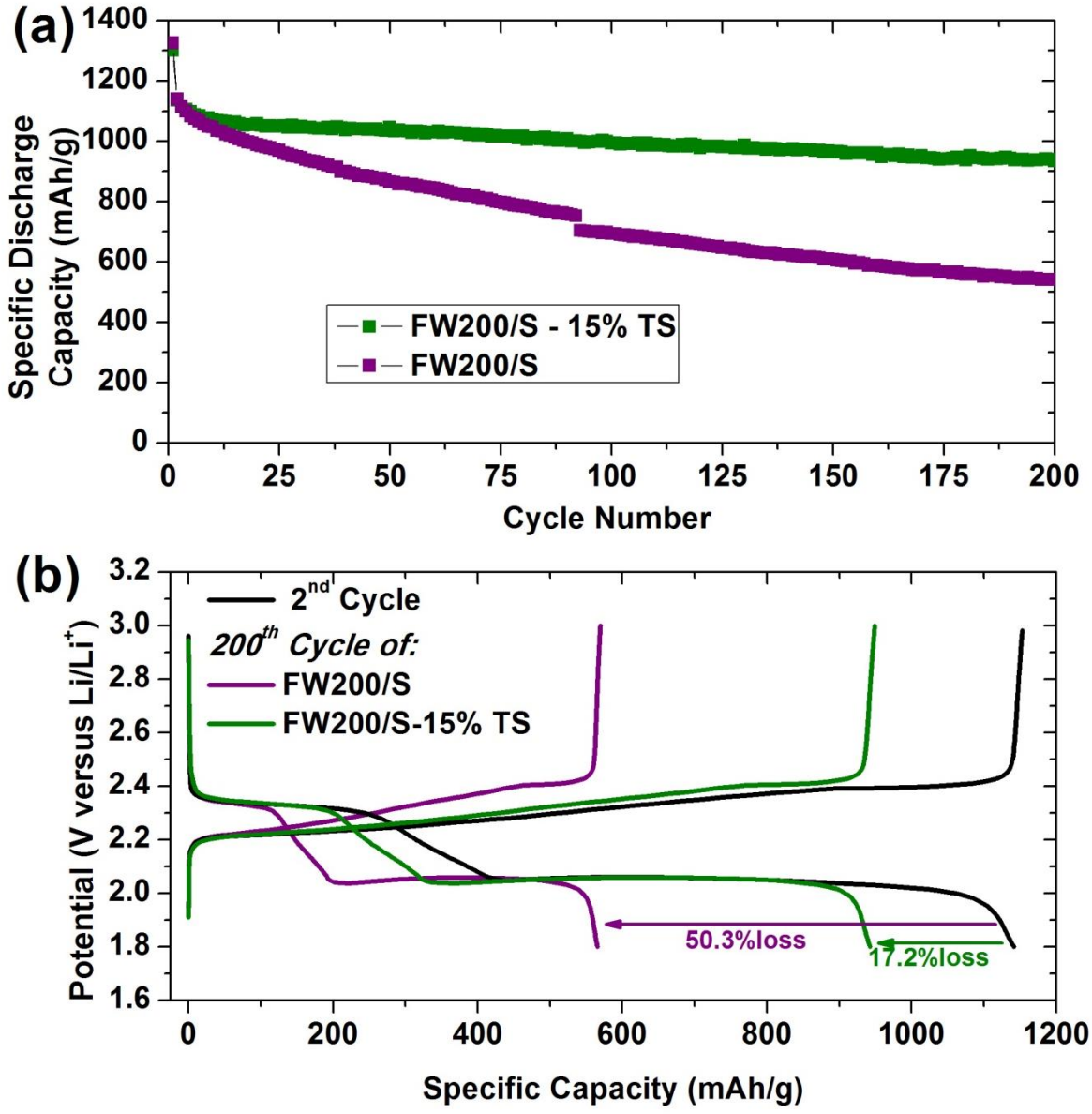

Figure 4.12: (a) Galvanostatic cycling of FW200 composite materials at C/2 rate after an activation cycle at C/20, (b) cycling provide of FW200 composite materials.

4.4 Conclusion

The search for a practical sulfur host material that is conductive, and inhibits polysulfide diffusion into the electrolyte is ever evolving. Carbon is an ideal host material because its conductivity is sufficient to not limit cycling rate, and it is light weight to benefit energy density. Due to the non-polar nature of carbon, polysulfide diffusion is a limiting factor for its practical application. The addition of thiosulfate to carbon host materials invokes improved interaction between the soluble polysulfides through the formation of the polythionate complex. A high surface area FW200 carbon with 15 wt% thiosulfate is able to retain 33% more capacity over 200 cycles compared to the pristine FW200. After 200 cycles, the FW200 with 15 wt% thiosulfate retains 83% of its original capacity which corresponds to a fade rate of 0.085% per cycle. In section 3.5, a plot was established comparing critical properties of cathode hosts. With the addition of 15 wt% thiosulfate to FW200, the surface area decreased slightly, but the capacity retention and polysulfide adsorptivity increased causing a shift closer to the target for an ideal sulfur host.

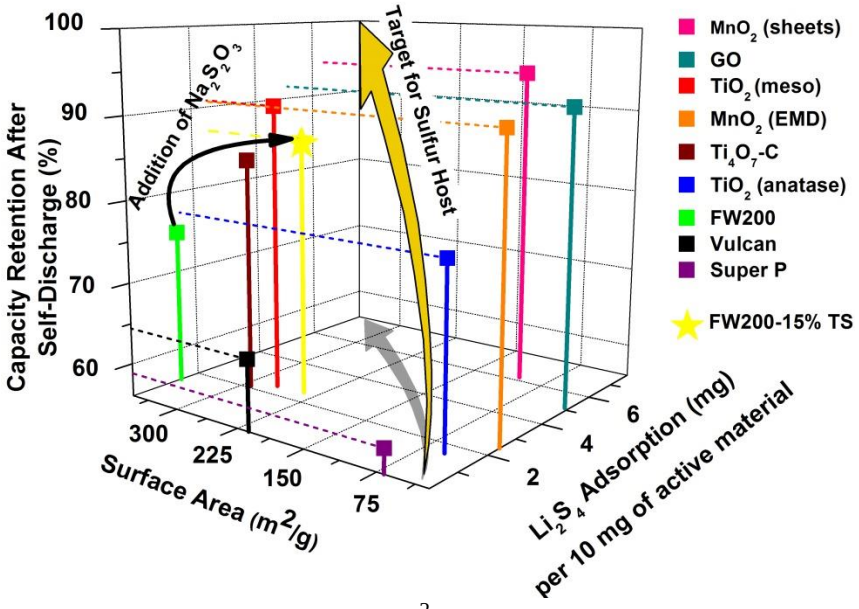

Figure 4.13: Target for sulfur host based on S_n^{2-} adsorption, surface area and capacity retention from Figure 3.13 with the addition of FW200-15%TS.

Future Prospective

It is with hope that the work in this thesis will aid in bringing the sulfur battery one step closer to commercialization. In order to realize a practical Li-S battery, the main technical issues must be addressed: polysulfide diffusion out of the positive electrode, the shuttle mechanism, volume expansion upon cycling and lithium dendrite formation/safety issues.

Chapter 3 focused on developing a diagnostic method to screen sulfur host materials. A diagnostic method provides advanced information about the Li-S system and informs researchers about where to target their focus. Through the comprehensive study of various materials, it was discovered that materials with a high polysulfide adsorptivity realized prolonged cycling while mitigating the irreversible capacity loss as a result of self-discharge. The conclusions drawn from the results of this method focused my research into developing a material that adsorbs polysulfides, instead of solely relying on physical entrapment.

Chapter 4 then focused on a positive electrode material with a high polysulfide adsorptivity for carbonaceous materials. The key reason to focus on the positive electrode is because one of the main issues hindering the commercialization of the Li-S battery is the diffusion of the intermediate polysulfides. Through the addition of thiosulfate to a high surface area carbon host, the polysulfide adsorptivity increased and as a result the capacity retention during long-term cyclability increased. In fact, the polysulfide adsorptivity FW200-15%TS is now comparable to that of a polar metal oxide.

Future work for incorporating polysulfide adsorbing functional groups into a carbon matrix must ensure there is no additive sitting freely on the surface of the carbon not participating in the thiosulfate mechanism. One tactic that could be pursued is the

functionalization of carbon under oxidative conditions in the presence of sodium thiosulfate to encourage more uniform and successful functional group addition.

Beyond discovering a new material, in order to realize a practical positive electrode material, the sulfur loading will need to be increased. It is now a common target in Li-S battery research to aim for 5 mg/cm^2 sulfur loading in the positive electrode. However, full sulfur utilization is a large issue when increasing the sulfur loading in the positive electrode and must be addressed.

In any case, research funding from governments and industrial partners need to continue to support Li-S battery research as it is hopeful that it can be the next high energy density battery. If this happens, then less pressure on fossil fuels will be needed and our world will become more environmentally friendly through driving electric vehicles and storing more energy from renewable sources.

References

[1] Goodenough, J.B., and Park, K-S., The Li-Ion Rechargeable Battery: A Perspective. *J. Am. Chem. Soc.*, **2013**, 135, 1167.

[2] Droege, P., Urban Energy Transition: From Fossil Fuels to Renewable Power, Elsevier Publications, **2008**.

[3] Tarascon, J-M., Armand, M., Issues and Challenges Facing Rechargeable Lithium Batteries, *Nature*, **2001,** 414, 359.

[4] Park, J.K., Principles and Applications of Lithium Secondary Batteries, Wiley-VCH, **2012**.

[5] Nazar, L.F., Cuisinier, M., Pang, Q., Lithium-Sulfur Batteries, *MRS Bulletin*, **2014**, 39, 436.

[6] Mizushima, K., Jones, P.C., Wiseman, P.J., and Goodenough, J.B., Li_xCoO_2: A New Cathode Material for Batteries of High Energy Density, *Mat. Res. Bull.*, **1980**, 15, 783.

[7] Zaghib, K., Dontigny, M., Guerfi, A., Charest, P., Rodrigues, I., Mauger, A., and Julien, C.M., Safe and fast-charging Li-ion battery with long shelf life for power applications. *J. Power Sources*, **2011**, 196, 3949.

[8] Bruce, P.G., Freunberger, S.A., Hardwick, L.J., and Tarascon, J-M., Li-O_2 and Li-S Batteries with High Energy Storage, *Nature Mater.*, **2012**, 11, 19.

[9] Herbert, D., and Ulam, J., US Patent 3,043,896, **1962**.

[10] Wang, D-W., Zhou, G., Li, F., Wu, K-H., Lu, G., Cheng, H-M., and Gentle, I., A Durable Cathode with Sub-Nanometer Confined Sulfur for High Energy Batteries, *Angew.*, DOI: 10.1002/anie.200, 2013.

[11] Guo, J., Yang, Z., Yu, Y., Abruna, H., and Archer, L., Lithium-Sulfur Battery Cathode Enabled by Lithium-Nitrile Interaction, *J. Am. Chem. Soc.*, **2013**, 135, 763.

[12] Ji, X., Lee, K., and Nazar, L.F. A Highly Ordered Nanostructured Carbon-Sulfur Cathode for Lithium-Sulfur Batteries, *Nature Mater.*, **2009**, 8, 500.

[13] Cuisinier, M., Cabelguen, P.-E., Evers, S., He, G., Kolbeck, M., Garsuch, A., Bolin, T., Balasubramanian, M., and Nazar, L. F., Sulfur Speciation in Li-S Batteries Determined by Operando X-Ray Absorption Spectroscopy, *J. Phy. Chem. Lett.*, **2013**, 4, 3227.

[14] Manthiram, A., Fu, Y., Chung, S-H., Zu, C., and Su Y-S., Rechargeable Lithium-Sulfur Batteries, *Chem. Rev.*, **2014**, 114, 11751.

[15] Cuisinier, M., Cabelquen, P-E., Adams, B., Garsuch, A., Balasubramanian, M., and Nazar, L.F., Unique Behaviour of Nonsolvents for Polysulfides in Lithium-Sulfur Batteries, *Energy Environ. Sci.*, **2014**, 7, 2697.

[16] Cuisinier, M., Hart, C., Balasubramanian, M., Garsuch, A., and Nazar, L.F., Radical or Not Radical: Revisiting Lithium-Sulfur Electrochemistry in Nonaqueous Electrolytes, *Adv. Energy Mater.*, **2015**, 1401801.

[17] Patel, M.U., Arcon, I., Aquilanti, G., Stievano, L., Mali, G., and Dominko, R., X-ray Absorption Near-Edge Structure and Nuclear Magnetic Resonance Study of the Lithium-Sulfur Battery and its Components, *Chem. Phys. Chem.*, **2014**, 15, 894.

[18] Patel, M.U., Demir-Cakan, R., Morcrette, M., Tarascon, J-M., Gaberscek, M., and Dominko, R., Li-S Battery Analyzed by UV/Vis in Operando Mode, *Chem. Sus. Chem.*, **2013,** 6, 1177.

[19] Nelson, J., Misra, S., Yang, Y., Jackson, A., Liu, Y., Wang, H., Dai, H., Andrews, J.C., Cui, Y., and Toney, M.F.J., In Operando X-Ray Diffraction and Transmission X-ray Microscopy of Lithium Sulfur Batteries, *J. Am. Chem. Soc.*, **2012**, 134, 6337.

[20] Dominko, R., Demir-Cakan, R., Morcrette, M., and Tarascon, J-M., Analytical Detection of Soluble Polysulfides in a Modified Swagelok Cell, *Electrochem. Commun.*, **2011**, 13, 117.

[21] Jayaprakash, N., Shen, J., Moganty, S.S., Corona, A., and Archer, L.A., Porous Hollow Carbon@Sulfur Composites for High-Power Lithium-Sulfur Batteries, *Angew. Chem., Int. Ed.*, **2011**, 50, 5904.

[22] He, G., Evers, S., Liang, X., Cuisinier, M., Garsuch, A., and Nazar, L.F., Tailoring Porosity in Carbon Nanospheres for Lithium-Sulfur Battery Cathodes, *ACS Nano,* **2013,** 7, 10920.

[23] He, G., Hart, C.J., Liang, X., Garsuch, A., and Nazar, L.F., Stable Cycling of a Scalable Graphene-Encapsulated Nanocomposite for Lithium-Sulfur Batteries, *ACS Appl. Mater. Interfaces*, **2014**, 6, 10917.

[24] Wang, H., Yang, Y., Liang, Y., Robinson, J.T., Li, Y., Jackson, A., Cui, T., and Dai, H., Graphene-Wrapped Sulfur Particles as a Rechargeable Lithium-Sulfur Battery Cathode Material with High Capacity and Cycling Stability, *Nano Lett.,* **2011**, 11, 2644.

[25] Su, Y-S., Fu, Y., and Manthiram, A., Self-weaving sulfur-carbon composite cathodes for high rate lithium-sulfur batteries, *Phys. Chem. Chem. Phys.,* **2012**, 14, 14495.

[26] Guo, J., Xu, Y., and Wang, C., Sulfur-Impregnated Disordered Carbon Nanotubes Cathode for Lithium-Sulfur Batteries, *Nano Lett.,* **2011**, 11, 4288.

[27] Seh, Z., Li, W., Cha, J., Zheng, G., Yang, Y., McDowell, M., Hsu, P-C., and Cui, Y., Sulfur-TiO_2 yolk-shell nanoarchitecture with internal void space for long-cycle lithium-sulfur batteries. *Nat. Commun.*, **2013**, 4, 1331.

[28] Pang, Q., Kundu, D., Cuisinier, M., and Nazar, L.F., Surface-enhanced redox chemistry of polysulfides on a metallic and polar host for lithium-sulfur batteries. *Nat. Commun.*, **2014**, 5, 4759.

[29] Liang, X., Hart, C., Pang, Q., Garsuch, A., Weiss, T., and Nazar, L.F., A highly efficient polysulfide mediator for lithium-sulfur batteries, *Nat. Commun.,* **2015**, 6, 5682.

[30] Liang, X., Kwok, C.Y., Hart, C., Pang, Q., Houtarde, D., Huang, H., Karsp, K., and Nazar, L.F., Tuning transition metal oxide-sulfur interactions for long life lithium sulfur batteries: the goldilocks principle, *Adv. Energy Mater.,* **2015**, submitted.

[31] Azimi, N., Xue, Z., Rago, N.D., Takoudis, C., Gordin, M.L., Song, J., Wang, D., and Zhang, Z., Fluorinated Electrolytes for Li-S Battery: Suppressing the Self-Discharge with an Electrolyte Containing Fluoroether Solvent, *J. Electrochem. Soc.*, **2015**, 162, A64.

[32] Qiu, Y., Li, W., Zhao, W., Li, G., Hou, Y., Liu, M., Zhou, L., Ye, F., Li, H., Wei, Z., Yang, S., Duan, W., Ye, Y., Guo, J., and Zhang, Y., High-Rate, Ultralong Cycle-Life Lithium/Sulfur Batteries Enabled by Nitrogen-Doped Graphene, *Nano Lett.*, **2014,** 14, 4821.

[33] Hart, C., Cuisinier, M., Liang, X., Kundu, D., Garsuch, A. and Nazar, L.F., Rational design of sulfur host materials for Li-S batteries: correlating lithium polysulfide adsorptivity and self-discharge capacity loss. *Chem. Comm.,* **2015**, 51, 2308.

[34] Bragg, W.L., The Diffraction of Short Electromagnetic Waves by a Crystal, *Proc. Camb. Phil. Soc.*, **1913**, 17, 43.

[35] Davies, O.L., and Goldsmith, P.L., Statistical Methods in Research and Production, Hafner Publishing Company, **1972**.

[36] Manthiram, A., Materials Challenges and Opportunities of Lithium Ion Batteries, *J. Phys. Chem. Lett.,* **2011,** 2, 176.

[37] Peled, E., Gorenshtein, A., Segal, M., and Sternberg, Y., Rechargeable Lithium-Sulfur Battery, *J. Power Sources,* **1989**, 26, 269.

[38] Aurbach, D., Pollak, E., Elazari, R., Salitra, G., Kelley, C.S., and Affinito, J., On the Surface Chemical Aspects of Very High Energy Density Rechargeable Li-Sulfur Batteries, *J. Electrochem. Soc.,* **2009**, 156, A694.

[39] Gordin, M.L., Dai, F., Chen, S., Xu, T. Song, J., Tang, D., Azimi, N., Zhang, Z., and Wang, D., Bis (2,2,2-trifluoroethyl) Ether As an Electrolyte Co-Solvent for Mitigating Self-Discharge in Lithium-Sulfur Batteries, *ACS App. Mater. Interfaces*, **2014**, 6, 8006.

[40] Ehi, R.G., and Ihde, A., Faraday's Electrochemical Laws and the Determination of Equivalent Weights, *J. Chem. Ed.*, **1954**, 31, 226.

[41] Urbonaite, S., and Novak, P., Importance of 'unimportant' experimental parameters in Li-S battery development, *J. Power Sources*, **2014**, 249, 297.

[42] Janakiraman, U., and Miller, G., *US Pat.*, 0 079 989, **2014.**

[43] Yin, Y.X., Xin, S., Guo, Y.G. and Wan, L.J., Lithium-sulfur batteries: electrochemistry, materials and prospects. *Angew. Chem. Int. Ed.*, **2013,** 52, 2.

[44] Zhang, B., Qin, X., Li, G.R. and Gao, X.P., Enhancement of Long-Stability of Sulfur Cathode by Encapsulating Sulfur into Micropores of Carbon Spheres, *Energy Environ. Sci*., **2010**, 3, 1531.

[45] Geim, A.K., and Novoselov, K.S., The Rise of Graphene, *Nat. Mater.*, **2007**, 6, 183.

[46] Wang, J., Chen, J., Konstantinov, K., Zhao, L., Ng, S.H., Wang, G.X., Guo, Z.P., and Liu, H.K., Sulfur-polypyrrole Composite Positive Electrode Materials for Rechargeable Lithium-Bateries, *Electrochim. Acta*., **2006**, 51, 4634.

[47] Wu, F., Chen, J., Li, L., Zhao, T., and Chen, R.J. Sulfur/Polythiophene with a Core/Shell Structure: Synthesis and Electrochemical Properties of the Cathode for Rechargeable Lithium Batteries, *J. Phys. Chem. C*, **2011**, 115, 24411.

[48] Yin, L., Wang, J., Ln, F., Yang, J., and Nuli, Y., Polyacrylonitrile/graphene composite as a precursor to a sulfur-based cathode material for high-rate rechargeable Li-S batteries, *Energy Environ. Sci.*, **2012**, 5, 6966.